

DATA-DRIVEN CONTROL AND OPTIMAL MANAGEMENT OF ELECTRIC  
DISTRIBUTION GRID WITH HIGH PENETRATION OF DISTRIBUTED  
ENERGY RESOURCES (DERS) BASED ON SPECTRAL CLUSTERING

by

Shyamal Patel

A dissertation submitted to the faculty of  
The University of North Carolina at Charlotte  
in partial fulfillment of the requirements  
for the degree of Doctor of Philosophy in  
Electrical Engineering

Charlotte

2022

Approved by:

---

Dr. Sukumar Kamalasan

---

Dr. Valentina Cecchi

---

Dr. Abasifreke Ebong

---

Dr. Vincent (Tobi) Ogunro

©2022  
Shyamal Patel  
ALL RIGHTS RESERVED

## ABSTRACT

SHYAMAL PATEL. Data-driven control and optimal management of electric distribution grid with high penetration of distributed energy resources (DERs) based on spectral clustering. (Under the direction of DR. SUKUMAR KAMALASADAN)

Motivated by the government's clean energy targets, the penetration of Distributed Energy Resources (DER) is increasing. These DERs interconnections bring the added generation and storage capacity at the distribution level. Also, with the increasing implementation of smart inverters and Advanced Distribution Management Systems (ADMS), the flexibility of the DERs can be leveraged to solve the distribution grid issues like abnormal voltages, intermittencies, and thermal overloads. The proposed work focuses on the development of a robust distributed control architecture to control and optimally manage the load and PV variations using energy storage by creating the virtual clusters of the distribution grid. The approach is based on a spectral clustering distributed control methodology that partition the grid into manageable clusters. The cluster of the distribution grid represents a good balance of local load and DER generation. An approach for reactive power to voltage sensitivity is also proposed for voltage regulation purposes at the cluster level based on the grid measurements. The cluster configurations adapt to accommodate the varying grid topology or changing load and DER generation. For the distribution grids receiving the set-points at the substation level for management of transmission power flow, an Alternating Direction Methods of Multipliers (ADMM) based optimization is proposed to share the area set-points among the clusters based on the state of charge of each cluster. The controllable assets of each cluster (BESS) are managed through model predictive control. The improvement in the grid resiliency is demonstrated through the implementation of the complete framework to support the loads on the healthy part of the grid without interruptions during the contingency/outage scenarios on the distribution grid.

## DEDICATION

This work is dedicated to my wife, Ghata, who has been a constant source of support and encouragement during the challenges of graduate school and life. This work is also dedicated to my parents, Haresh Patel and Daksha Patel, who have always motivated me and loved me unconditionally.

## ACKNOWLEDGEMENTS

I would first like to thank my research guide, Dr. Sukumar Kamalasan, whose guidance was invaluable in formulating the research questions and methodology. I would also like to thank the members of my dissertation committee, Dr. Valentina Cecchi, Dr. Abasifreke Ebong, and Dr. Vincent Ogunro, for the continued evaluation, support, and guidance.

I would like to acknowledge the research grants - UNCC Awards, NSF Award, DOE Award and Siemens for financially supporting the research activities. I would also like to acknowledge the research facility, Power Energy and Intelligent Systems Laboratory (PEISL), at EPIC UNCC for hosting the research.

A special thanks to Jonathan Hou, Consulting Director at Hitachi Energy, for the constant motivation and for helping me balance my professional commitments and my Ph.D. research. I would also like to acknowledge the support from my family and friends throughout the research.

## TABLE OF CONTENTS

LIST OF TABLES	xi
LIST OF ABBREVIATIONS	1
CHAPTER 1: INTRODUCTION	2
1.1. Background and Motivation	5
1.1.1. Resiliency related challenges	6
1.1.2. Power Quality	8
1.2. Research Objective	11
1.3. Research Challenges	12
1.4. Research Approach	13
1.5. Thesis Flowchart	14
CHAPTER 2: Literature review on clustering, distributed optimization and control	16
2.1. Introduction	16
2.2. Review: Clustering	16
2.2.1. Kernel based Clustering	16
2.2.2. Swarm Intelligence based Clustering	17
2.2.3. Density Based Clustering	17
2.2.4. Spatial Clustering	18
2.2.5. Hierarchical Clustering	18
2.2.6. Graph Theory Based Clustering	18
2.3. Review: Distributed optimization	19
2.3.1. Analytical Target Cascading	19

2.3.2.	Auxiliary Problem Principle	19
2.3.3.	Optimality Condition Decomposition	20
2.3.4.	Dual decomposition	20
2.3.5.	Consensus+Innovation	21
2.3.6.	Alternating direction method of multiplier	21
CHAPTER 3: New Method for Grouping Distributed Energy Resources to support Power Distribution System		23
3.1.	Introduction-Spectral Clustering	23
3.1.1.	Algorithm	24
3.2.	Evaluation of the cluster quality	26
3.2.1.	Quality of individual clusters	26
3.2.2.	Quality of overall cluster formations	27
3.2.3.	Factors affecting the cluster quality	28
3.3.	Active power flow based clustering of distribution grids	30
3.3.1.	Drawback of the conventional spectral clustering approach	30
3.4.	Proposed Approach: Two Layer Spectral Clustering	33
3.4.1.	Preliminary Study	35
3.5.	Voltage sensitivity based clustering of distribution system	40
3.6.	Sensitivity based spectral clustering	40
3.7.	Implementation of the proposed approach	43
3.7.1.	Result and Discussion: Active Power-flow based clusters.	44
3.7.2.	Result and Discussion: Sensitivity based clusters.	47

3.8. Chapter Summary	51
CHAPTER 4: Optimal management of power distribution system with clustering for effective utilization of DERs	52
4.1. Introduction	52
4.2. Cluster net-load management	53
4.2.1. Least Square Estimation based Active power-based cluster control for cluster net-load management	54
4.2.2. Inter-cluster set-point segregation	56
4.3. Sensitivity based reactive power control for voltage management	60
4.4. Implementation: IEEE 123 bus system	62
4.4.1. Net-load smoothing through dynamic cluster and control	63
4.4.2. Voltage control through dynamic clusters and control	68
4.5. Chapter Summary	71
CHAPTER 5: Dynamic distributed model of power grid for optimization and control	72
5.1. Introduction	72
5.2. ADMM based sharing optimization	72
5.3. Area Set-point segregation	74
5.3.1. Use-cases for SOC based set-point generation	77
5.4. Reference set-point tracking	85
5.5. Implementation: IEEE 123 bus system	89
5.5.1. Use case 1: Dynamically varying area set-points.	90
5.5.2. Use case 2: Net-load minimization	93

5.6. Chapter Summary	94
CHAPTER 6: Model predictive control approach for DER clusters in power distribution system	96
6.1. Introduction	96
6.2. Model Predictive Control	97
6.3. Theoretical Formulation: Plant Model Estimator	98
6.4. Theoretical Formulation: Optimizer	104
6.5. Implementation: 650 bus system	113
6.5.1. Use case 1: Area Control with Set-point Tracking	115
6.5.2. Use case 2: Active and Reactive Power Control	117
6.5.3. Computational time and overall integration time frame	120
6.6. Chapter Summary	121
CHAPTER 7: Resiliency Management of power distribution system with DERs	122
7.1. Introduction	122
7.2. Resiliency Metrics	122
7.2.1. Loss of loads	124
7.2.2. Economic loss	125
7.2.3. Loss in social discomfort	126
7.3. Situational awareness based cluster formation	127
7.3.1. Partial outage of the distribution feeder	128
7.3.2. Grid re-configuration	129
7.3.3. Switch location based clusters	130

7.4. Resilient cluster control through management of loads	131
7.4.1. Load Management Problem Formulation	132
7.4.2. Prioritization of the objectives	135
7.4.3. Effect of BESS SOC level and the event time on the critical load support	137
7.5. Implementation on IEEE 123 bus system	141
7.5.1. Results and discussion	142
7.6. Chapter summary	145
CHAPTER 8: CONCLUSIONS AND FUTURE WORK	149
8.1. Conclusions	149
8.2. Future Works	151
REFERENCES	154
APPENDIX A: Simulator	163
APPENDIX B: Measurements	164

## LIST OF TABLES

TABLE 1.1: US utility clean energy targets	6
TABLE 3.1: Effect of optimal $k$ on the clustering quality	29
TABLE 3.2: Spectral clustering cases	36
TABLE 3.3: Locations and ratings of DERs on IEEE 123 bus system	45
TABLE 3.4: Improvement of the proposed approach on cluster quality	45
TABLE 4.1: Inter-cluster set-point segregation	59
TABLE 4.2: Effect of cluster control on the net-load smoothing	65
TABLE 4.3: Improvement in the cluster net-load support through dynamic clustering	68
TABLE 5.1: Test cases illustrating ADMM based area set-point sharing	78
TABLE 5.2: Effect of control time-resolution on the tracking error	88
TABLE 5.3: Tracking error at cluster level	92
TABLE 6.1: Effect of output weight ( $Q$ ) on the reference tracking	108
TABLE 6.2: Effect of input weight ( $R$ ) on the reference tracking and BESS SOC	110
TABLE 6.3: Effect of input rate weight ( $E$ ) on the reference tracking and BESS dispatch	111
TABLE 6.4: Tracking Error for different disturbance models	113
TABLE 6.5: DER Ratings for 650 bus system	114
TABLE 6.6: Average Error: Use case 1	115
TABLE 7.1: Sample loads for the sensitivity study	135
TABLE 7.2: Inter-correlation of objectives and weights	136
TABLE 7.3: Load Information	142

TABLE 7.4: Loads during an islanded operation: Base Case and With proposed load management	146
TABLE 7.5: Quantification of the resilience for the impacted loads and the corresponding cluster	147
TABLE 7.6: Improvement in the resiliency of the cluster through the proposed management of the loads	148

## PREFACE

If you decide to have an introduction page, your introduction text would go here.

Depending on the discipline or the requirements of the student's advisory committee, an Introduction may be included as a preliminary page.

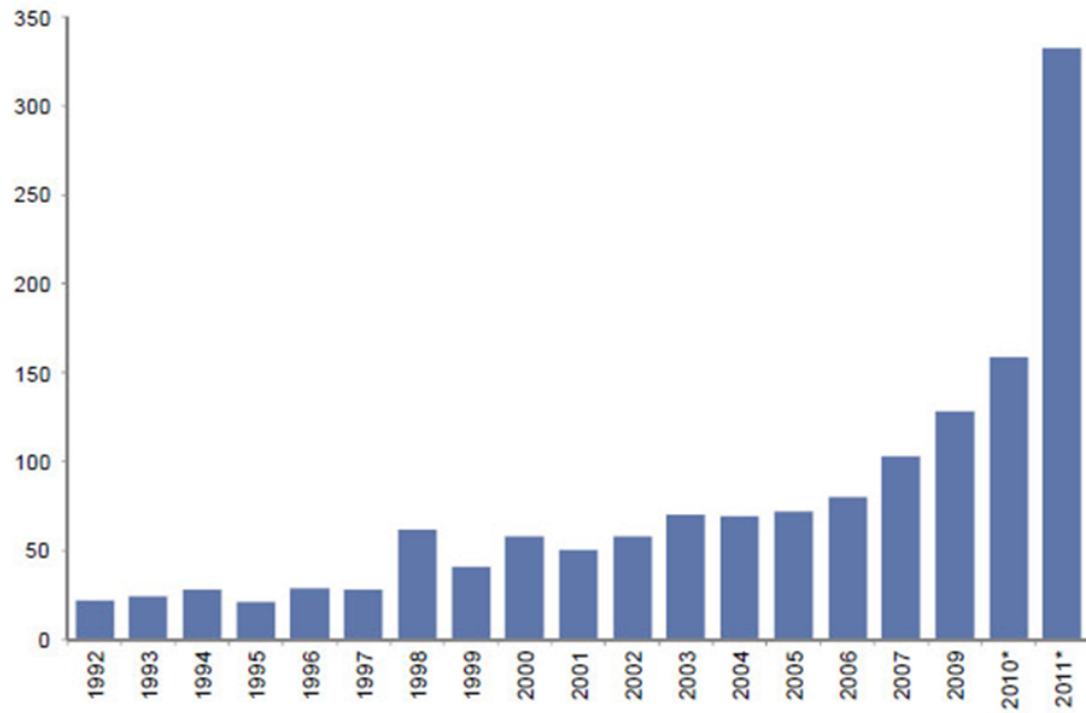
## CHAPTER 1: INTRODUCTION

There is an increasing trend in power outages and the impact of the power outages in the U.S. (Figure. 1.1). For example, it has been reported that more than 10 million customers were affected due to power outages between 2003 and 2012 [1]. According to Fig. 1.2, the majority of outages are weather-related. Between 2003 to 2012, weather-related events were responsible for 80% of the major outages in the U.S. [2] [1]. On the other hand, no significant increase in the frequency of hurricanes is observed during the specified period indicating that, with the aging grid infrastructure, increasing size and complexity of the power grid, the resiliency of the same is being compromised (Figure. 1.3).

In addition to the conventional causes of a power outage, cyber-threats and cyber-attacks are emerging challenges that compromise the power grid's reliability. Digitization of the power grid makes the power grid more vulnerable to cyber threats. For instance, including a more significant number of digital and smart devices in the grid has introduced a higher number of Internet Protocol (IP) based access points. These access points, if not adequately secured, act as a gateway for the cyber-attacks [3] [4].

At the same time, increasing adaptation of distributed energy resources (DERs) such as solar photovoltaics and batteries have introduced new technology options for energy resilience (Fig. 1.4). Renewable energy portfolios back growth in renewable energy and goals set by more than half of US states (Fig. 1.6). In addition to the same, many US utilities are targeting 100% clean energy generation. On the other hand, there is no significant increase in the overall energy consumption of US Fig. 1.5. With the current trends, the distribution grids would soon become self-sufficient to host the critical load demand during a power outage. In addition to the same,

## Power outages have risen sharply over the last decade Major power disturbances in North America



*Note: \* NERC equivalent data estimated based on the trends seen in the Eaton Blackout tracker for number of outages affecting over 50,000 people.  
Source: NERC, Eaton Blackout Tracker, Goldman Sachs Research estimates.*

Figure 1.1: Number of major outages (1992-2011)

compared to conventional power backup options, DERs (primarily PV and BESS) have a lower carbon footprint.

The organization of the chapter is as follows. Section II presents the major problems faced by critical loads. Section III presents the conventional load support approaches. Section IV discusses the clean-energy alternatives for providing power backup. Section V illustrates the effects of increasing DER interconnections on the power quality of the distribution grid. Section VI presents the additional planning challenges for DER interconnections on the distribution grid. Section VII discusses the possibilities for critical load management using DERs. Section VII summarizes the conclusion and

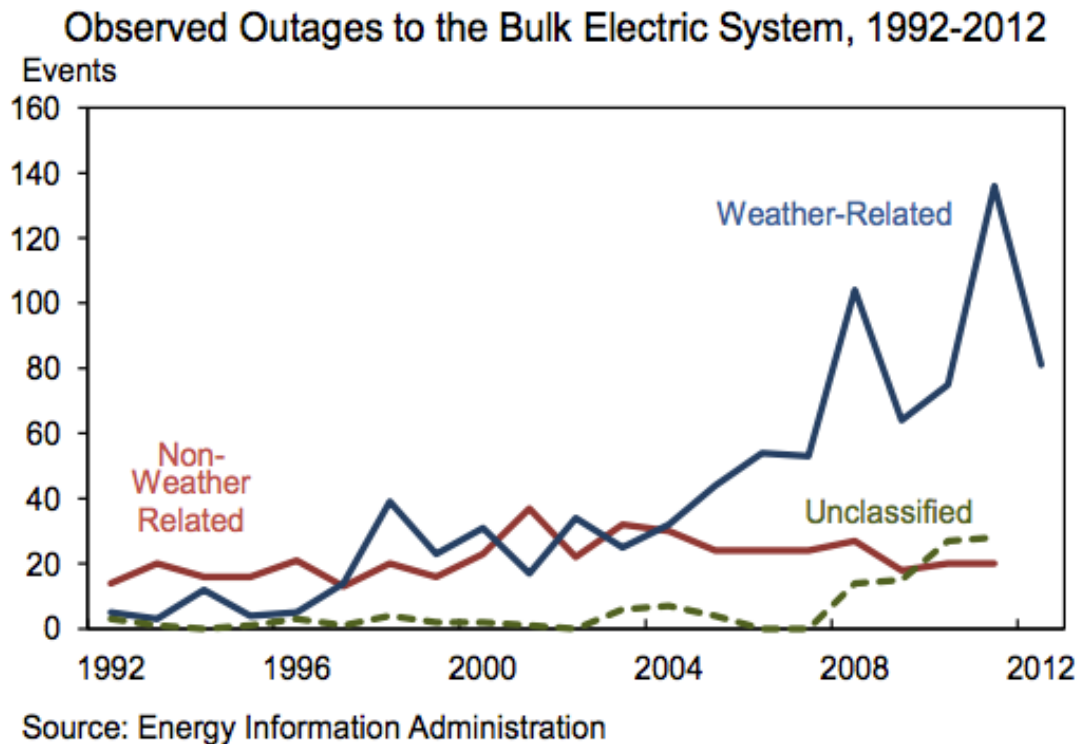


Figure 1.2: Common causes of major power outages (1992-2012)

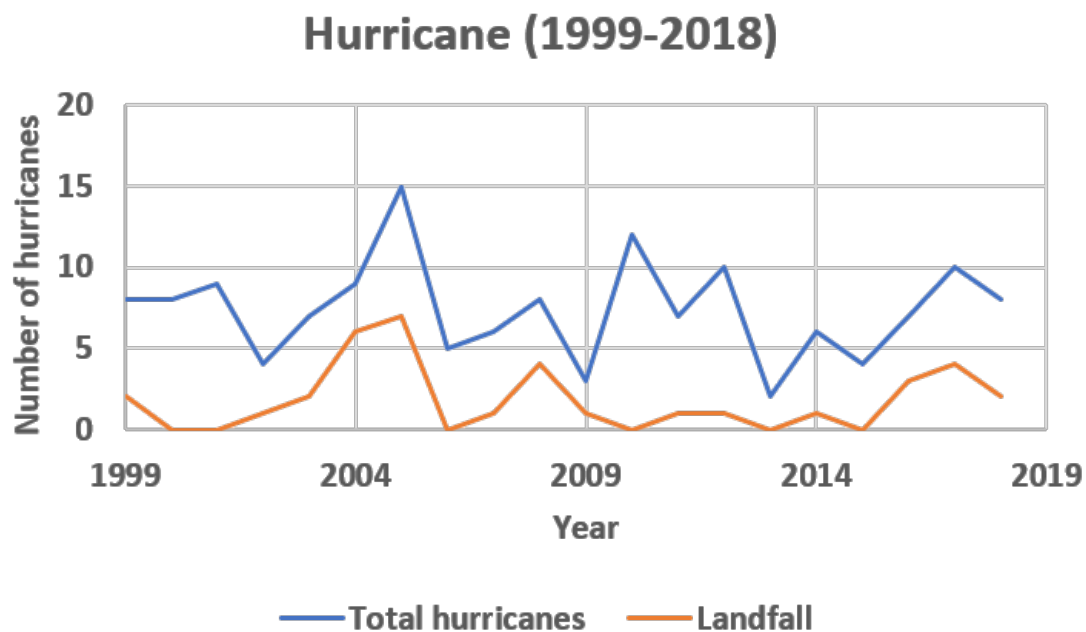


Figure 1.3: Hurricane faced by US (1999-2018)

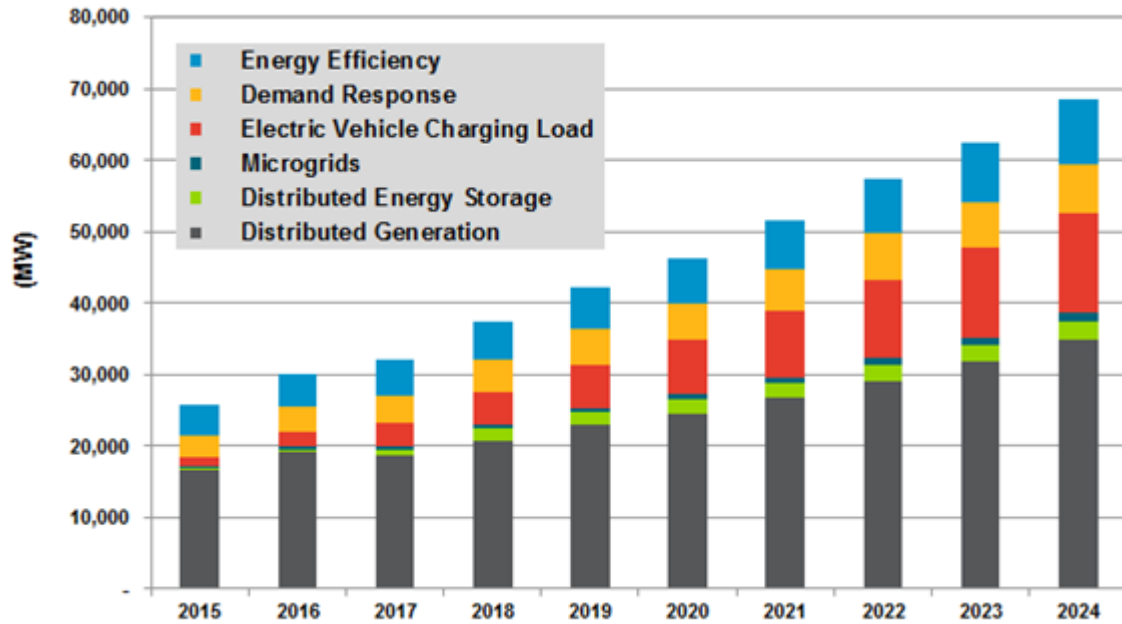


Figure 1.4: Forecasted growth of DERs

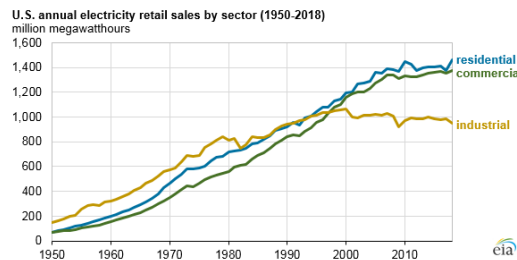


Figure 1.5: Power consumption by consumer category

future work.

## 1.1 Background and Motivation

Currently, the power grids face challenges in terms of resiliency and power quality. The increasing penetration of the renewable energy resources tied with the storage capacities provides the flexibility of controlling the generated energy and the resulting net load. Also, increasing penetration of Electric Vehicles with bi-directional charging capabilities and distributed generation may provide an opportunity to address the resiliency issues of the power grid locally. This section provides a detailed description of the challenges in terms of grid resiliency and power quality.

Table 1.1: US utility clean energy targets

Utility	Target deadline	States served
Avista	2045	WA, ID, OR
Duke Energy	2050	OH, KY, TN, NC, SC
Green Mountain Power	2025	VT
Idaho Power	2045	ID, OR
Public Service Co. of New Mexico	2040	NM
Xcel Energy	2050	MN, MI, WI, ND, SD, CO, TX, NM

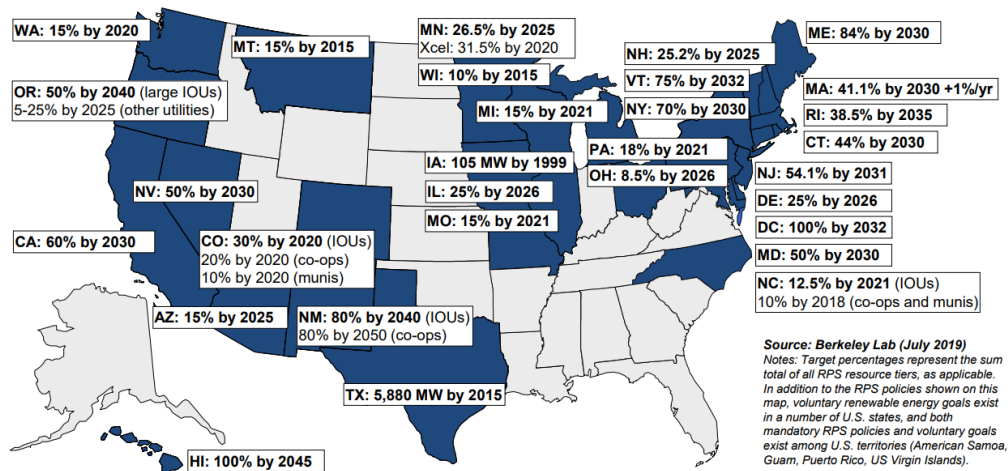


Figure 1.6: Renewable energy portfolios and goals for US states

### 1.1.1 Resiliency related challenges

Interruptions in power systems are the primary factors affecting the distribution grid resiliency. The interruptions can be broadly classified into Momentary Interruptions and Sustained Interruptions based on the duration.

#### 1.1.1.1 Momentary Interruptions

According to IEEE Std 1159 (2019) [5], a momentary interruption occurs when the supply voltage decreases to less than 0.1 pu for less than 1 min. The primary causes of interruptions in the distribution grid are power system faults, equipment failures,

transient faults, and control malfunctions. Reclosures detect and clear these faults by series of close-open operations [6]. Sensitive equipment are vulnerable to momentary faults. Induction machines can experience negative torque and transients during momentary interruptions [7]. Electronic loads are sensitive to voltage re-strikes. Voltage spikes during the restoration by reclosure can damage digital devices. Momentary interruptions of longer duration are more severe since reclosure is struggling to clear out the fault. After predefined number of reclosing operations, the reclosure opens up, and interruption becomes sustained by nature. [8].

#### 1.1.1.2 Sustained interruptions

According to IEEE Std 1159 (2019) [5], a momentary interruption occurs when the supply voltage decreases to less than 0.1 pu for less than 1 min. The primary causes of interruptions in the distribution grid are power system faults, equipment failures, transient faults, and control malfunctions. Reclosures detect and clear these faults by a series of close-open operations [6]. Sensitive equipments are vulnerable to momentary faults. Induction machines can experience negative torque and transients during momentary interruptions [7]. Electronic loads are sensitive to voltage re-strikes. Voltage spikes during the restoration by reclosure can damage digital devices. Momentary interruptions of longer duration are more severe since reclosure is struggling to clear out the fault. After a predefined number of reclosing operations, the reclosure opens up, and interruption becomes sustained by nature. [8].

Hospitals are considered to be the most critical loads. According to [9], in 2012, during the mid-Atlantic storms, around 30% of dialysis centers were impacted by power outages. REf. [10] analyzes the economic impact of power outages in the US. The overall economic impact is distributed among electricity consumers' residential, commercial, and industrial classes. Commercial loads account for the maximum economic impact of 72% because of power outages. Industrial loads account for 26% of the total economic impact, whereas residential loads account for less than 2% of the total. The

analysis, however, does not quantify the psychological and physiological impact of power outages. The study also claims that the frequency of interruptions affects the economic loss more than the duration of the interruption. The short-term/momentary interruptions account for 67%, whereas sustained interruptions contributed 33% towards the total economic loss.

### 1.1.2 Power Quality

Poor power quality is an indication of a potential power outage. Also, if the quality issues are not rectified locally before having a critical load connected to the distribution grid, it may affect the performance or even damage the sensitive loads. Power quality issues on the distribution grid can be classified into the following.

#### 1.1.2.1 Momentary voltage issues

Industrial loads are more sensitive to abnormal voltage-related problems. Failures due to such disturbances may create a high impact on production costs. Depending on the period and magnitude of voltage fluctuations, they can primarily be classified as follows.

- Sag: A voltage sag can be defined as a decrease in RMS voltage (between 0.1 to 0.9 pu) or current at the power frequency for durations from 0.5 cycles to 1 minute [5]. The voltage sags are generally caused by switching heavy load, an inrush while starting large motors, or a fault on the adjacent feeder until it is cleared, resulting in a voltage drop at the substation bus. The impact of voltage sag depends on the duration of the sag and sensitivity of the critical load on voltage sag [11]. The sensitive equipment includes adjustable speed drive controls, PLCs, motor starters, and control relays. Voltage sag is the most severe power quality problem faced by industrial customers. Voltage sag is a common reason for malfunctioning in production plants. [12]
- Swell: A voltage sag can be defined as an increase in RMS voltage (between 1.1

to 1.2 pu) or current at the power frequency for durations from 0.5 cycles to 1 minute [5]. The voltage swells are generally caused by switching off a heavy load, switching on the capacitor banks, or single phase-ground faults. Voltage swell is less severe than voltage sag because they are less common in the distribution system. The voltage swell may result in control delay, tripping, overheating and many times complete damage to electrical/electronic equipment [13].

- Flicker Flicker is a random or continuous voltage variation of voltage within the acceptable range of 0.95 to 1.05 pu [5]. As the name indicates, the human eye can perceive these voltage variations in the form of variations in lamp illumination intensity. Any load with significant periodic variations in reactive power consumption can cause voltage fluctuations. Flicker is also experienced because of high variation in DER output. IEEE Std 1453-2015 [14] discusses the standard practice for analyzing the flicker on power systems. Flicker maybe a concerning issue for critical loads using incandescent bulbs. However, with the increasing use of led/energy-efficient lighting systems, the issues concerning flicker may decrease in the future. [15].

#### 1.1.2.2 Sustained voltage issues

Regulators or tap-changing transformers and capacitors primarily provide voltage regulation at the distribution level. As per the ANSI standard, the voltage throughout the distribution grid should remain within the range of 0.95 to 1.05 pu [16]. If voltage regulating infrastructure is inadequate or malfunctioning, the violation of voltage operating limits may occur. Depending on the voltage magnitude, the voltage violation is categorized as follows-

- Overvoltage: An overvoltage is an RMS increase in ac voltage greater than 1.05 pu for a duration longer than 1 min. Overvoltage conditions are normally caused by poor distribution grid voltage regulation or mal-functioning voltage regula-

tors. Sustained overvoltage situations affect the insulation of the connected equipment. Also, the current drawn into the equipment increases resulting in additional heating of the equipment/devices. [13].

- Undervoltage: An undervoltage is an RMS decrease in ac voltage lesser than 0.95 pu for a duration longer than 1 min. Undervoltage conditions can occur in a distribution grid with high demand. This increases the current from the feeder head and the grid losses. Loads at the feeder end are more susceptible to the under-voltage scenarios because of higher voltage drop. [13]. Since the torque in the induction motor depends on the stator voltage, the loads running on the induction motor (eq. HVAC) are affected by undervoltage scenario. Prolonged undervoltage may also lead to overheating of the motor because of higher than rated current intake.

### 1.1.2.3 Frequency issues

Power frequency variations are the power system's fundamental frequency deviation from its specified nominal value (60 Hz). The steady-state power system frequency is directly related to the rotational/synchronous speed of the generators on the system. Frequency is an indicator of the power grid's balance of generation and demand. The magnitude of the frequency shift and its duration depends on the load characteristics and the response of the generation system to load changes. Small, instantaneous frequency changes occur almost continuously due to load switching, etc. These changes are limited to the local distribution zone of the grid. High variations on the power grid frequency are caused by sudden switching of significant generation sources because of fault, outage/disconnection of major load center from the power grid, and fault on a weak system. Islanded distribution systems that are relatively weak can have higher frequency variations due to low inertia. Motor loads are more sensitive to frequency variations. High-frequency variations would make the motor run faster

or slower. Hence all the applications depending on the motor rotational speed are impacted [17].

## 1.2 Research Objective

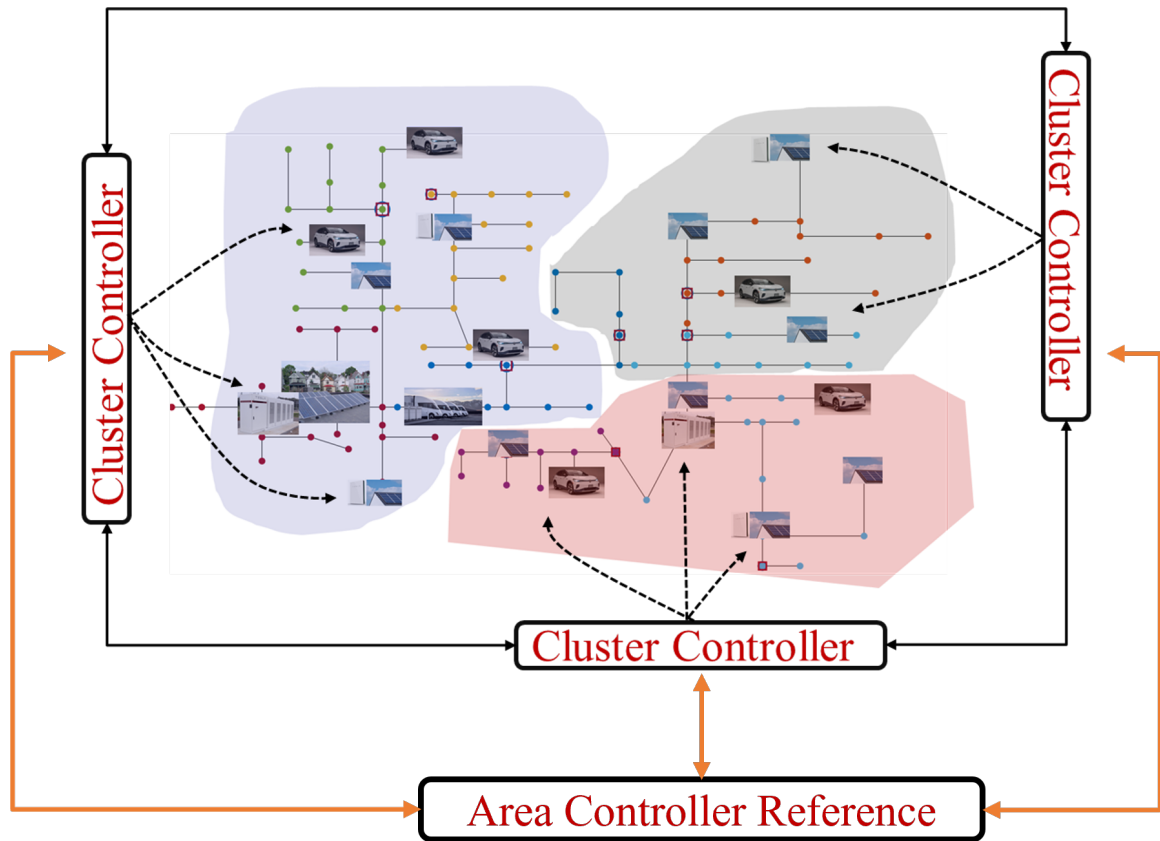


Figure 1.7: Thesis Objective

As discussed in the previous sections, increasing penetration of the distributed energy resources and storage (static or EVs) provides flexibility over the feeder net-load. This flexibility over the net load can facilitate the applications like net-load smoothing, management of thermal loading, market participation, etc through active network management. In addition, the advanced inverters with 4 quadrant operations can also provide reactive power support.

The objective of the current research work is to create clusters of load and distributed generation as shown in figure 1.8. Each cluster would represent a local

balance of load and PV generation. The clusters configurations are expected to vary dynamically depending on the load and PV generation. The research work also proposes a distributed cluster control of active and reactive power approach for net-load support applications. The final objective of the proposed approach is to demonstrate the potential of resilient operation and support of critical loads during the grid outage.

### 1.3 Research Challenges

The following research challenges are addressed in the current research:

- **Simulation environment:** To demonstrate the distribution grid management applications, 12 hours of time-series simulation is required which would capture variations in PV and load. The capability to transition from one topology to other is also helpful to demonstrate the universal adaptability of the management application. The commercially available simulation platforms capable of 24-hour simulation have the license limitation for parallel execution. Also, the flexibility of interacting with simulators during the simulation could be a challenge.
- **Clustering Approach:** The clustering of a graph is an NP-hard problem. Various graph-based clustering approaches aim to provide the approximate solution for graph partitioning.
- **Distributed Control:** The concept of distributed control is popular among the transmission grid management for the voltage and frequency control based on the generator coherency. Multiple approaches have been adopted to calculate the solution of power-flow problems through distributed optimization techniques. However, no significant work has been done on managing distribution grids through distributed controls.

## 1.4 Research Approach

Following approaches were adopted to address the research challenges mentioned above:

- **Co-simulation Environment Development:** The distribution grid with DERs is modelled in OpenDSS. The OpenDSS platform, being an open-source platform, does not limit the number of parallel executions. Also, extensive Common Object Model (COM) based APIs are available for automation and external control of the simulation platform. Hence, the python APIs are leveraged to develop two parallel co-simulating instances of OpenDSS.
  1. **Grid Simulator Instance:** This process simulates the distribution grid at 1s time interval. The irradiance and load profiles are separated for different zones on the distribution grid to emulate the difference in PV generation and load consumption pattern. At every 5 second time interval, the measurements from each device are captured in the JSON format and sent to the controller through a TCP channel.
  2. **Controller Instance:** The controller instance is an independent process co-simulating with the simulator. The measurements received from the simulator are used to run an OpenDSS based power-flow at every 3 minute time interval. The control modules are designed to operate at a resolution between 5 seconds and 1 minute. The controller module calculates the set-points for each DER and sends them to the simulator through the TCP channel.
- **Clustering Approach:** An improved two-layer spectral clustering approach is developed to accurately identify the naturally occurring islands with a balance of DER generation and the load on the distribution grid. Chapter 3 discusses the approach in detail.
- **Distributed Control:** The research proposes a distributed control approach to

calculate the active and reactive power set-points for the power balance and voltage management purposes at very clusters. The efficiency of the approach is demonstrated for multiple applications: Net-load smoothing, Net-load minimization, and External Set-point tracking.

### 1.5 Thesis Flowchart

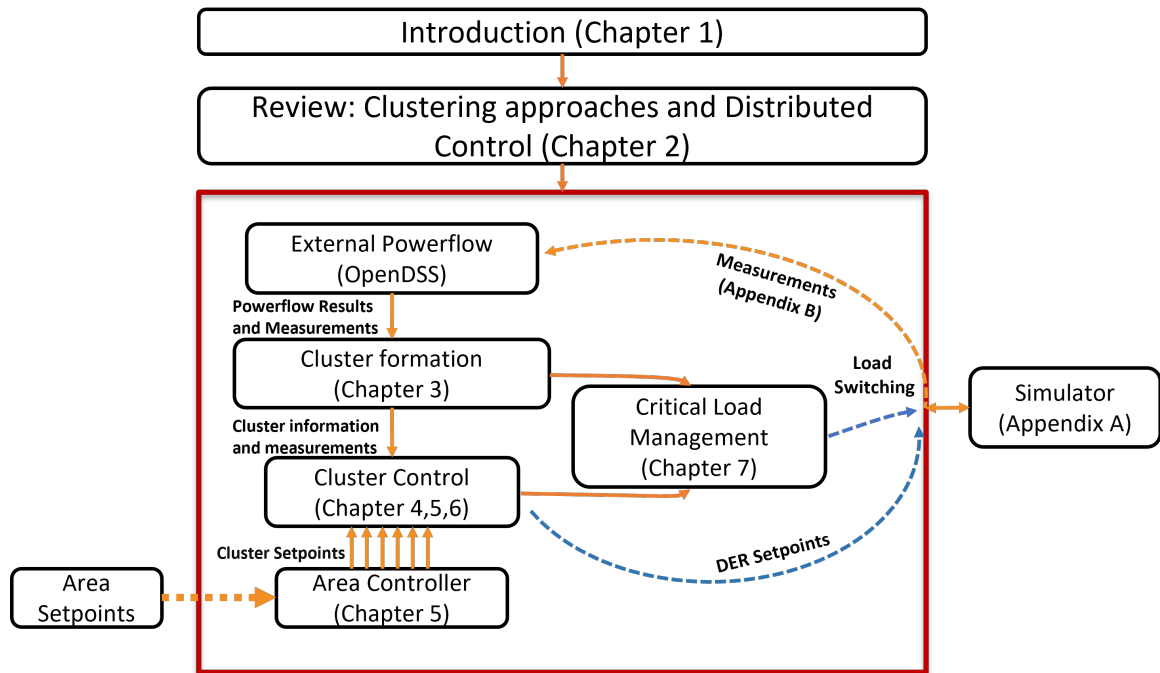


Figure 1.8: Thesis flowchart

- Chapter 2 reviews the clustering methodologies and distributed optimization approach and their application on the power grid.
- Chapter 3 discuss the development of a two-layer spectral clustering approach for active power flow-based clusters for active power management and reactive power sensitivity-based clusters for the voltage management on the distribution grid.
- Chapter 4 proposes the least square-based optimization techniques for controlling active power and reactive power at each cluster for the smoothing applica-

tion. Chapter 5 proposes the ADMM based cluster SOC-based power-sharing approach for each cluster to meet the substation's overall goal/set points. The approach is demonstrated for the feeder net-load minimization and feeder head set-point tracking applications.

- Chapter 6 proposes model predictive control of cluster DERs. An ADMM based transfer function generation approach is also proposed for accurately estimating the model and state of the clusters based on the measurements.
- Chapter 7 proposes an approach for critical load management and demonstrates the cluster control architecture for increasing the distribution grid resiliency.

## CHAPTER 2: Literature review on clustering, distributed optimization and control

### 2.1 Introduction

As discussed in Chapter 1, the objective of the current research is to cluster the distribution grid based on the load and PV generation and coordinate the control among the clusters to meet the required goals (local and global). Hence, the current chapter extensively reviews the clustering and distributed optimization techniques currently used for power system applications.

### 2.2 Review: Clustering

#### 2.2.1 Kernel based Clustering

- Method: Kernel based clustering is performed through non-linear mapping of data in the feature space. The relation among the data points is established through one of the kernel approaches- Polynomial kernels, Guassian Kernals, Sigmoid Kernel, etc. Once the data-points are projected in the feature space, the clustering is performed using the linear clustering approaches such as K-means, SOM (Self organizing maps), SVDD (Support Vector Domain Description), Fuzzy C-Means, etc. The kernel based clustering approaches are efficient in separating the cluster overlaps. Also, the prior knowledge of data topology is not required. However, the relations between the data-points is highly sensitivity to the kernel values. The issue of sensitivity to Gaussian kernel values is addressed in the current research work.
- Method: Power-system Application: Intentional Islanding [18], Multi-Machine Equivalence [19], Bad data detection [20]

### 2.2.2 Swarm Intelligence based Clustering

- Method: Swarm intelligence approaches are inspired from the biological behaviours of the swarm. The swarm techniques are developed to solve the optimization problems. The swarm based algorithms are initialized by generating the set of random solutions within the search space. Based on the fitness of the solutions, the velocity and the direction of the swarm particles are then updated till the optimum solutions are determined. The approach leverages the conventional clustering approaches like k-means to determine the fitness of each agent vector. The clustering approach typically has high time complexity because of higher number of iterations. Particle swarm optimization, Ant Colony Optimization and Shuffled frog leaping algorithms are adopted for the clustering purposes.
- Method: Power-system Application: Security assessment in power systems so1, Coherency detection [21]

### 2.2.3 Density Based Clustering

- Method: Here the clusters are formed based on the density of the data points. The area with relatively higher density of the data points forms a cluster. DBSCAN is the widely adopted approach for the density based clustering. OPTICS overcomes the shortfalls of the DBSCAN approach: Sensitivity to radius and minimum data-points in the neighbourhood area [22]. The density based clustering approach are memory intensive for larger data-sets.
- Power-system Application: Electricity theft detection [23], Generator Coherency detection [24]

### 2.2.4 Spatial Clustering

- Method: The spatial clustering approaches are one of the widely adopted approaches for grouping of the data based on the feature similarities. The approaches can also be used along with the other clustering approaches to achieve the clustering objective. For example, k-means is used in graph partitioning as well as kernel based clustering. Few of the most used spatial clustering approaches are K-means, K-medoids, DBSCAN, CLARANS, Wavecluster, etc
- Power-system Application: Fault location identification [25], Bad data detection [26], Forecasting [27] [28], reactive power management [29]

### 2.2.5 Hierarchical Clustering

- Method: Hierarchical clustering techniques are among the widely used techniques for clustering. The clustering approaches are divided into two categories: Agglomerative and Divisive. IN Agglomerative clustering, each data point is initialized as an individual cluster and merged with the most similar data-point. The process is repeated till all data points are grouped into one cluster. The process flow of clustering is reverse in Divisive approach. Dendogram is generally used to represent the cluster hierarchy. Commonly used agglomerative clustering approaches are BIRCH (Balanced Iterative Recursive and Clustering using Hierarchies), CURE (Clustering Using Representatives) and ROCK (Robust Clustering Using Links).
- Power system application: Grouping of generators [30], Distance based power-grid partitioning [31], optimal PMU placement [32], power quality analysis [33]

### 2.2.6 Graph Theory Based Clustering

- Method: The graph based clustering approaches identifies the boundaries of the clusters characterized by the lowest similarity. If the data-set is not represented

as a graph, similarity indexes (ex. Gaussian similarity index) is used to assign the branch weights and connect the data points. Spectral clustering approach is one of the widely used approach for the graph clustering. Current research work discusses in detail of the application of spectral clustering for partitioning the distribution grid based on active power flow and reactive power sensitivity. Few of the other graph clustering approaches are Markov Clustering, Nearest Neighbour clustering, Minimum spanning tree, and CLICK [34].

- Power system application: Power grid partitioning [35] [36], islanding application [37], powergrid restoration [38]

## 2.3 Review: Distributed optimization

### 2.3.1 Analytical Target Cascading

- Method: This approach was originally developed to translate the system level design objectives to the design specifications of the components. It follows a hierarchical structure to achieve the overall target. [39] proposes the non-hierarchical structure for solving the problem. The optimization problem is split into multiple sub-problems. The variables are shared among the parent and children sub-problems. The coupling among the sub-problems is modelled as a penalty function. Here, a central coordinator is required to manage the distributed computations.
- Power system application: Unit Commitment [40], Optimal Power Flow [41]
- Pros: Guaranteed convergence for the convex problems

### 2.3.2 Auxiliary Problem Principle

- Method: The approach decomposes the problem into sub-problems. The sub-problems are connected to the adjacent sub-problems through shared variables. This sub-problems are solved sequentially or in parallel [42]. An augmented

Lagrangian ensures the consistency among the sub-problems from the adjacent regions.

- Power system application: Optimal powerflow [43] [44]
- Pros: Guaranteed convergence for the convex problems

### 2.3.3 Optimality Condition Decomposition

- Method: Every sub-objective functions are assigned a primal and dual variable. Every agent performs optimization only on it's assigned variables. The remaining variables are fixed while an agent is solving for it's objective function. Upon solving, the agent shares it's updated variables with the neighbouring agents. The approach is decentralized and does not require a central coordinator. The method is further modified to Heterogeneous Decomposition Algorithm where the agents are regarded as the difference computational units sharing the boundary information.
- Power system application: Distributed MPC for storage and generation dispatch [45] [46], voltage management [47], Dynamic Economic dispatch [48], Economic dispatch of coupled TD system (Heterogeneous Decomposition (HGD) algorithm) [49]
- Pros: Low computational time, applicable to real time systems and control, parallel computation capability.

### 2.3.4 Dual decomposition

- Method: Dual decomposition approach dates back to 1960s [50]. The method is based on Dual Ascent algorithm and is a precursor to the ADMM. If the objective is separable into sub-objectives, the sub-objectives are solved in parallel at the beginning of each iteration. Then the residue for each sub-objectives is

gathered for the computation of the dual variable. The dual variable is then broadcasted to each sub-objectives for the next iteration. Here, a central coordinator is required for the calculation of dual variable at the end of each iteration.

- Power system application: Large-Scale Power Balancing [51], OPF [52], MPC based building energy management [53], vehicle energy management [54], Electric vehicles charging [55]
- Pros: Classical and widely adopted approach.
- Cons: Does not guarantee the convergence.

### 2.3.5 Consensus+Innovation

- Method: The Consensus+Innovation approach performs distributed optimization based on KKT conditions. Here an agent exchanges the information with the neighbouring agents. Hence a central coordinator is not required and computation is completely distributed in nature. An agent may represent a single node or a cluster of nodes for the scalability of the approach. The convergence of the approach is further improved by establishing the communication between the non-connected areas [56].
- Power system application: Micro-grid Coordination [57], DC-OPF [58] [56], State Estimation and Energy Management [59]
- Pros: Good convergence, Less computations required per entity, Facilitates parallel computations.

### 2.3.6 Alternating direction method of multiplier

- Method: The ADMM approach solves the optimization problem by decomposing it into smaller sub-problems. At each iteration, the local objectives of the

sub-problems are solved in parallel and the updated local variables are shared to solve for the global variable. The ADMM approach has combined advantage of dual decomposition and augmented Lagrangian methods for constrained optimization. Since the approach needs a central coordinator, the ADMM is not fully decentralized. The approach is further modified through proximal message passing to achieve full decentralization. Current research work adopts the ADMM based distributed optimization for consensus and sharing applications.

- Power system application: Distributed OPF [60] [61], Coordination and Control of PV and storage [62], Micro-grid energy management [63].
- Pros: Simple implementation, Robust, Flexibility in adoption for different problem types.

## CHAPTER 3: New Method for Grouping Distributed Energy Resources to support Power Distribution System

### 3.1 Introduction-Spectral Clustering

In the modern grid, distributed generators (DGs) are playing a vital role in fulfilling the increasing demand [64]. An increasing number of controllable devices and flexible generation assets on the distribution grid would increase the scale and thereby the complexity of distribution grid level control and optimization [65]. Also, the load distribution, as well as the variation, is not uniform in the distribution grids. Hence, the centralized control for all the flexible assets may not be efficient and optimal and often a distributed control approach is adopted by creating the virtual clusters of the distribution grid and assigning the zones of control to the groups of DERs. Power grids partitioning has a wide spectrum of applications. In planning and analysis of the power grids, the partitioning is used in network reduction and parallel processing of the grid partitions. Ref. [66–68] discusses the network partitioning based on the generator coherency to improve the reliability of the network and [69] and [70] proposes the use of network clustering to restart the power grid zones in from a blackout scenario.

In the distribution grids, the clustering methods have been primarily applied to identify the micro-grids during grid contingencies for an islanded operation [71] [72]. Since a power network can be modeled as a graph, various graph-based methods can be applied for the partitioning. Hierarchical and spectral based clustering approaches are the commonly used approaches of power grid clustering [73]. Even though the approach is very effective, the results of the spectral clustering are an approximate solution and may not ensure the minimum k-way partition of a graph. In addition

to that, the spectral clustering clusters' results are often found to be discontinuous. The issues of discontinuity and non-optimum cut are not addressed in the literature. Ref. [66] proposes the pre-processing and post-processing approaches to improve the cluster quality and remove the discontinuities. However, considering the iterative nature of these approaches, the application in real-time applications of a larger distribution network may not be feasible.

### 3.1.1 Algorithm

Spectral clustering is a graph-based partitioning algorithm treating the data points as graph nodes and partitions the graph based on the weight of the connections among the graph nodes [74] [75] [76]. In this approach, the distribution grid can be modeled as an undirected graph  $G = (V, E)$ . The vertex ( $V$ ) of the graph represents the network buses and the edges ( $E$ ) represent the connections among the vertices. The weight ( $w$ ) of an edge is any physical parameter on which the clustering has to be performed. It represents the "strength" of the connection between the vertices. In this chapter, we represent weights as an active power flow through power distribution lines. For an edge with  $N_p$  phases, the equivalent weight is

$$w_{ij} = \sum_{n=1}^{N_p} P_{ij}(n) \quad (3.1)$$

Further, for a graph with  $N$  vertices, the adjacency matrix ( $A$ ) can be formulated as an  $N \times N$  matrix such that,  $A(i, j) = 0$ , if vertex  $i$  and  $j$  are not connected and  $A(i, j) = w_{ij}$ , if vertex  $i$  and  $j$  are connected. The degree of a vertex is defined as the sum of weights of all edges connecting with the vertex. The "degree matrix"  $D$  is defined as a diagonal matrix representing the degree of all the vertices  $d_1, d_2, d_3, \dots, d_N$  in a graph with  $N$  vertices. For  $m$  edges connected through a common vertex  $i$ , the

degree of a vertex  $i$  is represented as

$$d_i = \sum_{j=1}^N w_{ij} \quad (3.2)$$

Based on the  $A$  and  $D$  matrices, the Laplacian matrix  $L$  is defined and normalized as follows [77].

$$L = D - A \quad L_n = D^{-\frac{1}{2}} L D^{-\frac{1}{2}} \quad (3.3)$$

The Laplacian matrix, both normalized and un-normalized, is symmetric and positive semi-definite. The eigenvalues of  $L_n$  are  $0 = \lambda_1 \leq \lambda_2 \leq \lambda_3 \leq \dots \leq \lambda_N \leq 2$ . For un-normalized Laplacian, there is no definite upper bound value. For the required number of clusters  $k$ , the first  $k$  eigenvectors  $(v_1, v_2, \dots, v_k)$  are calculated. These eigenvectors are then normalized to unit length as  $u_i = \frac{v_k}{\|v_k\|}$ . Each row  $i$  of the normalized matrix is an individual point in  $k$  dimensional Euclidean space and corresponds to the  $i^{th}$  vertex of the system. These points in the spectral embedding are clustered using vector quantization approaches like K-means or K-medoids. Both the K-means and K-medoids algorithms are partitional (breaking the data set up into groups). K-means attempts to minimize the total squared error, while K-medoids minimizes the sum of dissimilarities between points labeled to be in a cluster and a point designated as the center of that cluster. The major component in the spectral clustering process is the clustering of eigen vectors points in the  $k^{th}$  dimensional euclidean space using a vector quantization method. In the spectral embedding, the vertices of an edge with lower weights are more separated compared to the vertices connected with higher weights. The K-means and K-medoids are the widely accepted methods used to identify these gaps representing the weak connection between the vertices in the spectral embedding. It has been observed that this approach injects discontinuity in cluster formation.

### 3.2 Evaluation of the cluster quality

The quality of clusters is assessed based on three main factors a) individual cluster quality b) overall cluster quality and, c) the factors affecting the cluster quality. Each of these is discussed in the next subsections.

#### 3.2.1 Quality of individual clusters

- Volume: The volume of a cluster indicates the sum of weights for all connections within the clusters. For an active power flow based clusters, the volume represents the total power flow through all the lines within the cluster. A larger volume represents the higher interconnection or higher power flow through the lines within the clusters. Volume can be expressed as

$$vol(s) = \sum_{i,j \in s}^n P_{ij}(t). \quad (3.4)$$

- Cut: The cut or boundary of a cluster indicates the sum of weights of all the tie-lines connecting the cluster with the adjacent clusters. For active power-based clustering, the boundary value for a cluster indicates the dependency of the cluster on the adjacent clusters for the power exchanges where the lower value of the boundary indicating the balance between the demand and generation within the cluster.

$$cut(s) = \sum_{i \in s, j \notin s}^n P_{ij}(t) \quad (3.5)$$

- Expansion: The expansion of a cluster is a ratio of cut over the volume of the respective cluster. The lower expansion represents a better clustering quality. From a distribution grid's perspective, the lower expansion represents either or both of higher power flow within the cluster and lower power exchanges with

the adjacent cluster.

$$\phi(s) = \frac{cut(s)}{vol(s)} \quad (3.6)$$

### 3.2.2 Quality of overall cluster formations

- Ncut: Normalized cut or Ncut gives the measure of the overall partitioning quality by taking the sum of expansion  $\phi(s)$  for all clusters. Since the Ncut value increases with an increase in the number of clusters, the average Ncut ( $Ncut_k$ ) is used in our work. This can be expressed as

$$Ncut_k = \frac{1}{k} \sum_{s=1}^k \frac{cut(s)}{vol(s)} \quad (3.7)$$

- Maximum expansion: The expansion or  $\phi(k)$  represents the individual cluster quality of the  $k^{th}$  cluster. The lower value of the  $\phi(k)$  is an indicator of the good cluster quality. The maximum expansion correlates the overall clustering quality with respect to the quality of the worst of the  $k$  clusters.

$$\phi(max) = maximum(\phi(1), \phi(2), \dots, \phi(k)) \quad (3.8)$$

- Discontinuity: The clustering of the graph nodes using K-means and K-medoids results in the discontinuity of the clusters [78]. This is more visible while clustering the distribution power grids with low interconnections. In our work, a discontinuity flag (1 or 0) is used to indicate the clustering discontinuity for any particular instances.
- Cluster size ratio: Lower expansion of the cluster can be obtained either by lowered boundary value or higher size of the clusters. Hence the cluster size ratio, represented by the ratio of the number of nodes in smallest cluster ( $N^s$ ) with respect to the largest cluster ( $N^l$ ), is used to represent the balance between

the smallest and largest cluster given as

$$R(k) = \frac{N^s}{N^l} \quad (3.9)$$

### 3.2.3 Factors affecting the cluster quality

- Laplacian normalization: Normalized Laplacian helps in better approximation for minimizing the Ncut. Upon normalization, the off-diagonal elements of the original Laplacian matrix ( $L$ ) can be written as

$$L_n(i, j) = \frac{L(i, j)}{\sqrt{(D_i * D_j)}} \quad (3.10)$$

An example of a feeder-end power flow snapshot with and without normalization of Laplacian is shown in Fig. 3.1. The  $P$  is the actual active power flow which can be seen decreasing while moving from node number 105 to nodes 111, 107, and 114. This is expected there is only one generating source (a PV farm). However, the normalized power flow values represented by  $Pn$  does-not follow the same trend since the normalization is performed with the total power flowing through the connecting nodes as shown in (3.10). Normalization helps in avoiding un-wanted cluster cuts near the feeder-end where the magnitude of power-flow is small and thereby improving the size ratio. Fig. 3.2 shows the improvement with normalization in the size ratio for 1000 active power-flow based clustering instances.

- Number of clusters ( $k$ ): Spectral clustering provides an approximate clustering of a graph which numerically is an NP hard problem. The closeness of an approximate clustering solution to an optimum solution is represented by Cheeger inequality [79] where  $\rho_g$  is the minimum of maximum expansion  $\phi(max)$ . Based on the inference derived from Cheeger inequality [80], the relative eigengap for

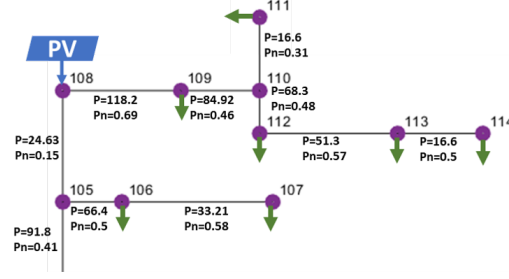


Figure 3.1: Edge weights with and without Laplacian normalization.

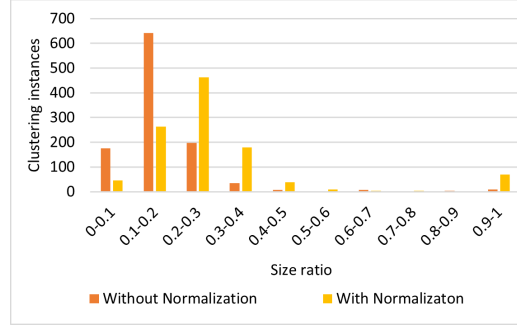


Figure 3.2: Effect of normalization on the size ratio of the clusters.

optimum number of clusters can be found. Highest value of  $\lambda_k^g$  indicates the optimal clustering into  $k$  islands so can  $k$  be defined as optimum number of clusters. This can be considered as  $\frac{\lambda}{2} \leq \rho_g \leq \sqrt{(2\lambda)}$ .  $\lambda_k^g = \frac{\lambda_{k+1} - \lambda_k}{\lambda_k}$ , and  $k_{opt} = index(max(\lambda_k^g))$ . On running the spectral clustering over the normalized Laplacian for  $k_{opt}$  clusters, considerable improvement in the clustering quality has been observed. To illustrate this a clustering algorithm was performed over

Table 3.1: Effect of optimal  $k$  on the clustering quality

Quality Parameter	Random $k \in \{2, 10\}$	$k_{opt} \in \{2, 10\}$
Ncut	0.14	0.06
Maximum expansion	0.32	0.12
Discontinuities for every 10 clustering instances	2.27	0.25
Size Ratio	0.295	0.31

120 snapshots of power flow scenarios and compared against the 120 clustering scenarios with optimum  $k$  clusters obtained using the relative eigengap, with  $k$

ranging from 2 to 10. The summary of the analysis is presented in Table 3.1.

### 3.3 Active power flow based clustering of distribution grids

The spectral clustering approach proposed in section is used to identify the clusters in the distribution system. The clusters are characterised by the local generation feeding the active power to the local loads with the lower power exchange between the adjacent clusters. Since the grid condition dynamically changes, the cluster configuration and count also dynamically changes. For example, if the DERs within the particular clusters are cut-off because of cyber-physical issues, the re-clustering of the distribution grid would merge the deficient cluster with the nearby clusters. Hence, the spectral clustering approach is required to identify the optimal number and the configuration of the clusters.

#### 3.3.1 Drawback of the conventional spectral clustering approach

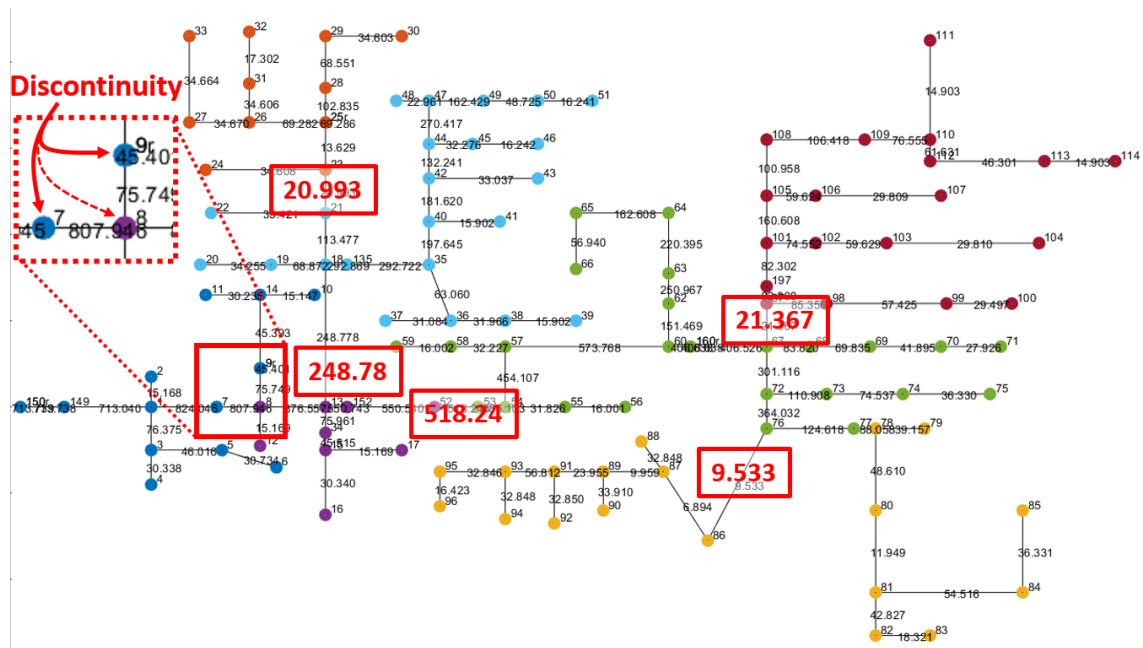


Figure 3.3: Clustering of 123 bus system with Kmeans eigenvector clustering.

Figure 3.3 shows the output of conventional spectral clustering approach when applied over a snapshot of grid condition. The optimal number of cluster ( $k$ ) was

identified from the relative eigen gap heuristics. However the cluster configuration suffers from the following drawbacks:

1. Discontinuity: As shown in the figure, the nodes 7 and 9 belongs to the same cluster. However they are separated at node 8. The discontinuity in the cluster configuration may not be desirable for the cluster control approaches. The discontinuity among the clusters is by the kmeans clustering of the eigen vectors. Discontinuity occurs because the points 7,8 and 9 are close to each other because of lower weight of the branch connecting nodes 8 and 9. Hence, the centroid of corresponding to "blue" cluster is closer to point 9 causing the discontinuity among the "blue" cluster.
2. Non optimal cluster boundaries: The power flowing from "indigo" cluster and "green" cluster is 518 kW. This issue is caused by the non-linear nature of the normalized eigen vector space. Figure 3.4 shows the points corresponding to each nodes in the eigen vector space for a set of 100 nodes connected sequentially to each other and having same branch weight. It can be noted that the distance among the eigen vector points at the corresponding to the middle of the graph is greater compared to the remaining points and thereby increasing the probability of the cluster cuts at the middle of the graph. Additional post processing is required here to merge the non-optimal cluster configuration.
3. Sub-optimal cluster cuts: The major component in the spectral clustering process is the clustering of eigenvectors points in the  $k^{th}$  dimensional euclidean space using a vector quantization method. In the spectral embedding, the vertices of an edge with lower weights are more separated compared to the vertices connected with higher weights. The K-means and K-medoids are the widely accepted methods used to identify these gaps representing the weak connection between the vertices in the spectral embedding. It can be illustrated that these

methods are based on balancing the total distance of points from each cluster with respect to the centroid. Hence, they may not always be efficient in identifying the gaps as clustering as the vector quantization methods may fail to identify the distribution lines with the lowest weights. To illustrate this, an example clustering process is explained. In this example, 123 data points are connected with edges having weight=1. As one of the edge weights is changed to 0.4, a weak connection can be visually seen as a gap between the eigenvector points. In active power-based clustering of the distribution grid, these dips in the edge weight would indicate the downstream DERs supporting the local loads in that area. By accurately identifying these dips in the active power flow, the local zones where the DERs are supporting the loads in the distribution network can be established. For both K-means and K-medoids methods, the total distance of all points in blue cluster and orange cluster to their respective centroids is balanced. Hence, the traditional approaches fail to identify these gaps while forming the clusters.

All the three drawbacks can be resolved if the distance between the eigen vector points in spectral clustering can be re-scaled while keeping the node-connectivity information in the spectral embedding intact. Since Kmeans is unable to retain the graph connectivity information in the spectral embedding, another layer of spectral clustering is proposed by establishing the relation among the nodes in the eigen-vector space.

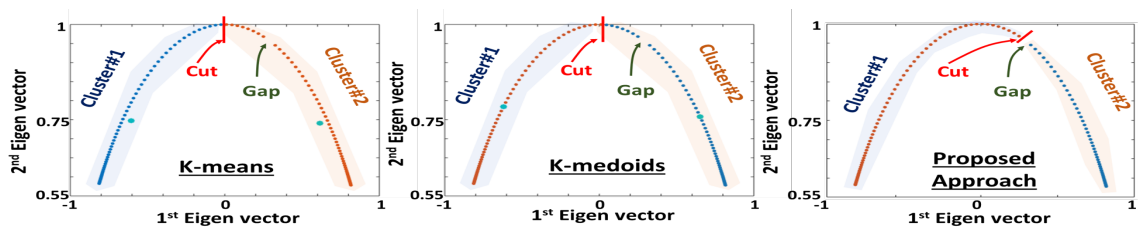


Figure 3.4: Eigenvector clustering using Kmeans, K-medoids, and the proposed approach. Remove the proposed approach plot

### 3.4 Proposed Approach: Two Layer Spectral Clustering

The proposed approach of two-level spectral clustering uses the information regarding the distance among the eigenvectors points in spectral embedding and their actual connectivity from the graph of distribution grid to perform spectral clustering of the eigenvector points. The proposed approach is summarized in the Fig. 3.5. In this approach, normalized Laplacian of the active power flowing through the distribution grid is used. Since the optimum number for the clusters identified from relative eigengap ensures the better clustering quality,  $k$  is determined using optimal conditions discussed earlier. Based on the distance between the eigenvector points in the spectral embedding and connectivity information from the graph, a similarity index is calculated using a Gaussian similarity index presented as

$$S(i, j) = e^{-\left(\frac{Dist(i, j)}{\sigma}\right)^2} \quad (3.11)$$

$$S'(i, j) = \begin{cases} e^{-\left(\frac{Dist(i, j) - \mu}{2\sigma}\right)^2}, & \text{for } Dist(i, j) > \mu \\ 1, & \text{for } Dist(i, j) \leq \mu \end{cases} \quad (3.12)$$

where  $\sigma$  is Gaussian kernel which helps in scaling the similarity index values between 1 and 0. With  $\sigma \rightarrow 0, S \rightarrow 0$  and  $\sigma \rightarrow \infty, S \rightarrow 1$ . Hence, a properly tuned value of sigma is required to distribute the similarity index between 0 and 1. Hence, the Gaussian similarity function is converted to normal distribution function represented in (3.12). Here,  $\mu$  is the average of the distances and  $\sigma$  is the variance of all the distances between the connecting eigenvector points.

The major component in the spectral clustering process is the clustering of eigenvectors points in the  $k^{th}$  dimensional euclidean space using a vector quantization method. In the spectral embedding, the vertices of an edge with lower weights are more separated compared to the vertices connected with higher weights. The K-means

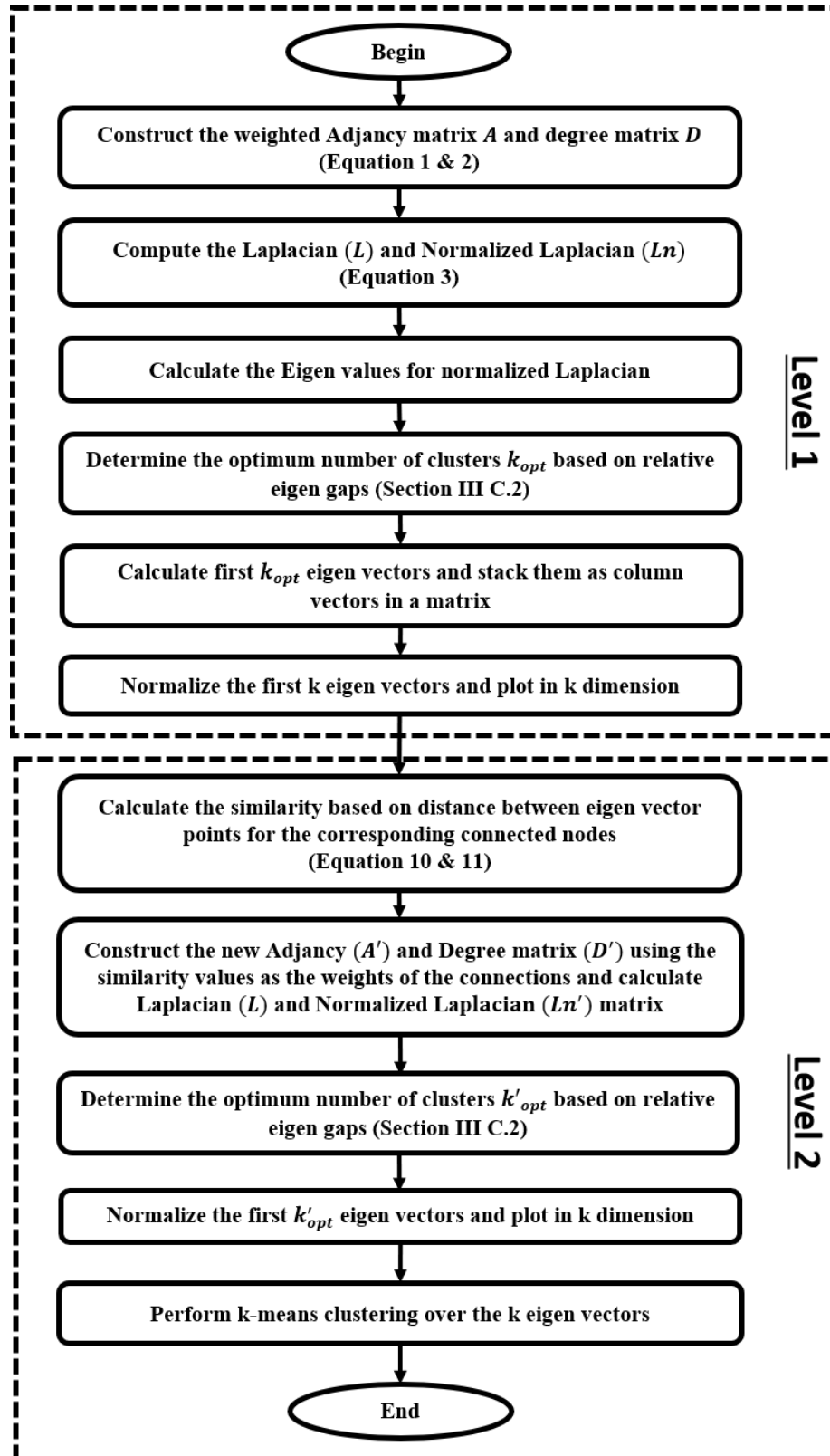


Figure 3.5: Flowchart: Proposed approach- 2 level spectral clustering.

and K-medoids are the widely accepted methods used to identify these gaps representing the weak connection between the vertices in the spectral embedding. It can be illustrated that these methods may not always be efficient in identifying the gaps as clustering as the vector quantization methods may fail to identify the distribution lines with the lowest weights. To illustrate this, an example clustering process is explained. In this example, 123 data points are connected with edges having weight=1. As one of the edge weight is changed to 0.4, a weak connection can be visually seen as a gap between the eigenvector points. In active power-based clustering of the distribution grid, these dip in the edge weight would indicate the downstream DERs supporting the local loads in that area. By accurately identifying these dips in the active power flow, the local zones where the DERs are supporting the loads in the distribution network can be established. Both K-means and K-medoids method fails to identify these gap while forming the clusters. Next, the spectral clustering using the proposed approach was performed for the same example. Fig. 3.4 illustrates the comparisons. It can be seen that with the proposed approach the cut happens at the gap indicating that cluster cut is happening optimally at the branch with the lowest weight. It is worth noting that the number of points is the same for this analysis and the ratio is similar. This illustration explains the advantages of the proposed approach.

#### 3.4.1 Preliminary Study

Figure 3.6 shows the additional cases with the second layer of the spectral clustering. Table 3.2 summarizes the 5 cases identified to evaluate the clustering quality. Case 1 and 2 are the conventional spectral clustering use cases for the bench-marking the results from case 3, 4 5. The use cases were evaluated on IEEE 123 bus system with 15 DERs for 600 powerflow snapshots for total clusters ( $k$ ) ranging from 2 to 6. The quality of cluster configurations are quantified in terms of discontinuities (3.7), NCut(3.8), Maximum expansion (3.9) and size ratio (3.11). The maximum boundary

Table 3.2: Spectral clustering cases

	Case 1	Case 2	Case 3	Case 4	Case 5
Eigen Vector Clustering	Kmeans	Kmeans	Spectral	Spectral	Spectral
Laplacian Type (First Layer)	Un-normalized	Normalized	Un-normalized	Normalized	Normalized
Laplacian Type (Second Layer)	-	-	Un-normalized	Un-normalized	Normalized

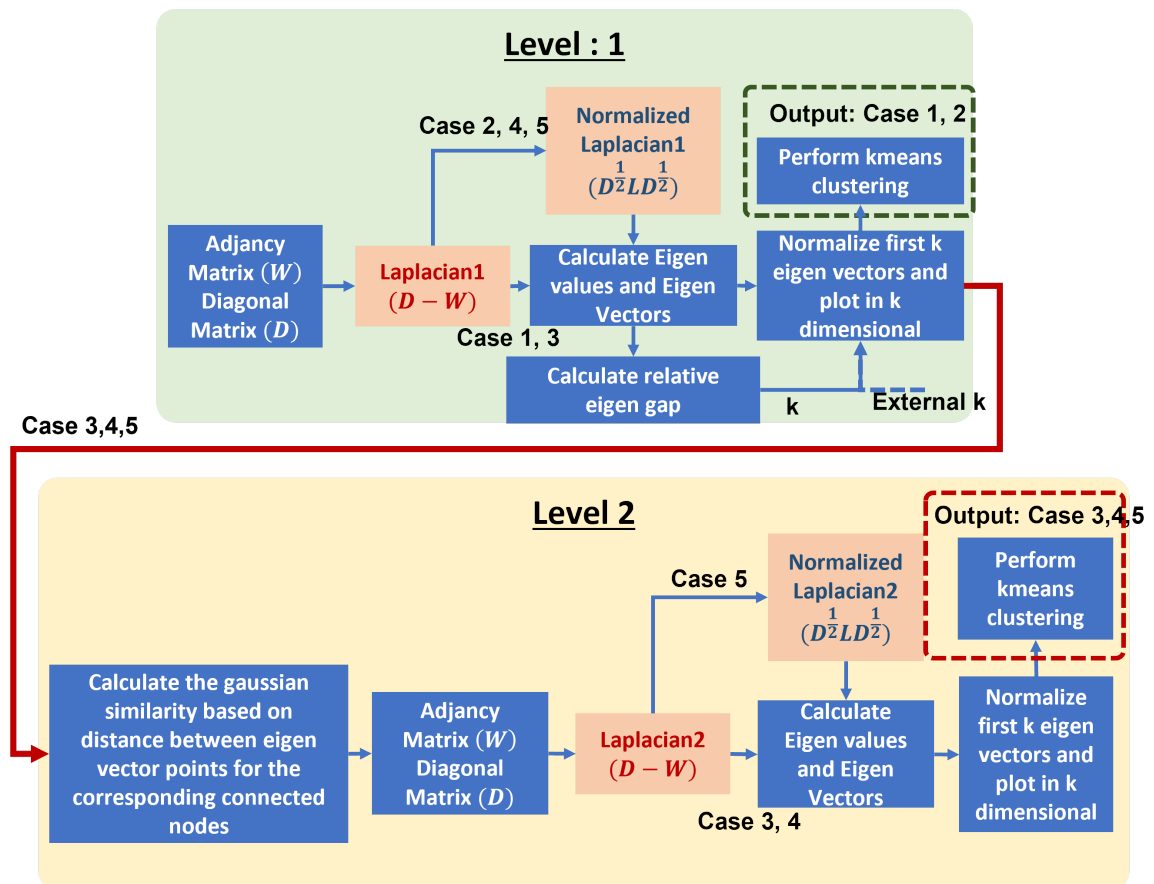


Figure 3.6: Effect of normalization on the size ratio of the clusters.

powerflow for the cluster configuration (3.10) is also analysed to relate the NCut and the Size ratios.

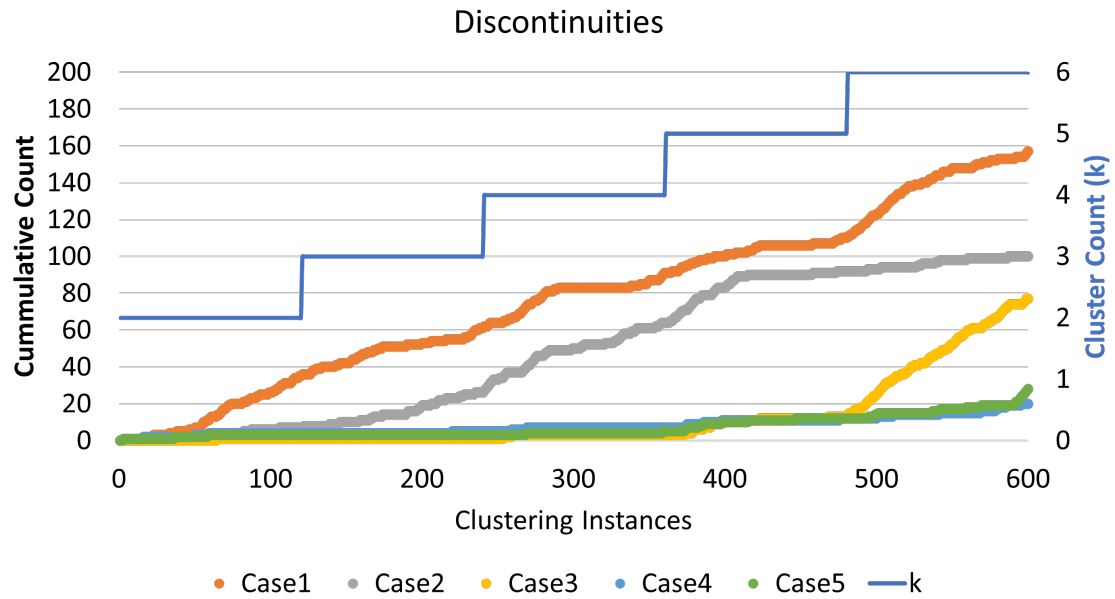


Figure 3.7: Cumulative count of discontinuities in the cluster configuration for 600 power-flow snapshots with varying  $k$  requirements

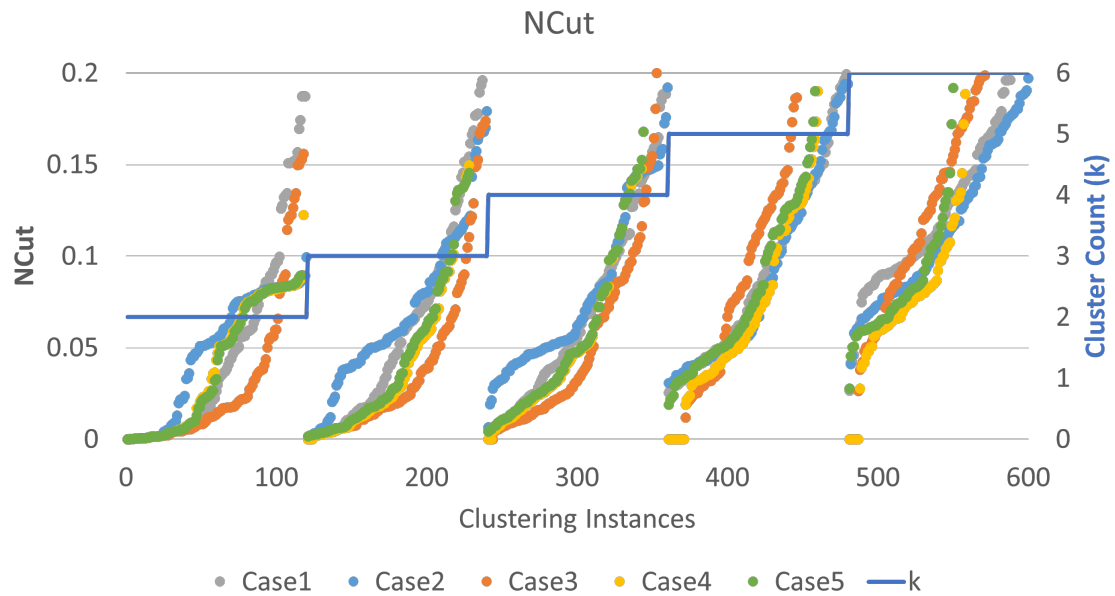


Figure 3.8: Variations in the NCut for 600 power-flow snapshots with varying  $k$  requirements

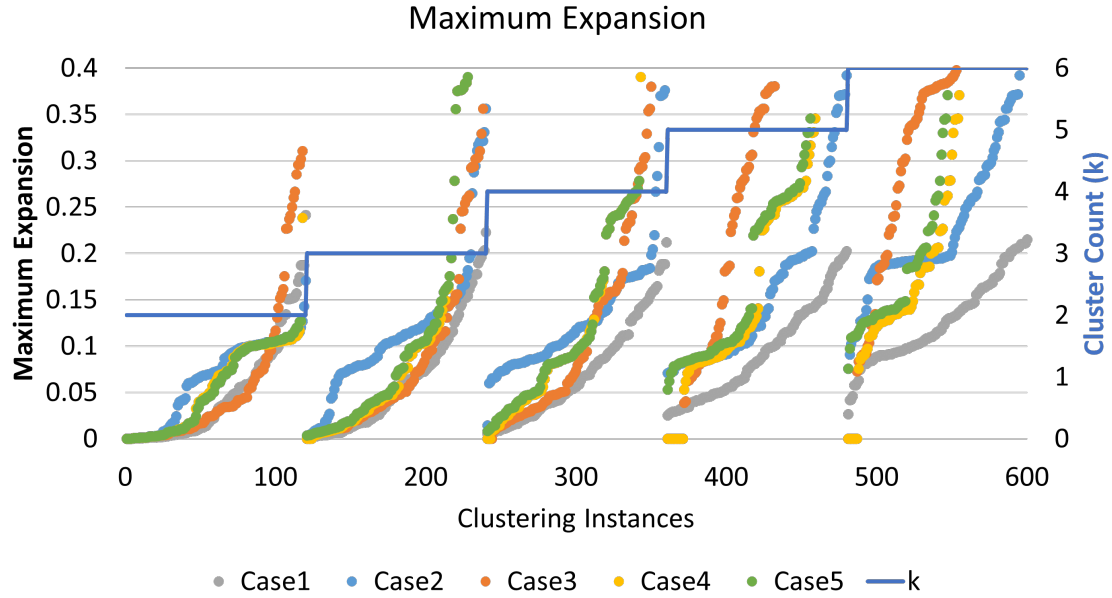


Figure 3.9: Variations in the maximum expansion for 600 power-flow snapshots with varying  $k$  requirements

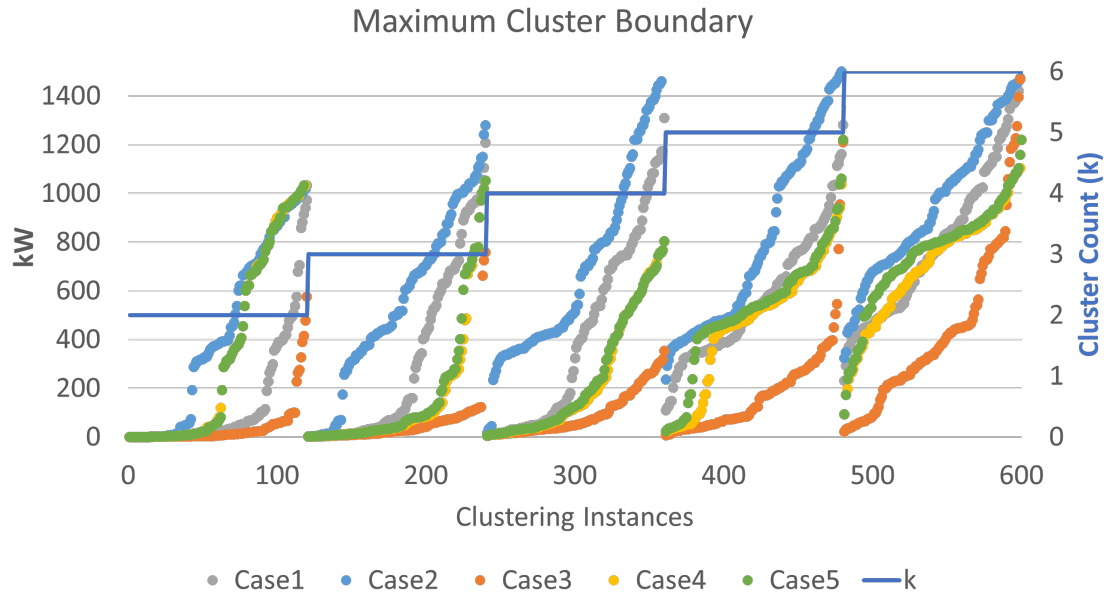


Figure 3.10: Variations in the boundary powerflow for 600 power-flow snapshots with varying  $k$  requirements

- Case 1: Conventional spectral clustering approach without the normalization of the laplacian

Conventional spectral clustering without normalization is based on actual pow-

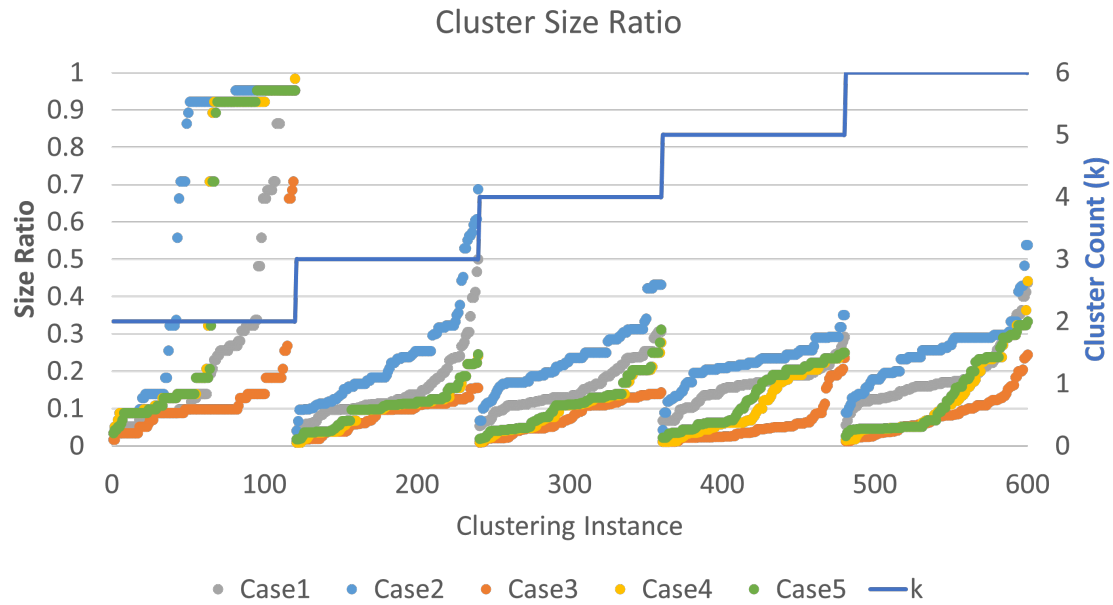


Figure 3.11: Effect of normalization on the size ratio of the clusters.

erflows through the grid. The discontinuities in the cluster configurations are the highest among all the cases analysed (Figure 3.7). Hence this case is not desirable for the realtime clustering and control applications.

- Case 2 Conventional spectral clustering approach with the normalized laplacian  
The normalization of the laplacian reduces the discontinuities among the cluster configuration as compared to case 1. However, the count of overall discontinuities is still considerably higher compared to other cases. Also, the clustering configurations are not always optimal. Figure 3.10 shows the high power flowing though the cluster boundaries. Hence, this case is not suitable for the cluster load balancing applications.
- Case 3 represents the conventional spectral clustering approach with the unnormalized laplacian at both levels  
The discontinuities decreases by 50% with the second level of spectral clustering. Also the boundary powerflow is the lowest for this case. However, the cluster size ratio is extremely low indicating huge difference among the cluster

sizes. Hence, the possibilities of not having any controllable DER asset within the clusters are higher and hence the approach is not adopted for the cluster and control application.

- Case 4: Two layer spectral clustering approach with the normalized laplacian in the first layer and non normalized laplacian in the second layer A significant improvement in terms of cluster configurations is observed for this case. The discontinuities decreases by 81%. Also the NCut and maximum expansion values are lower for this case.
- Case 5: Two layer spectral clustering approach with the normalized laplacian at the second layer

Case 4 and Case 5 are almost comparable in terms of clustering quality (Discontinuities, NCut and boundary powerflow). However, the the size ratio is comparatively higher then case 5. Hence, the case 5 is adopted for the active power based clustering of the distribution system.

### 3.5 Voltage sensitivity based clustering of distribution system

Previous approach discusses the active power flow based clustering of the distribution grids. With the increasing adoption of 4 quadrant inverters, the volt=var based reactive power control is gaining the traction. By performing the clustering of the distribution grids based on the reactive power to voltage sentivity, the voltage of the distrubution grids can be localized. This section proposes an approach to identify the sensitivity based virtual cluster of the distribution grid.

### 3.6 Sensitivity based spectral clustering

This design is based on the assumption that measurements available only at legacy device controller such as a) capacitors, b) transformers, and c) regulators. Also we are assuming that measurements are available on all DERs, a) PhotoVoltaic (PV) and b) Battery Energy Storage (BESS). It will be beneficial that we have measurements

for critical loads even though it is not mandatory. For the voltage sensitivity based clustering, first the sensitivity matrix is calculated. The sensitivity matrix is defined as the inverse of power grid Jacobian. The steps for the sensitivity based clustering are as follows:

- For every time instant when the sensitivity based clustering is performed, first the Jacobian is calculated as follows. For the Jacobian calculation, the power grid model with the current status is used. First, with the loads disconnected the power flow is performed. Then the load  $Y$  bus and the voltages is used to prepare the  $\mathbf{J}$  submatrices.

$$\mathbf{J}_{2nx2n} = \frac{d\mathbf{f}}{d\mathbf{x}} = \begin{bmatrix} \frac{\partial \mathbf{f}}{\partial x_1} & \cdots & \frac{\partial \mathbf{f}}{\partial x_n} \end{bmatrix} = \begin{bmatrix} \frac{\partial f_1}{\partial x_1} & \cdots & \frac{\partial f_1}{\partial x_n} \\ \vdots & \ddots & \vdots \\ \frac{\partial f_m}{\partial x_1} & \cdots & \frac{\partial f_m}{\partial x_n} \end{bmatrix} \quad (3.13)$$

This can be expressed as

$$\begin{bmatrix} \mathbf{J}_{1x1} & \cdots & \mathbf{J}_{1xn} \\ \vdots & \ddots & \vdots \\ \mathbf{J}_{nx1} & \cdots & \mathbf{J}_{n xn} \end{bmatrix} = \begin{bmatrix} \mathbf{J1}_{n \times m} & \mathbf{J2}_{m \times n} \\ \mathbf{J3}_{n \times m} & \mathbf{J4}_{m \times n} \end{bmatrix} \quad (3.14)$$

- With this, the reactive power sensitivity can be written as

$$\mathbf{S}_{n \times n} = \begin{bmatrix} \mathbf{J1}_{n \times m} & \mathbf{J2}_{m \times n} \\ \mathbf{J3}_{n \times m} & \mathbf{J4}_{m \times n} \end{bmatrix}^{-1} \quad (3.15)$$

where

$$\mathbf{S4}_{m \times n} = \left[ \mathbf{J4}_{m \times n} \right]^{-1} = \left[ \frac{\partial \mathbf{V}}{\partial Q} \right]$$

Assuming  $n$  nodes and  $m$  DERs on the distribution system:  $\mathbf{S4}_{m \times n}$  can be

defined as

$$\begin{bmatrix} \mathbf{S}_{(\text{DER}_{1,1})} & \cdots & \mathbf{S}_{(\text{DER}_{1,m})} \\ \vdots & \ddots & \vdots \\ \mathbf{S}_{(\text{DER}_{n,1})} & \cdots & \mathbf{S}_{(\text{DER}_{n,m})} \end{bmatrix}$$

- Further, based on active power dispatch from each DER available reactive power  $Q$  for each DER can be calculated as  $Q_m = \sqrt{S^2 - P_{set}^2}$ .
- Thus, maximum voltage support limit at each node on the system can be calculated as

$$\begin{bmatrix} dv_1^u \\ \vdots \\ dv_n^u \end{bmatrix} = \begin{bmatrix} \mathbf{S}_{(\text{DER}_{1,1})} & \cdots & \mathbf{S}_{(\text{DER}_{1,m})} \\ \vdots & \ddots & \vdots \\ \mathbf{S}_{(\text{DER}_{n,1})} & \cdots & \mathbf{S}_{(\text{DER}_{n,m})} \end{bmatrix}^T * \begin{bmatrix} Q_1 \\ \vdots \\ Q_m \end{bmatrix} \quad (3.16)$$

- Every node has value of the maximum available voltage support limit. For the nodes connected by the distribution lines, the branch weight can be calculated based on Gaussian Similarity index:(3.17)

$$W_{ij} = \exp\left(-\frac{\|dv_i^u - dv_j^u\|^2}{2\sigma^2}\right) \quad (3.17)$$

where  $dv_i^u$  and  $dv_j^u$  are upper limits of voltages on the bus  $i$  and  $j$  respectively,  $\sigma$  is the variance.

- The sensitivity to available reactive power, unlike power-flow, increases towards the downstream of the feeder. Equation 3.17 assigns weights between 0 and 1 to all branches based on the variation in  $dv^u$ . For nodes with similar  $dv^u$  values, the weights are assigned as 1. The weights are 0 for higher difference in the  $dv^u$  values among the connected nodes. The lower  $dv^u$  values indicate a potential cut for the clusters. For IEEE 123 node system, 30% nodes with potential cuts are identified. Two layer spectral clustering may yield larger number of small sensitivity based clusters. Such cluster configuration is not

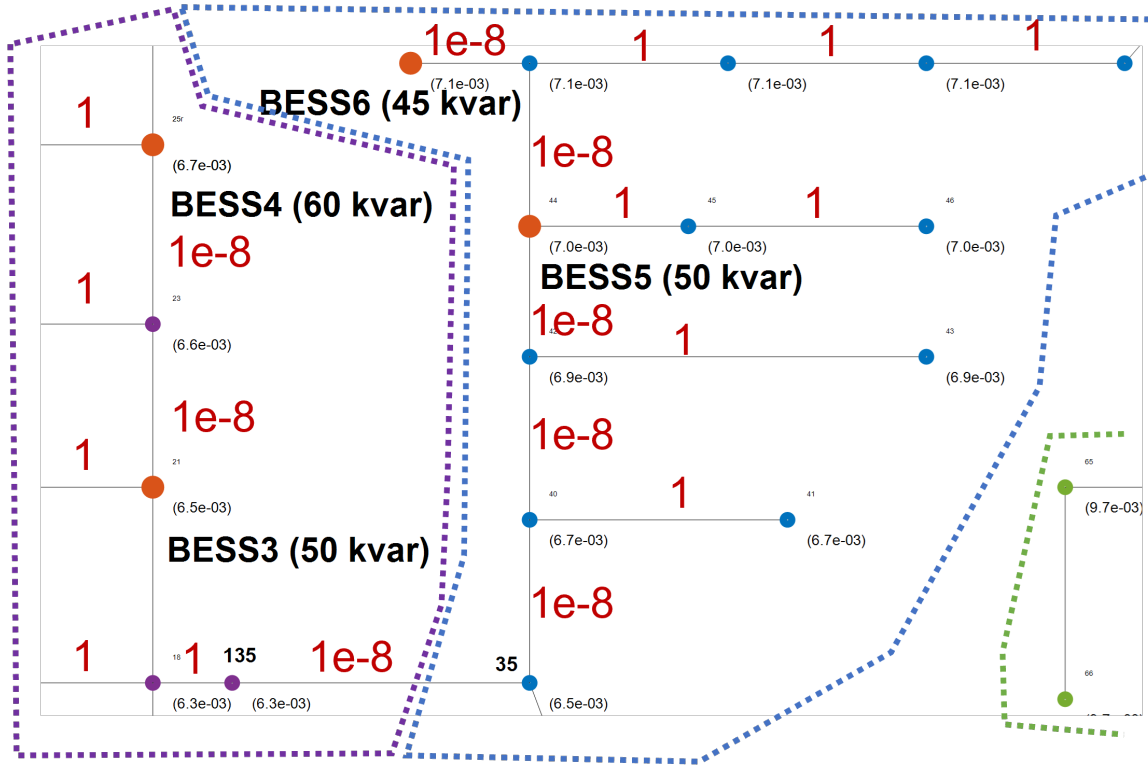


Figure 3.12: Typical reactive power sensitivity based cluster on distribution system

desirable for reactive power control as it may create hunting of controls among multiple clusters. Hence, the conventional clustering approach is adopted here. The ideal cluster for reactive power control has more number of nodes, multiple DERs and cluster cut characterized by at-least one of the following:

- New branch
- Larger distribution line length or higher distribution line impedance
- Difference in the reactive power availability of reactive power support

### 3.7 Implementation of the proposed approach

The proposed approach of active power and sensitivity based spectral clustering was implemented on IEEE 123 bus system with 15 PV and Battery Energy Storage Systems (BESS). Figure 3.13 shows the architecture for online clustering of distri-

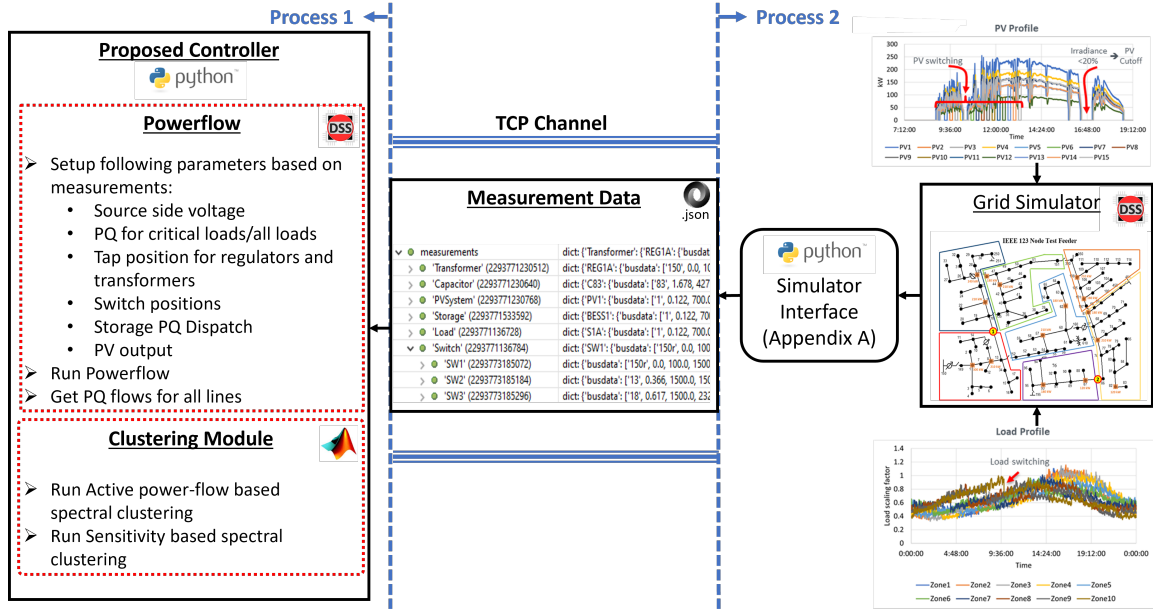


Figure 3.13: Co-simulation of cluster formation module and grid simulator

tribution grids based on the measurements. IEEE 123 bus system with 15 DERs is modelled in OpenDSS simulator. The ratings and locations of the PV and BESS are summarized in Table. 3.3. The locations and ratings of PVs were assumed based on the local loads connected in the respective areas of the feeder. Considering the futuristic scenario of distribution feeders with high PV interconnections, the total PV penetration was assumed to 80% of the total load on the feeder. The BESS  $kW$  ratings are assumed to be 25% of the connected PVs at the same node. The simulator is configured to run at 1s time interval in time-series mode. The load and PV profiles is also shown in 3.13. The measurements from grid simulator are logged in form of JSON file and transmitted to the cluster controller at every 5 second time interval through TCP channel. The detailed JSON structure for each device category is shown in Appendix B.

### 3.7.1 Result and Discussion: Active Power-flow based clusters.

The load and PV variation for 6 hours was captured in a total of 120 power flow scenarios at an interval of 3 minutes. The performance of clustering algorithms was

Table 3.3: Locations and ratings of DERs on IEEE 123 bus system

PV Rating	BESS Rating	NodeIDs
120 kW	30kW/120kWh	82, 87
180 kW	45kW/135kWh	48, 62, 93, 97, 101
210 kW	50kW/150kWh	8, 21,44, 57, 72, 108
240 kW	60kW/180kWh	25
300 kW	75kW/225kWh	1

evaluated based on the quality parameters explained in section 3.2.3. First, the two-level clustering approach presented in this chapter is compared with conventional K-means eigenvector based spectral clustering. Fig. 3.3 shows the conventional K-means eigenvector based spectral clustering scenario over a snapshot of the distribution power flow. The spectral clustering for the "8" clusters (the value of  $k_{opt}$  for the normalized Laplacian is 8) shows the discontinuity within the *blue* cluster. The power flowing through the lines connecting each cluster is also indicated. Similarly 3.14 shows the proposed approach. It can be seen that there is no discontinuity for the proposed approach as the eigengaps are amplified based on the proposed similarity index. Also, it can be seen that the power flowing through the lines connecting each cluster is the same or less when compared to conventional approach.

Table 3.4: Improvement of the proposed approach on cluster quality

Quality Parameter	Spectral clustering	Proposed approach	Improvement
Ncut	0.06	0.029	51.67%
Maximum expansion	0.12	0.051	57.5%
Discontinuities for every 10 clustering instances	0.25	0	100%
Size Ratio	0.31	0.24	-22.6%

The performance of the proposed approach against the conventional spectral clustering approach is summarized in Table 3.4. It can be seen that the proposed architecture improves the quality of the cluster. Fig. 3.15 and 3.16 compares the Ncut and maximum expansion values for 120 powerflow instances. These values are sorted

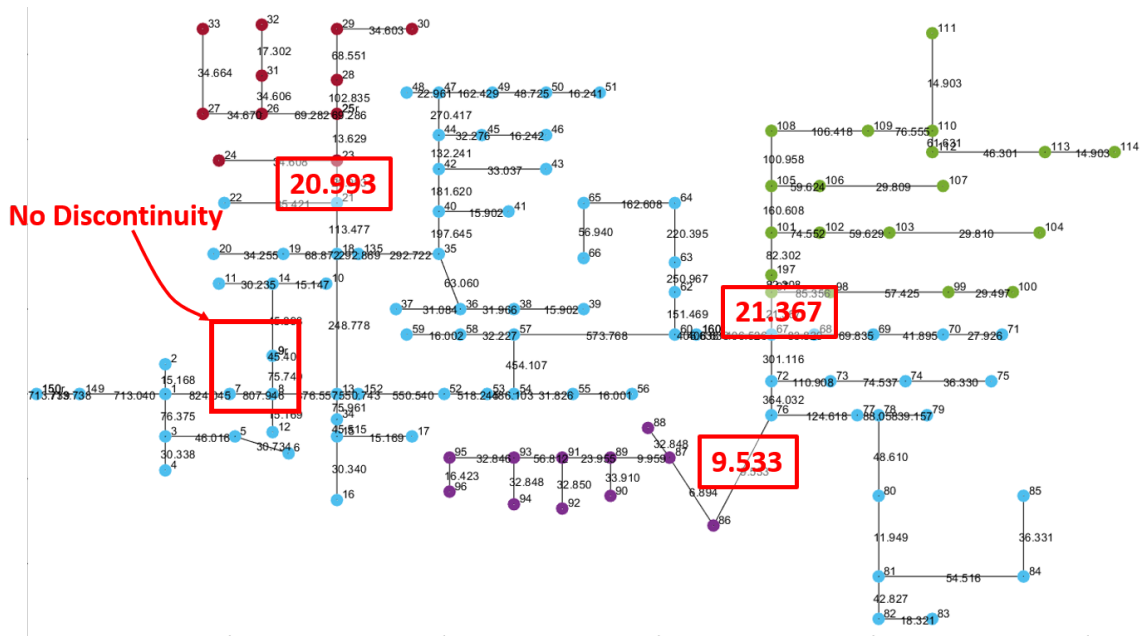


Figure 3.14: Clustering of 123 bus system with the proposed approach.

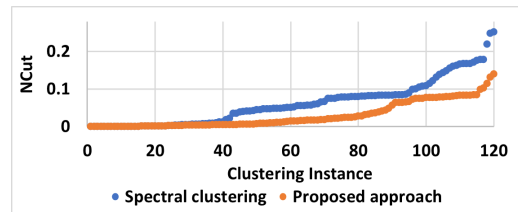


Figure 3.15: Ncut for 120 instances of IEEE 123 bus system.

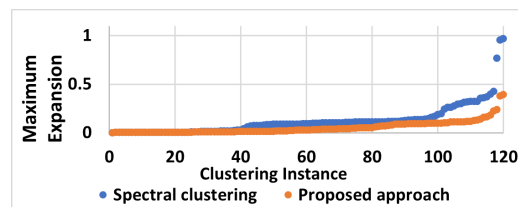


Figure 3.16: Maximum expansion for 120 instances of IEEE 123 bus system.

in ascending order to improve the plot visibility. The improvement in the Ncut and Maximum expansion values comes against the reduction in the size ratio. It was also found that the size ratio is reduced. This is expected as the total number of cluster was changing to reduce the edge powerflow. It is also observed that the major advantage of the proposed approach lies in the improvement brought on the aspect of the cluster discontinuities and reduction in the edge powerflow.

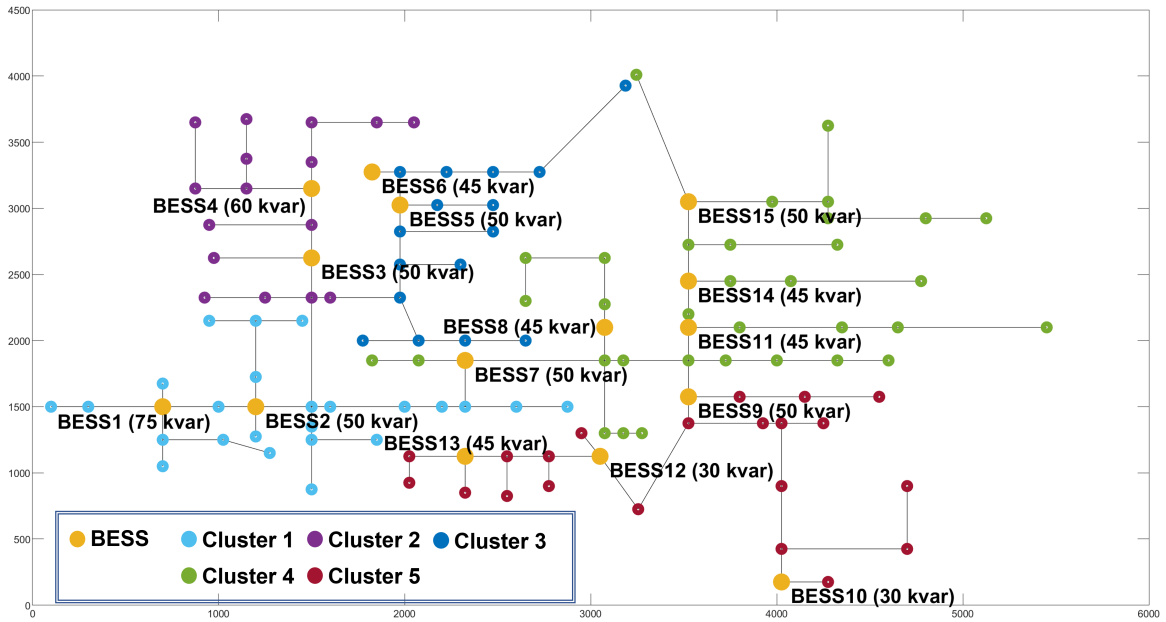


Figure 3.17: Reactive power clusters for full availability of reactive power at each DERs

### 3.7.2 Result and Discussion: Sensitivity based clusters.

The sensitivity based clusters are constructed based on the available reactive power at each BESS. Current implementation does not implement active or reactive power control through BESS. Hence, all the availability of reactive power is equal to the rates kVA of the BESS inverters. Figure 3.17 shows 5 sensitivity based cluster configuration for complete availability of the reactive power at each DER. The configuration is not expected to change in the absence of reactive power at each BESS (Figure 3.18). In this case, the cluster represents the cuts at the lines with higher impedance. The dynamic changes in the cluster configuration is based on the availability of the reactive power at every BESS. Based on the variation on the available reactive power at each BESS, figure 3.19 to figure 3.22 demonstrates the variation in cluster configuration.

- Case 1: Figure 3.19 shows a scenario where BESS 3 and BESS 4 do not have any reactive power available for the support. Here, the cluster 2 merges with cluster 3 for the voltage support from BESS 5 and BESS 6.

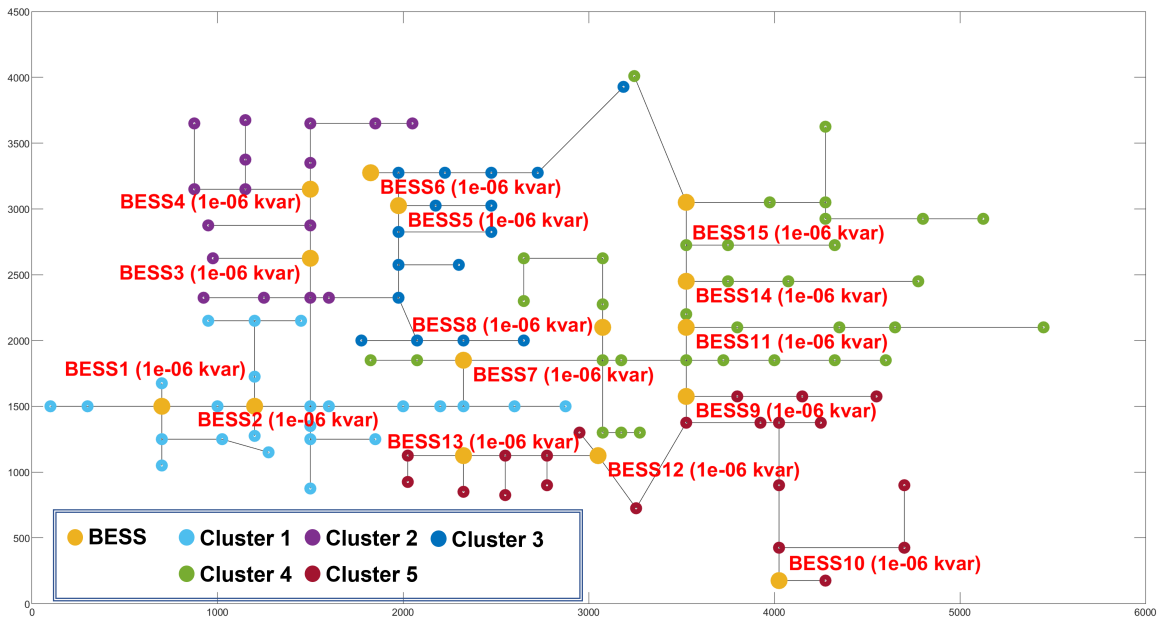


Figure 3.18: Reactive power clusters for no availability of reactive power at each DERs

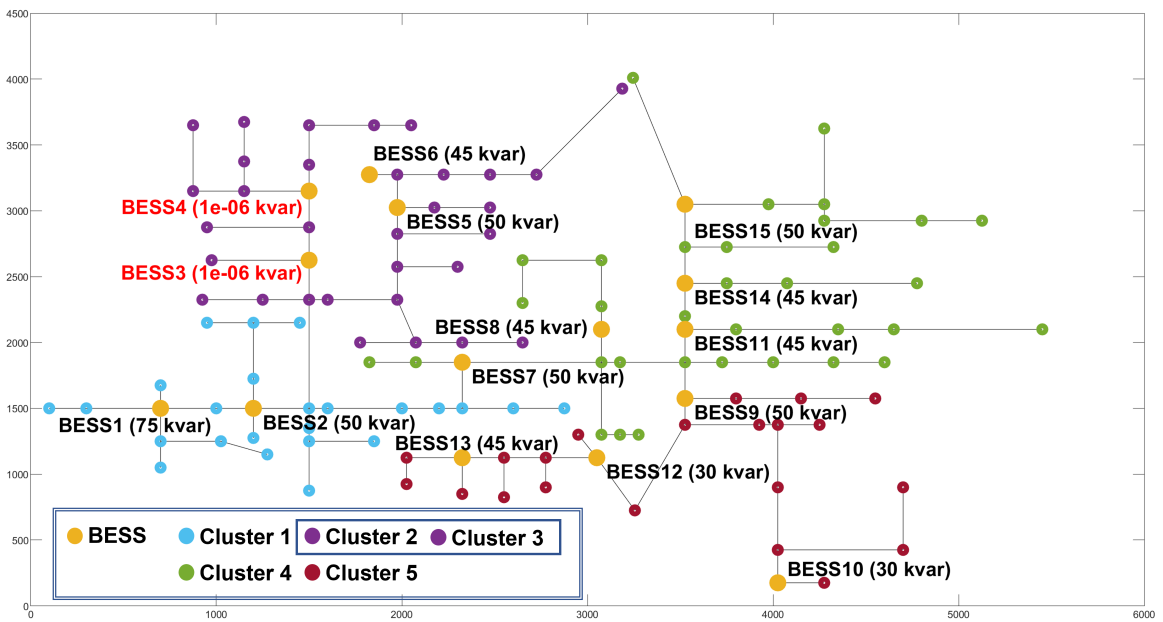


Figure 3.19: Reactive power clusters for availability of reactive power at BESS 3 and BESS 4

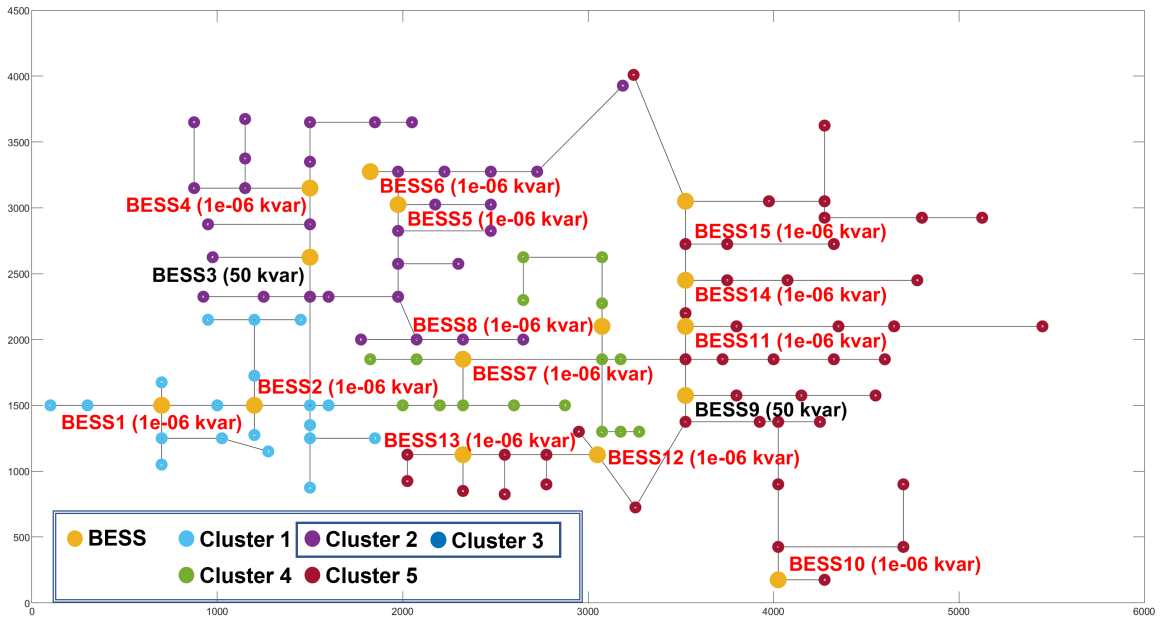


Figure 3.20: Reactive power clusters for availability of reactive power at BESS 3 and BESS 9

- Case 2: Figure 3.20 shows a scenario where only BESS 3 and 9 has reactive power available. Here cluster 2 and 3 merges for the reactive power support from BESS 3. Whereas, cluster 5 coverage area increases to include nodes from cluster 4.
- Case 3: Figure 3.21 shows a scenario where only BESS 3, 9 and 15 has reactive power available. Here the merged configuration for cluster 3 and 4 remains intact. A new cluster-cluster 6 emerges from the reactive power support of cluster 15.
- Case 4: Figure 3.22 shows a scenario where only BESS 3, 6, 9 and 15 has reactive power available. Here the cluster 3, previously merged with cluster 2, receives an independent voltage support from BESS 6. The rest configuration remains similar to case 3

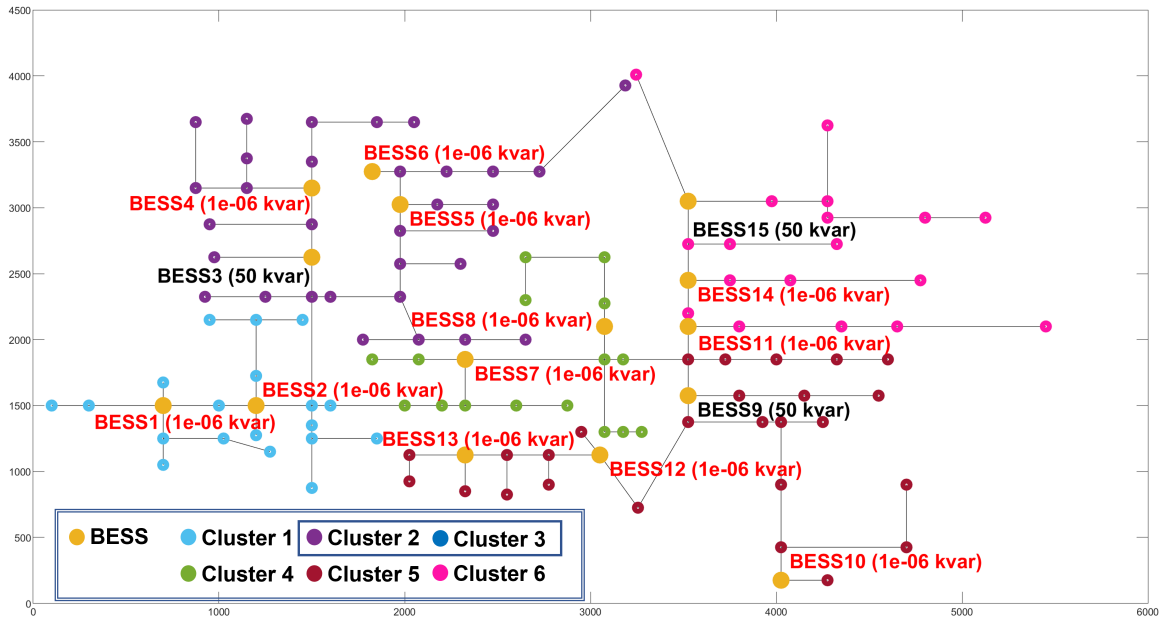


Figure 3.21: Reactive power clusters for availability of reactive power at BESS 3,9 and 15

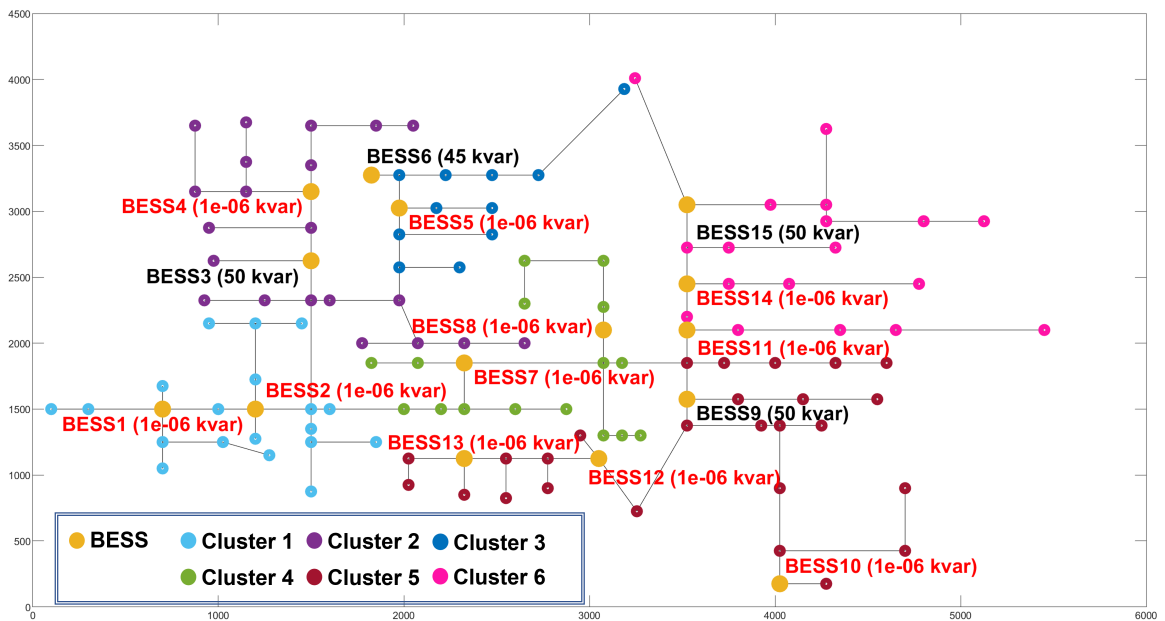


Figure 3.22: Reactive power clusters for availability of reactive power at BESS 3,9,6 and 15

### 3.8 Chapter Summary

The chapter presents an approach to perform clusters of distribution grid for distributed active and reactive power controls. The active power based clusters are performed through an improved two layer spectral clustering approach. The approach significantly improves the cluster quality and accurately identifies the clusters with load and generation balance. The clusters would dynamically vary based on grid operating condition (Load and PV variation). The distributed cluster level controls can be further used to maintain this balance. The chapter also proposes an approach to cluster based on the voltage sensitivity to reactive power support from DERs. The sensitivity clusters varies dynamically based on the reactive power available at each DER. The future works would include implementation of the proposed approach of active and reactive power based clusters on a larger distribution network.

## CHAPTER 4: Optimal management of power distribution system with clustering for effective utilization of DERs

### 4.1 Introduction

In the modern grid, distributed generators (DGs) are playing a vital role in fulfilling the increasing demand [81–84]. An increasing number of controllable devices and flexible generation assets on the distribution grid would increase the scale and thereby the complexity of distribution grid level control and optimization. Also, the load distribution, as well as the variation, is not uniform in the distribution grids. Hence, the centralized control for all the flexible assets may not be efficient and optimal. The challenges mentioned above can be mitigated if the distributed control approach is adopted by creating the virtual clusters of the distribution grid and assigning the zones of control to the groups of DERs. Various methods for distribution system clustering or partitioning have been developed [81–84]. It is demonstrated that the management of the distribution system with distributed energy resources as one of the potential applications of the smart power grid [85,86]. Several applications have focused on DER integrated power distribution management architecture including the outage management [87], situational awareness [88], and, phasor measurement unit applications [89], including the report from agencies such as the Department of Energy (DOE) [90–92].

For management of DER integrated power distribution grid, applications such as secondary voltage control including stability [93], splitting strategies [94], dynamic voltage control areas [95], voltage control area identification [96], and dynamic planning [97] has been proposed earlier. In our earlier works, we have developed control architectures for renewable energy management as well as [68,98–103]. These meth-

ods are focusing on partitioning the distribution networks into micro-grids during grid contingencies for an islanded operation, or generically managing the DER. However, the management of the power grid locally and at the same time integrated into a grid management framework such as ADMS is extremely critical. Higher penetration of DERs in the distribution grid leads to higher intermittencies. Most of the literature work deals with global supply from all the distributed generations to support the loads during normal as well as intermittent conditions. This may lead to inefficient utilization of the distributed generations during several scenarios.

Chapter 3 proposed an approach for clustering the distribution grid based on active power-flows and reactive power voltage sensitivities. Current chapter focuses on an efficient management of the distribution grid in grid-connected mode. The chapter presents a robust distributed control architecture control and optimally manage and support the net-load and voltage variations by leveraging the battery energy storage systems (BESS) available within that cluster.

The Chapter is organized as follows. Section 4.2 discusses presents an approach for net-load smoothing through cluster control. Section 4.3 presents an approach for measurement based voltage management on the grid. Section 4.4 implements the proposed approach on the IEEE 123 bus system.

## 4.2 Cluster net-load management

A distribution grid cluster consists of load, PVs and BESS. The cluster net-load is the results of total load and DER generation within the cluster. Typically the loads may be controllable upto an certain extent through utility's demand response programs, PV may be curtailable through curtailment approaches and BESS dispatch is controlled based on the targeted application. However, current chapter assumes PV and loads as the non-controllable assets and leverages the flexibility of BESS dispatch for the net-load smoothing application.

#### 4.2.1 Least Square Estimation based Active power-based cluster control for cluster net-load management

It is assumed that DERs are interconnected through smart inverters and can be controlled. The virtual clusters identified by the dynamic clustering module can be further controlled optimally by leveraging the capabilities of smart inverters. In this work, an active power-based cluster control is proposed, to support the local loads and reduce the perturbations caused by PV intermittencies and load variations within the clusters. The mathematical details of cluster control are as follows.

The net-load for cluster  $k$  at any time  $n$  is given by (4.1). Here  $P_{nl}(k, i)$  is the net-load without BESS for cluster  $k$  at time-step  $i$ . If the criticality level is known for the feeder-loads, the net-load ( $P_{nl}$ ) can be made same as the critical net-load ( $P_{nl}^c(k, i)$ ).

$$P_{nl}(k, n) = Pload(k, n) - P_{pv}(k, n) \quad (4.1)$$

In the proposed approach, the reference net-load  $P_{nl}^{ref}(k, n)$  for a  $k$  cluster is calculated by taking the moving average of the net-load ( $P_{nl}$ ) or the critical net-load ( $P_{nl}^c(k, i)$ ) for the past  $N$  measurements, as shown in (4.2).

$$P_{nl}^{ref}(k, n) = \frac{1}{N} \sum_{i=n-N}^n P_{nl}(k, i) \quad (4.2)$$

As shown in (4.3), the linear least square optimization approach is applied to optimize the error between the reference net-load  $P_{ref}^{nl}$  and the measured net-load ( $P_{nl}$ ) for the  $k^{th}$  cluster over past  $N$  measurements. Here  $x(k)$  is the optimization co-efficient.

$$\min U = \sum_{i=n-N}^n \frac{1}{2} * (P_{nl}(k, i) - x(k) * P_{nl}^{ref}(k, i))^2 \quad (4.3)$$

The net-load support provided by the BESS is limited by the active power rating ( $kW$ ) rating of the BESS within the cluster. For  $m$  BESS within the cluster, the

total active power support available for the cluster  $k$  is represented by  $P_{kW}(k) = P_1^{BESS} + P_2^{BESS} + \dots P_m^{BESS}$ . Based on the  $P_{kW}(k)$ , the upper and the lower bounds of the optimization coefficient  $x(k)$  can be formulated as shown in (4.4). Based on the value of  $x(k)$ , the optimal active support from the  $m$  number of BESS for cluster  $k$  can be calculated as

$$\frac{-P_{kW} + P_{nl}(n)}{P_{ref}} < x(k) < \frac{P_{kW} + P_{nl}(n)}{P_{ref}} \quad (4.4)$$

$$P_{BESS}(k, n) = P_{nl}(k, n) - x(k) * P_{nl}^{ref}(k, n) \quad (4.5)$$

The  $P_{BESS}(k, n)$  determines the total active power to be dispatched by the BESS of the  $k^{th}$  cluster. Based on the total  $P_{BESS}(k, n)$ , the dispatch from an individual BESS is distributed among the cluster BESS based on the decreasing order of the state of charge error ( $e_{soc}(j, n)$ ) and the storage capacity of the BESS ( $BESS_{kWh}$ ) as

$$e_{soc}(j, n) = SOC_t(j, n) - SOC(j, n) \quad (4.6)$$

$$ekWh_{soc}(j, n) = e_{soc}(j, n) * BESS_{kWh} \quad (4.7)$$

A PI-based approach is used to calculate the active power setpoints ( $P_{set}^i$ ) for the individual BESS. This approach aims to improve the SOC recovery for the targeted state of charge ( $SOC_t(j, n)$ ) and was found to be efficient in keeping the BESS state of charge within the upper and lower limits. For every BESS within the cluster, based on the  $e_{soc}(j, n)$  value, the ramp-rate coefficient ( $\zeta_{soc}^j$ ) is calculated as shown in (4.8). When the SOC error ( $e_{soc}$ ) is smaller compared to the error threshold  $e_{soc}^{th}$ , the proportional component ramp-rate coefficient is based on the proportional component ( $k_p$ ) which controls the sudden changes in the BESS dispatch. When the SOC error ( $e_{soc}$ ) is larger compared to the error threshold  $e_{soc}^{th}$ , the integral component based on errors for the last N measurements is used to control the BESS dispatch. The

values of  $K_i$  can be further varied dynamically based on charging and discharging opportunities to improve the SOC recovery.

$$\zeta_{soc}^j = \begin{cases} k_p, & \text{for } e_{soc}(j, n) \leq e_{soc}^{th} \\ k_i \sum_{i=n-N}^n e_{soc}(j, i), & \text{for } e_{soc}(j, n) \geq e_{soc}^{th} \end{cases} \quad (4.8)$$

Based on the  $\zeta_{soc}^j$ , the value of active power dispatch for every BESS within the cluster is calculated sequentially as shown in (4.9) limited by BESS kW limits  $P_{kW}^j$  as shown in (4.10).

$$P_{set}^j = \zeta_{soc}^j * \frac{P_{BESS}(k, n) - \sum_{\forall j>1, m=1}^{j-1} P_{set}^m}{N_k - j + 1} \quad (4.9)$$

$$-P_{kW}^j \geq P_{set}^j \leq P_{kW}^j \quad (4.10)$$

#### 4.2.2 Inter-cluster set-point segregation

Equation 4.9 segregates the cluster set-point for every BESS on the system based on the  $\zeta_{soc}^j$  coefficient. The sequential segregation of the set-point may not be optimal. Also, approach may not support inter-cluster power exchanges between the BESS. ie. A BESS with higher SOC may not be able to support BESS with lower SOC. Hence, an inter-cluster optimization was developed with the goal keeping the BESS SOC within the tolerance limit.

For every cluster( $k$ ), the objective function for BESS set-point segregation can be formulated as follows:

$$\min \frac{1}{2} \|SOC_i^{target} - SOC_i(t)\|^2 \quad (4.11)$$

subjected to the kW support limit of the BESS

$$-P_i^{kw} \leq P_i(t) \leq P_i^{kw} \quad (4.12)$$

Equation 4.12 can be represented based on the storage capacity of BESS as:

$$P_i(t) = Ebess_i(t - 1) - Ebess_i(t) \quad (4.13)$$

Since  $Ebess_i(t)$  can also be represented in form of state of charger, equation 4.13 can be modified to

$$P_i(t) = Ebess_i(t - 1) - SOC_i(t) * Ebess_i \quad (4.14)$$

Substituting  $P_i(t)$  in equation 4.12

$$-P_i^{kw} \leq Ebess_i(t - 1) - SOC_i(t) * Ebess_i \leq P_i^k W \quad (4.15)$$

Rearranging equation 4.15 to obtain the lower and upper bounds of the optimization variable  $SOC_i(t)$

$$P_i^k W - Ebess_i(t - 1) \leq x_i * Ebess_i \leq -P_i^{kw} - Ebess_i(t - 1) \quad (4.16)$$

$$\frac{P_i^k W - Ebess_i(t - 1)}{Ebess_i} \leq x_i \leq \frac{-P_i^{kw} - Ebess_i(t - 1)}{Ebess_i} \quad (4.17)$$

For multiple BESS within the cluster, the equality constraint to meet cluster set-point can be given by

$$\sum_{i=1}^N P_i(t) = P_{set}(t) \quad (4.18)$$

Substituting  $P_i(t)$  in equation 4.18

$$\sum_{i=1}^N Ebess_i(t - 1) - \sum_{i=1}^N SOC_i(t) * Ebess_i = P_{set}(t) \quad (4.19)$$

Re-arranging the equation 4.19, the equality constraint in terms of optimization vari-

able  $SOC_i(t)$  can be formulated as

$$\sum_{i=1}^N Ebess_i(t-1) - P_{set}(t) = \sum_{i=1}^N SOC_i(t) * Ebess_i \quad (4.20)$$

$$\frac{\sum_{i=1}^N Ebess_i(t-1) - P_{set}(t)}{\sum_{i=1}^N Ebess_i} = \sum_{i=1}^N SOC_i(t) \quad (4.21)$$

Meeting the cluster set-point may not always be possible because of limited support capability of BESS. Hence, the equality constraint is added to the objective function as a soft constraint with a penalty coefficient  $\rho$ . Equation represents the final optimization formulation for the inter-cluster setpoint segregation.

$$\begin{aligned} \min_{SOC_i(t)} \quad & \frac{1}{2} \|SOC_i^{target} - SOC_i(t)\|^2 + \frac{\rho}{2} \left\| \frac{\sum_{i=1}^N Ebess_i(t-1) - P_{set}(t)}{\sum_{i=1}^N Ebess_i} - \sum_{i=1}^N SOC_i(t) \right\|^2 \\ \text{s.t.} \quad & \frac{P_i^{kW} - Ebess_i(t-1)}{Ebess_i} \leq x_i \leq \frac{-P_i^{kW} - Ebess_i(t-1)}{Ebess_i} \end{aligned} \quad (4.22)$$

Table 4.1 presents 7 cases of inter-cluster set-point segregation for a fictitious cluster with 3 BESS. The rated  $kW$  capacities for three BESS is assumed to be 50, 75 and 25 kW. The rate storage capacity for the BESS is assumed to be 120, 150 and 50 kWh. The  $SOC_i^{target}$  for all cases is assumed to be 0.5 or 50%.

- Case 1: The SOC for all BESS is 0.5. The set-point for the cluster is equal to the combined rated kW of the cluster. Hence all BESS are discharges at the rated capacity.
- Case 2: The SOC for all BESS is 0.5. The set-point for the cluster is higher than the combined rated kW of the cluster. Hence all BESS are discharges at the rated capacity to minimize the tracking error.
- Case 3: The SOC for all BESS is 0.5. The set-point for the cluster is lower

Table 4.1: Inter-cluster set-point segregation

	BESS1	BESS2	BESS3
$P_{kW}$	50	75	25
Ebess	120	150	50
Case 1	Cluster Set-point = 150 kW		
SOC(t-1)	0.5	0.5	0.5
P(t)	50	75	25
Case 2	Cluster Set-point = 200 kW		
SOC(t-1)	0.5	0.5	0.5
P(t)	50	75	25
Case 3	Cluster Set-point = 100 kW		
SOC(t-1)	0.5	0.5	0.5
P(t)	34.2	59.05	6.65
Case 4	Cluster Set-point = 100 kW		
SOC(t-1)	0.5	0.2	0.5
P(t)	50	25	25
Case 5	Cluster Set-point = 75 kW		
SOC(t-1)	0.5	0.2	0.5
P(t)	50	0	25
Case 6	Cluster Set-point = 50 kW		
SOC(t-1)	0.5	0.2	0.5
P(t)	50	-25	25
Case 7	Cluster Set-point = 70 kW		
SOC(t-1)	0.8	0.3	0.4
P(t)	50	45	-25

then the combined rated kW of the cluster. Hence all BESS are discharges are proportionate to the rated storage capacity.

- Case 4: The SOC of BESS 2 is low (0.2). The set-point for the cluster is same as in case 3. But, the set-point for the BESS2 is reduced from 59 kW to 25 kW and the reduction in the discharge of BESS 2 is compensated by BESS1 and BESS2.
- Case 5: The SOC of BESS 2 is low (0.2). The cluster set-point for this case is 75 (lower than previous cases). The set-point is achievable through the discharge from the BESS1 and BESS3. Hence, the BESS 2 temporarily set to "idle" mode to avoid any further depletion of the SOC.
- Case 6: The SOC of BESS 2 is low (0.2). The cluster set-point for this case is 50 (lower than previous cases). Hence an additional headroom is available for the power exchange between the BESS after meeting the cluster set-point. Hence, the BESS 2 is assigned the set-point to restore the state of charge from the additional dispatch of BESS 1 and BESS2.
- Case 7: The SOC of BESS1 is 0.8, BESS 2 is 0.3 and BESS 3 is 0.4. The cluster set-point for this case is 70. Since BESS 1 is having the higher SOC, it is assigned the set-point to discharge at the rated capacity. Although the SOC of BESS2 is lower compared to BESS3, the rate storage capacity of BESS 3 is significantly lower (33%) than BESS 2. Hence, the SOC restoration of BESS 3 is prioritized compared to BESS 2 and the BESS 2 discharges at a reduced rate.

#### 4.3 Sensitivity based reactive power control for voltage management

Sensitivity based clustering is based on the sensitivity matrix obtained from the system Jacobin and available reactive power support from all DERs. However, the

voltage measurements are also available from additional nodes with distribution system devices connected to it. These measurements can be further used to calculate the reactive power set-points from each DER to holistically manage the voltage throughout the clusters. Current approach aims at controlling the voltage deviations from all measurement nodes of the cluster. The upper limit for voltage support for all measurement nodes is calculated by:

Based on the upper limit of voltage support, the constraint least square based optimization is formulated to calculate the optimum voltage setpoint for all measurement nodes( $n$ )

$$\min U = \sum_{k=t-\Delta t}^t \frac{1}{2} * ||(V_n(k) - \lambda_n * Vref_n(k))|| \quad (4.23)$$

for all nodes such that

$$\frac{(v_n(t) - dv^u)}{vref_n(t)} \geq \lambda_n \geq \frac{(v_n(t) + dv^u)}{vref_n(t)} \quad (4.24)$$

Here  $Vref_n$  is the reference voltage and  $\lambda_n$  is the optimization coefficient for  $n^{th}$  measurement node.

From 4.23 and 4.24, the optimal voltage for  $n^{th}$  node at time  $t+1$  can be calculated as

$$dv_n^{t+1} = v_n^t - \lambda_n * vref_n^t. \quad (4.25)$$

Based on the voltage reference setpoint for every measurement nodes, the optimal reactive power setpoint is calculated through a least square optimization problem. The  $Q$  for the time step  $t+1$  is calculated as follows

$$\min U = \sum_{i=1}^n \frac{1}{2} * ||dv_n^{t+1} - dQ_m^{t+1} * S^T|| \quad (4.26)$$

Since, the reactive power control is given the secondary priority after active power

control. The reactive power set-point for every DER is constrained by the availability of the reactive power from each DER.

$$Q_m = \sqrt{S_m^2 - P_m^{t+1}} - Q_m^t \geq dQ_m^{t+1} \geq Q_m = \sqrt{S_m^2 - P_m^{t+1}} + Q_m^t \quad (4.27)$$

From (29), the optimal reactive power setpoint for  $n^{\text{th}}$  node at time  $t + 1$  can be calculated as  $Q_m^{t+1} = Q_m + dQ_m^{t+1}$ .

#### 4.4 Implementation: IEEE 123 bus system

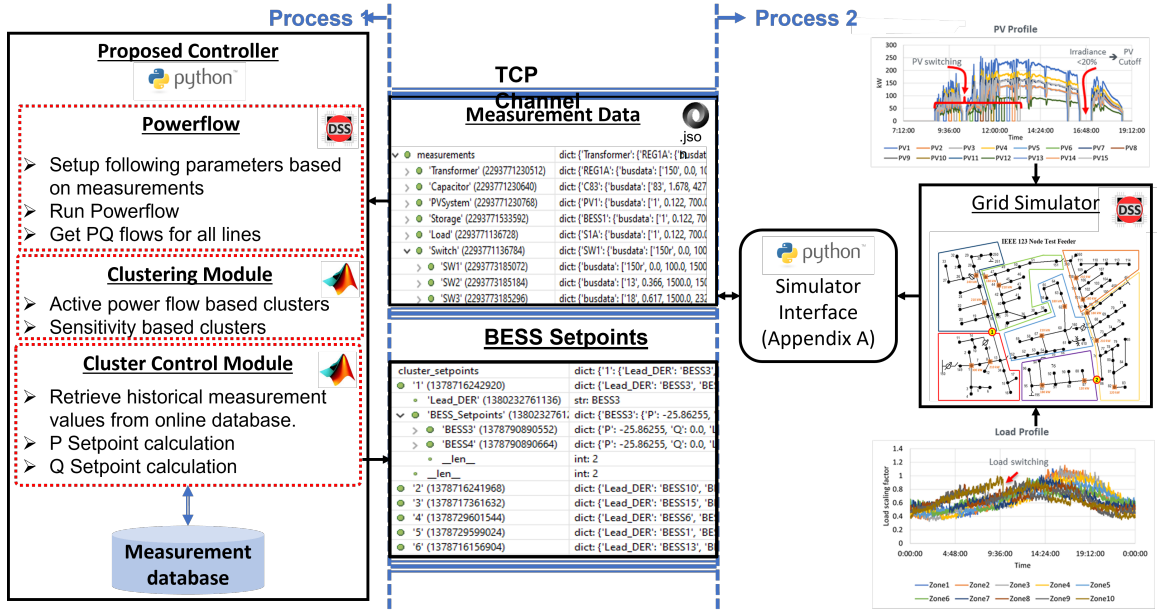


Figure 4.1: Implementation of active and reactive power control on IEEE 123 bus system

The active and reactive power management approaches presented in the chapter was implemented on the dynamically varying active and reactive power cluster configurations of IEEE 123 bus system. Figure 4.1 shows the flow of processes in the co-simulated environment. The measurements are collected at every 5 seconds and sent to the simulator. The active and reactive power clustering is performed at every 3 minute time intervals. For the required cluster configurations, the reactive and active power set-points for the BESS are calculated at every 5seconds. Since the proposed

approach uses the historical data to calculate the set-points, an online database of the past measurement is maintained. For every new cluster configurations, the historical measurements are extracted to re-establish the history of the new cluster based on the past time-step measurements.

The active and reactive power control is performed for the net-load minimization and voltage deviation minimization applications. Figure 4.2 shows the PV, load and the net-load profile through out the simulation time window.

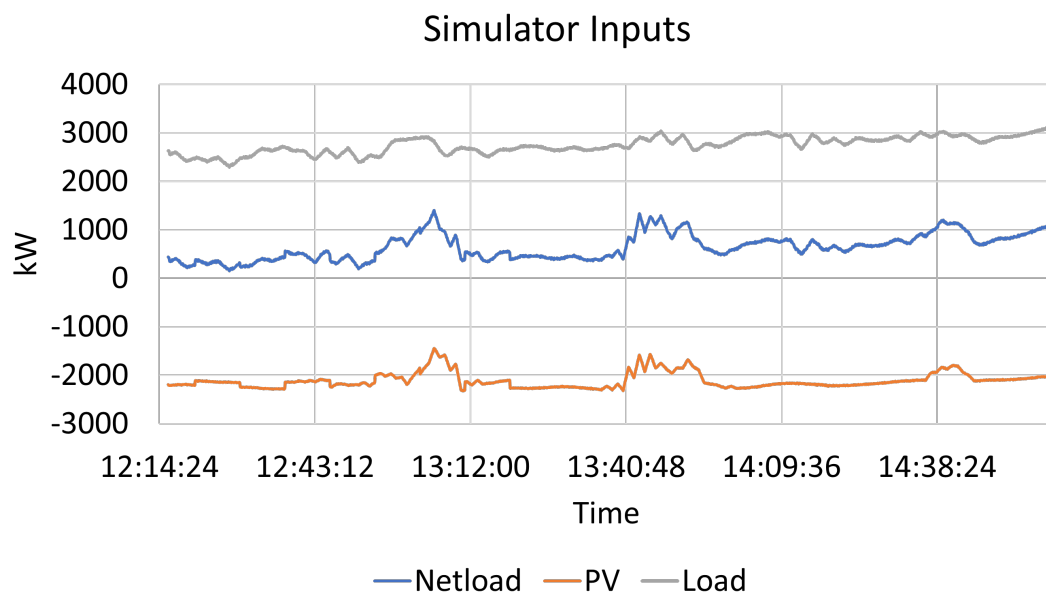


Figure 4.2: Load and PV generation profiles during the simulation window.

#### 4.4.1 Net-load smoothing through dynamic cluster and control

The section demonstrates and analyzes the performance of the cluster based net-load smoothing. To understand the benefits of cluster control and dynamically varying cluster, the following three cases are compared:

- **Centralized Control:** Here complete grid acts as a single cluster and the set-points are calculated based on the overall grid requirements.
- **Control with constant clusters:** Here the cluster configuration is kept constant

through out the simulation. Figure 4.3 shows the cluster configuration followed through out the simulation.

- Control with dynamic clusters: Here the cluster configuration is dynamically varying based on power-flows at every 3 minute time interval. Figure 4.4 shows the variation of clusters through out the simulation.

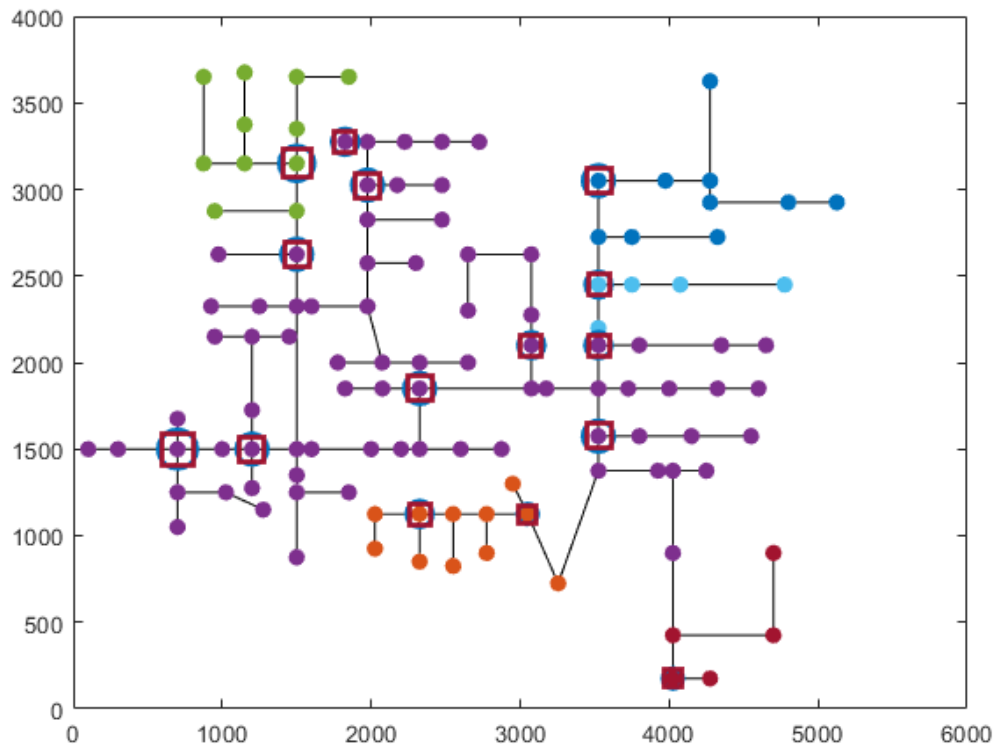


Figure 4.3: Active power-flow based clusters on IEEE 123 bus system

Figure 4.5 shows the feeder-head power-flow without control and with controls. The net-load smoothing strategy is based on the moving average as a reference. Hence, the measurements from the past time-steps helps in determining the set-points for the next time-steps. Due to the moving average window, the the resulting feeder-head power flow with controls shows the time-shifts. The approach addresses the inter-mittacies by reducing the magnitude of the variations and ramp rate of the variations

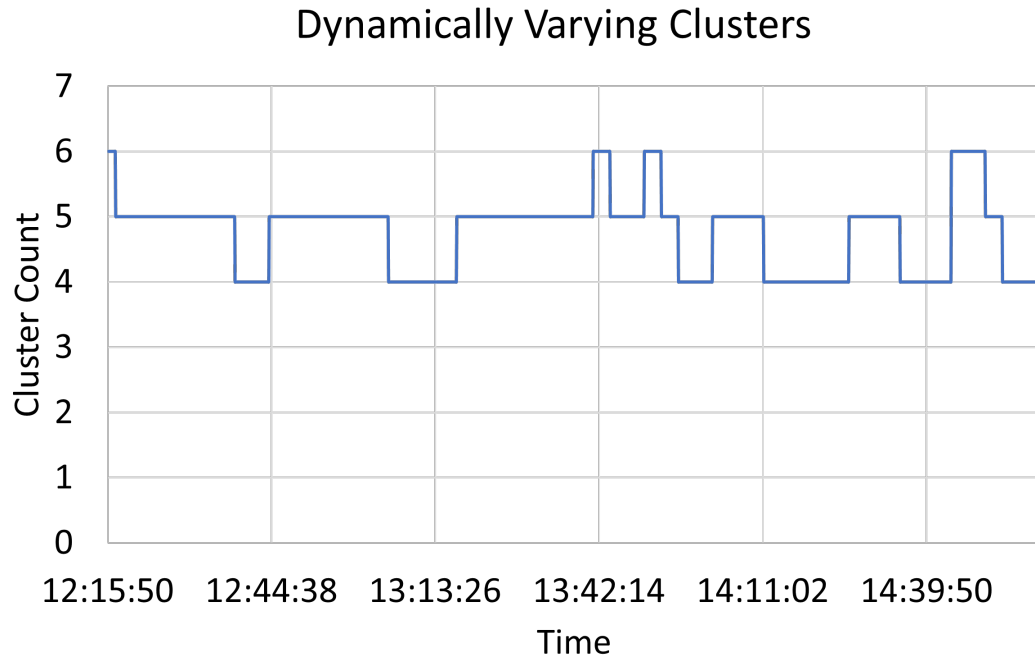


Figure 4.4: Dynamically varying active powerflow based clusters

Table 4.2: Effect of cluster control on the net-load smoothing

	Without Control	Centralized Control
Constant Cluster	0.57	0.96
Dynamic Cluster	0.58	0.98

in the net-load. The feeder-head power-flow for cluster based control is compared against the centralized control. The overlapping of the net-load profile validates the consistency of the distributed control approaches. A 1 minute regression based smoothing index is calculated to compare the improvement in the net-load smoothing. The cluster based smoothing approaches reduces the net-load intermittancies by 48%. The clustered net-load control efficient by 4% when compared against the centralized control in reducing the intermittancies.

Figure 4.6 compares the average active power-loss for all three net-load smoothing cases. The loses, as expected, are higher for centralized controls. It is to be noted here, that smoothing applications does not have significant power requirements. The

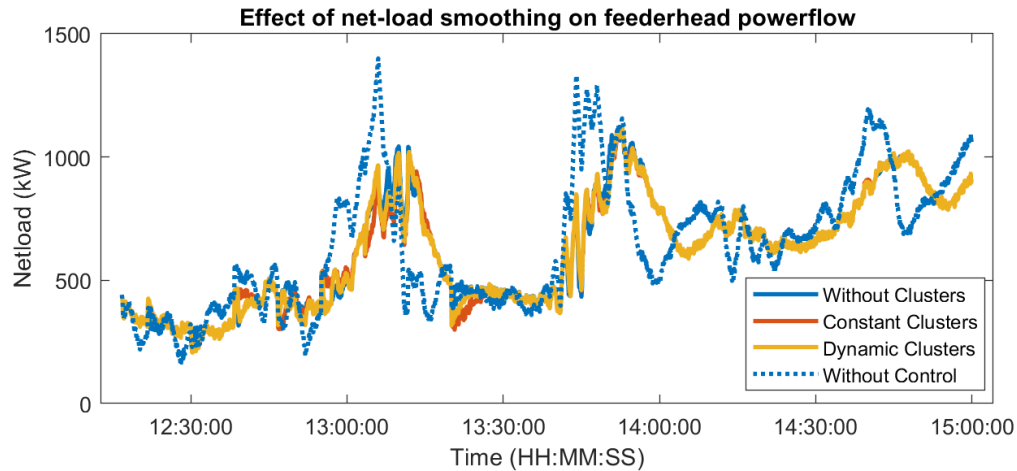


Figure 4.5: Feeder-head power-flow for net-load smoothing application

reduction in the losses would be higher for net-load minimization application discussed in the later chapters.

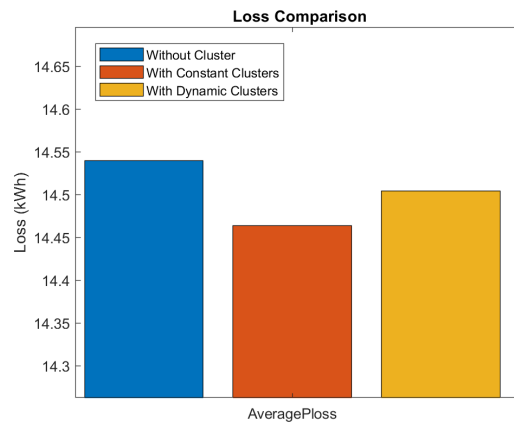


Figure 4.6: System active power losses

Figure 4.7 compares the voltage variations at all nodes on the distribution feeders. The nodes after 75 are near the end of the feeder. Here, the  $x/r$  ratio is higher and hence the voltage variations are also high. The centralized control does not address the variations in the load locally. Hence, the higher voltage variation is observed for centralized control approach. Constant and dynamic cluster configurations shows almost similar variations in the voltage magnitude.

Figure 4.8 and figure 4.14 shows the cluster net-load for static and dynamic clus-

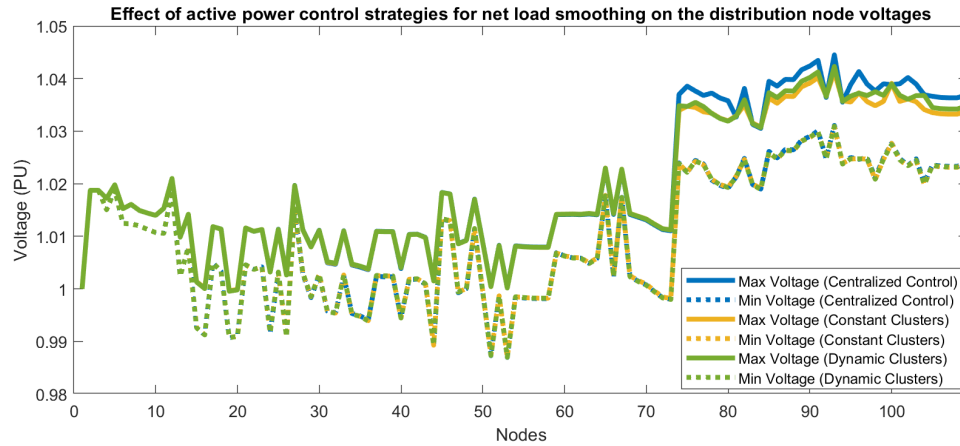


Figure 4.7: Effect of active power control strategies for net-load smoothing on the distribution node voltages

tering approaches. Since the dynamic clustering, re-configures the clusters with an improved balance of the net-load, the magnitude of cluster net-load is low. Current approach does not minimize the net-load. The balance of load and generation is achieved through re-clustering by the improved spectral clustering based approach. The improvement in the cluster net-load is summarized in the table ??

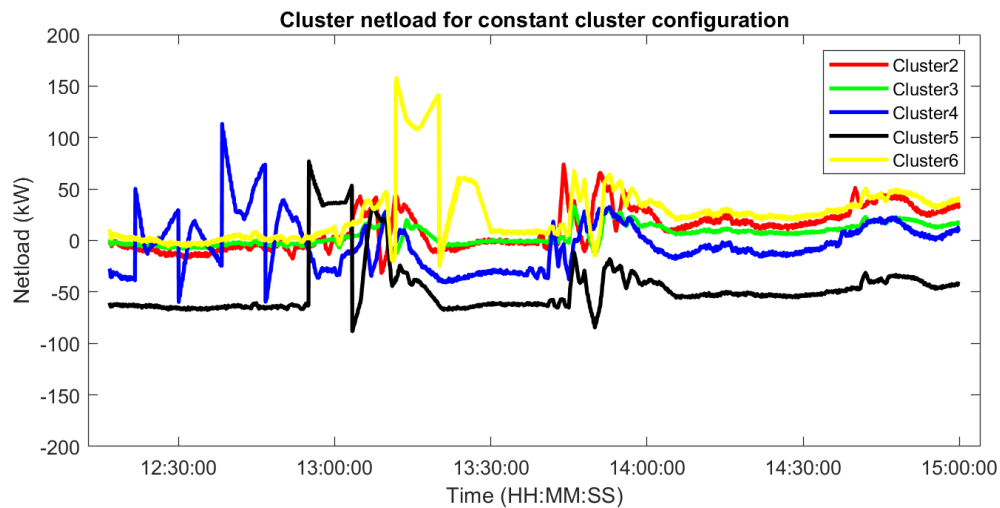


Figure 4.8: Cluster net-load for constant cluster configuration

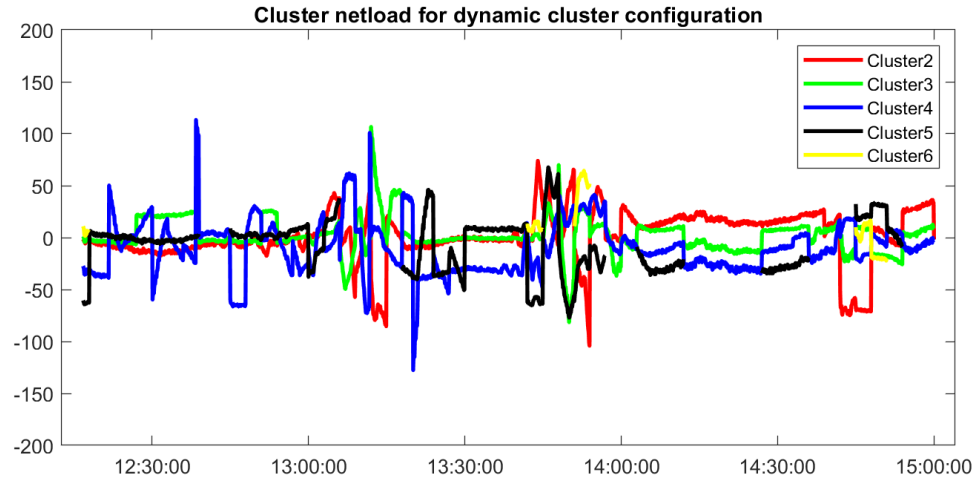


Figure 4.9: Cluster net-load for dynamic cluster configuration

Table 4.3: Improvement in the cluster net-load support through dynamic clustering

	Constant Clusters	Dynamic Clusters
Cluster 2	11.2	0.894
Cluster 3	5.47	1.2
Cluster 4	-4.04	9.9
Cluster 5	-46.53	-7.9
Cluster 6	26.27	11.26

#### 4.4.2 Voltage control through dynamic clusters and control

The sensitivity based clustering approach is discussed in the previous chapter 3. Since the IEEE 123 bus system is relatively small distribution grid, the number of reactive power based clusters are limited to three. The count on number of clusters would be relaxed later for the larger system. The the boundaries of voltage sensitivity to reactive power is not definite, the small size clusters would contribute to the hunting to the neighbouring clusters. A Measurement based voltage control approach is proposed for each clusters in this chapter. The measurement nodes could be: transformers, DERs, critical loads, capacitors. Based on the measurements, the proposed approach pro-actively manages the reactive power dispatch to control the voltages at the measured nodes. Since, the measurement nodes are distributed through out

the distribution grid, the effect of voltage management is also observed on the non-measurement grid.

Figure 4.10 compares the voltage profile for node 82. The measurements from this nodes are available since the BESS 10 is connected at this node. The variation in the node voltage is reduced substantially through the PQ control.

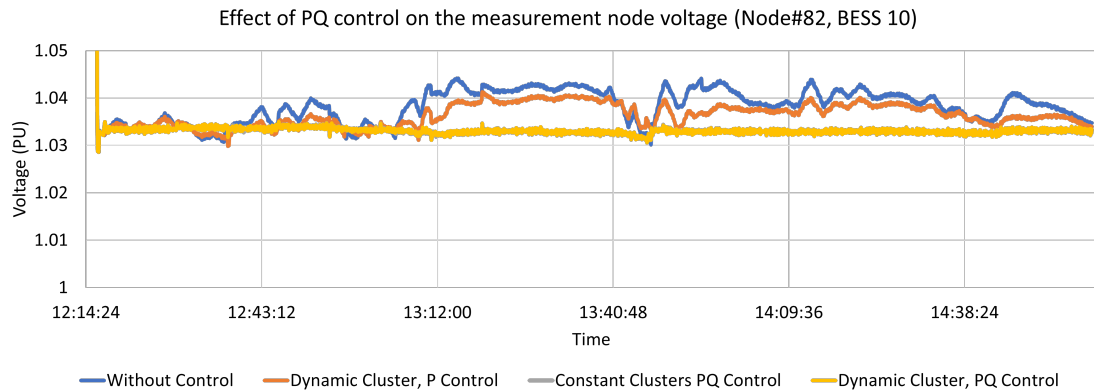


Figure 4.10: Effect of control on the measurement node voltage

Figure 4.11 compares the voltage profile for node 114. The node is connected through a single phase line and is located towards the feeder end. The sensitivity of the voltage to active and reactive power variation is high for this node. Figure 4.11 shows the voltage variation of 0.02 PU without any control. The nearest measurement node is node 108 with BESS interconnection. The reactive power based voltage control reduces the variation substantially.

Figure 4.12 and figure 4.13 shows the voltage for all-nodes on the feeder with P control and PQ control. It can be observed here, the variations in the voltage are substantially reduced for measurement as well as non-measurement nodes on the system.

The difference in the minimum and maximum voltage observed at all nodes is summarized in figure. The plot compares the improvement with PQ control against a stand-alone P control (net-load smoothing). Since the active power dispatches are small for net-load smoothing application, reactive power is always available at each

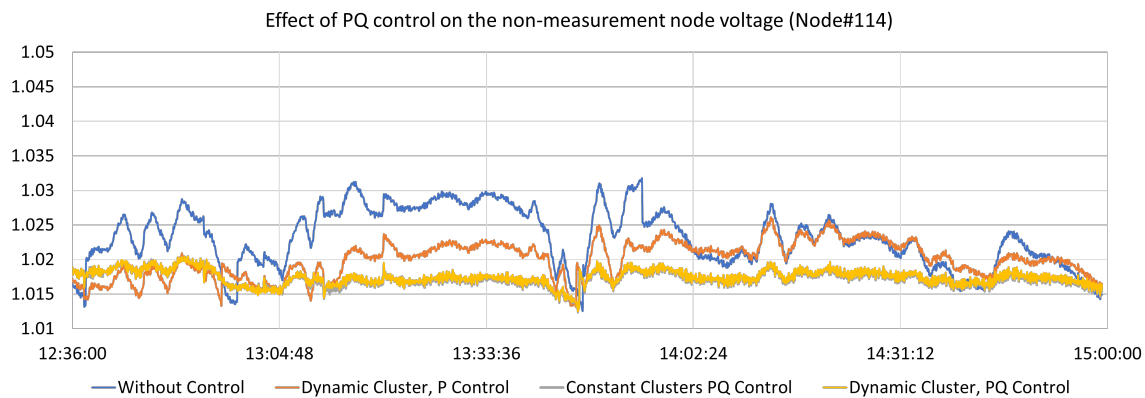


Figure 4.11: Effect of control on non-measurement node voltage

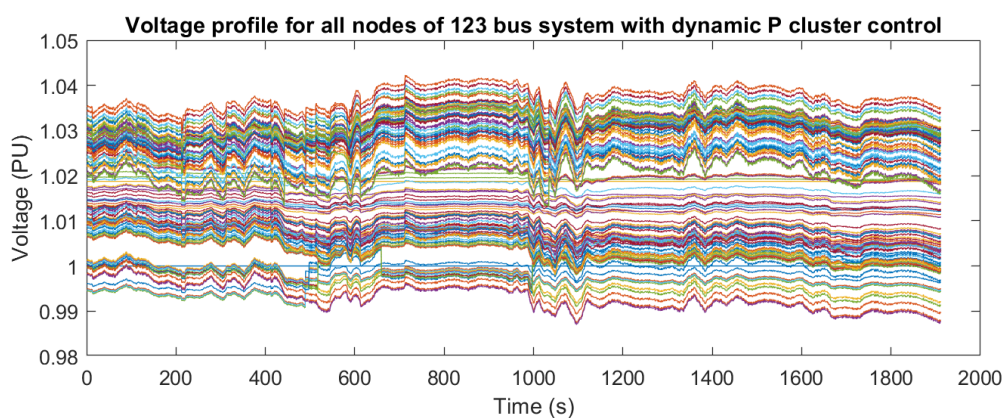


Figure 4.12: Voltage profile for all nodes of 123 bus system with dynamic P cluster control

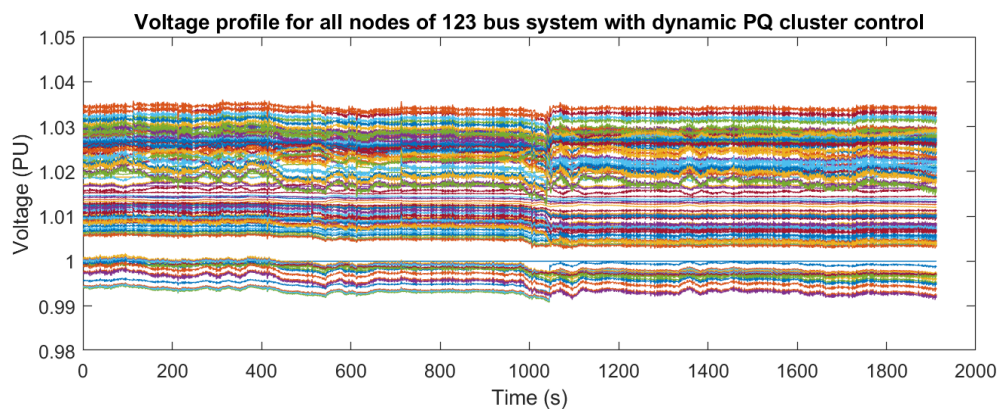


Figure 4.13: Voltage profile for all nodes of 123 bus system with dynamic PQ cluster control

BESS. Hence, no significant difference is observed here between static and dynamic clustering.

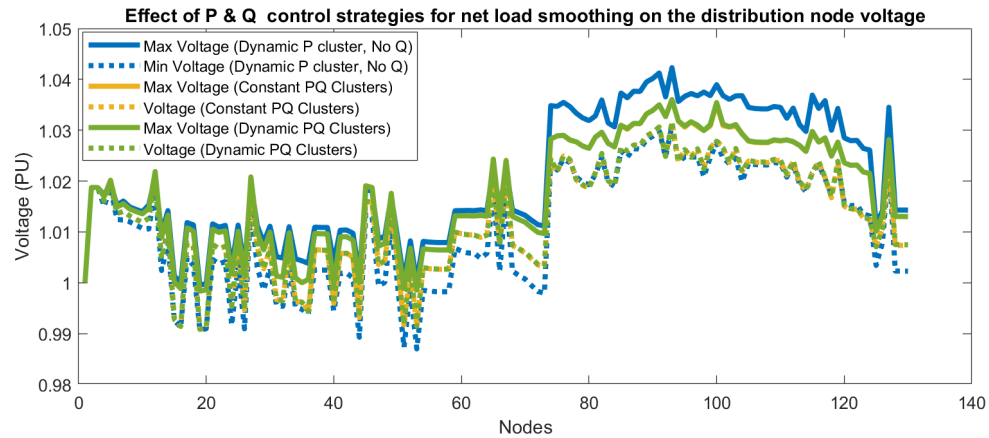


Figure 4.14: Effect of P and Q control strategies for net load smoothing on the distribution node voltage

#### 4.5 Chapter Summary

The chapter presents a distributed approach for net-load smoothing. Each clusters acts as stand-alone agents and minimize the load net-load variations through BESS active power control. The proposed approach is implemented on IEEE 123 bus system and validated against centralised control approach. A distributed reactive power management approach is also presented in the chapter. The reactive power set-points are calculated based on the voltage measurements and the reactive power available at each DER after active power dispatch. A substantial reduction in the voltage variation is observed through reactive power control for all measurement and non-measurement nodes of IEEE 123 bus system.

## CHAPTER 5: Dynamic distributed model of power grid for optimization and control

### 5.1 Introduction

The previous chapter discusses the approach for cluster control. Utilities employ the OPF algorithms at the sub-transmission levels to manage the losses and the aggregated demand at the substation level. Currently, active power management at the substation level is performed only to manage any issues related to thermal overloads. However, with increasing controllable assets at the distribution level, the setpoints may be provided at the substation level to include additional applications such as market participation or transmission grid management. The current chapter proposes an ADMM based approach to share the feeder head or area setpoints among the clusters on the distribution grid based on the SOCs of the cluster BESS.

Section 5.2 discusses the ADMM based sharing optimization formulation. Section 5.3 discusses the application of ADMM based sharing optimization problem for the area set-point sharing. Section 5.4 modifies the least square-based cluster control approach presented in chapter 4 for the reference set-point tracking application. Section 5.5 implements the sharing and tracking approaches on IEEE 123 bus system.

### 5.2 ADMM based sharing optimization

Sharing problem is a form of multiple objective optimizations consisting of multiple local and global cost minimization. Although the local optimization may be independent, the global optimization cost is dependent on all local variables. Hence, a sharing optimization problem aims to minimize the overall system cost, including the local optimizations. Figure 5.18 illustrates a sharing based optimization where  $f(x_i)$  are the local optimization cost functions and  $g(z_i)$  where is the global optimization cost

function. Here,  $x_i$  are the "local variables," and  $z$  is the global variable.

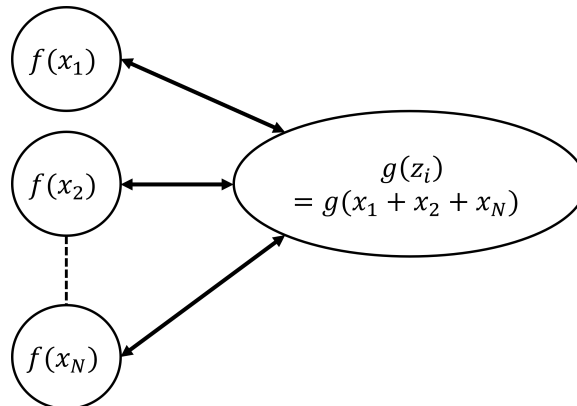


Figure 5.1: Sharing optimization problem

The sharing problem is formulated as shown in figure 5.18:

$$\min \sum_{i=1}^N f(x_i) + g\left(\sum_{i=1}^N x_i\right) \quad (5.1)$$

The sharing problem has a dual relationship with a consensus problem, where the contribution from the local variables to the global optimization problem can also be expressed as:

$$\min \sum_{i=1}^N f(x_i) + g\left(\sum_{i=1}^N z_i\right) \quad (5.2)$$

subject to  $x_i - z_i = 0, i = 1, 2, 3 \dots N$

If  $\bar{z} = \frac{1}{N} \sum_{i=1}^N z_i$ , the 5.1 can also be represented as:

$$\min \sum_{i=1}^N f(x_i) + g(N\bar{z}) \quad (5.3)$$

subject to  $\bar{x} - \bar{z} = 0$

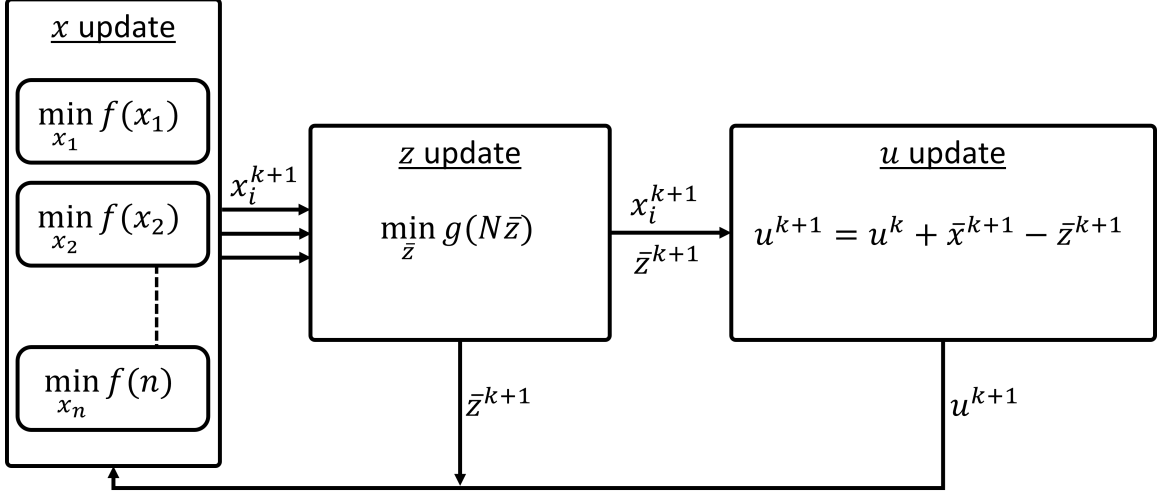


Figure 5.2: Sharing optimization problem

The flow of variables in the ADMM based sharing problem is represented in figure 5.2. The final scaled version of ADMM based sharing algorithm is as follows:

- $x$  update ( $N$  parallel executions):

$$x_i^{k+1} = \min_{x_i} (f_i(x_i) + \frac{\rho}{2} \|x_i - x_i^k + \bar{x}^k - \bar{z}^k + u^k\|^2) \quad (5.4)$$

- $z$  update:

$$z^{k+1} = \min_{\bar{z}} (g(N\bar{z}) + \frac{N\rho}{2} \|\bar{z} - u^k - \bar{x}^{k+1}\|^2) \quad (5.5)$$

- $u$  update:

$$u^{k+1} = u^k + \bar{x}^{k+1} - \bar{z}^{k+1} \quad (5.6)$$

### 5.3 Area Set-point segregation

A distribution grid with controllable generating assets provides flexibility in controlling the feeder-head power flow. The continuous monitoring-based control of active power generation on the distributed generating asset is often implemented to avoid the reverse power-flow conditions or the thermal loading on the sub-transmission lines.

Reference set-point tracking at the feeder head may also be required for advanced applications like loss minimizing OPFs or market participation.

Segregating the area set-point into multiple optimized cluster set-points is a *sharing-problem* requiring a global optimization for minimizing the area set-point error and multiple local optimizations running in parallel to optimize the local SOC level of energy storage present in each cluster. The sharing-based optimization problem is formulated as shown in (5.7).

$$J = \min_{x_N, u_N} \sum_{i=1}^{N_c} f(P_{cl}^i(k)) + g(z) \quad (5.7)$$

where  $i$  is the cluster number,  $N_c$  is the total number of clusters.

Here,  $f(P_{cl}^i(k))$  is a local optimization function for  $i^{th}$  cluster and  $g(z)$  is the global optimization function. Local optimization for every cluster is solved in parallel for a particular time period  $k(k = \Delta t)$ . Equation 5.8 represents the local optimization function formulated in the form of a least square problem to determine the cluster dispatch set-point  $P_{cl}^i$  and also manage the state of charge of BESS within the cluster  $i$ .

$$f(P_{cl}^i) = \frac{1}{2} \left\| E_i * soc_i(ref) - E_i * soc_i(k-1) + P_{cl}^i(k+1) * \frac{T_{ac}}{3600} \right\|^2 + \frac{1}{2} \left\| P_{cl}^i(k+1) - P_{ni}^i(k-1) \right\|^2 \quad (5.8)$$

Here,  $E_i$  is the total storage capacity of the cluster,  $soc_i(k-1)$  is the aggregated storage available in each cluster at time  $k$ , and  $T_{ac}$  is the time resolution at which the area controller is running.

The solution of the local optimization is constrained by total kW support limits  $+ - pKW_i$  for all BESS within the cluster. (See equation 5.9)

$$-pKW_i \leq P_{cl}^i(k) \leq pKW_i \quad (5.9)$$

Let  $err(k)$  be the area error (difference between reference and measured power

flow) at the time  $k$ . Since the dispatch from every cluster contributes towards the total power flow, the previous time-step contribution of the cluster dispatches is deducted from the error ( $\sum_{i=1}^{N_c} P_{cl}^i(k-1) - err(k)$ ). If  $z$  is the average dispatch from all clusters, the global optimization function ( $g(z)$ ) can be formulated as a least-square optimization problem to minimize the area error as shown in equation 5.10. Here  $z$  is also known as a global variable.

$$g(z) = \frac{1}{2} \left\| N_c * z - \sum_{i=1}^{N_c} P_{cl}^i(k-1) - err(k) \right\|^2 \quad (5.10)$$

where  $err(k) = P_{area}(k-1) - P_{ref}(k-1)$

An iteration ( $k+1$ ) of ADMM based optimization consists of three steps:

1. Local variable update  $P_{cl}^{i(k+1)}$ : Updating local variables  $P_{cl}^{i(k+1)}$ , where  $i = 1, 2..N_c$  in parallel using equation 5.11

$$P_{cl}^{i(k+1)} = \underset{z,u}{\operatorname{argmin}} (f(P_{cl})^{i(k)} + \frac{\rho}{2} \left\| P_{cl}^i - P_{cl}^{i(k)} + P_{cl}^{(k)} - z^{(k)} + u^{(k)} \right\|^2) \quad (5.11)$$

Here,  $P_{cl}^i$  is the local variable,  $P_{cl}^{i(k)}$  is cluster set-point from previous iteration,  $P_{cl}^{(k)}$  is an average set-point from previous iteration

2. Global variable update  $z^{(k+1)}$ : Requires all updated local variables to calculate the mean  $P_{cl}^{(k+1)}$  using equation 5.12 and then solving equation 5.13

$$P_{cl}^{(k+1)} = \frac{1}{N_c} \sum_{i=1}^{N_c} P_{cl}^{i(k+1)} \quad (5.12)$$

$$z^{(k+1)} = \underset{z}{\operatorname{argmin}} \left( g(z) + \frac{N_c * \rho}{2} \left\| z^{(k)} - u^{(k)} - P_{cl}^{(k+1)} \right\|^2 \right) \quad (5.13)$$

Here,  $\rho > 0$  is the penalty parameter and  $u^{(k)}$  is the dual variable, and  $z^{(k)}$  is the global variable value from the previous iteration.

3. Dual variable update  $u^{(k+1)}$ : Calculated based on the difference of the mean of local variables ( $P_{cl}^{(k+1)}$ ) and the updated global variable  $z^{(k+1)}$ , as shown in the equation 5.14

$$u^{(k+1)} = u^{(k)} + P_{cl}^{(k+1)} - z^{(k+1)} \quad (5.14)$$

The above theoretical formulation illustrates the ADMM based distributed optimization algorithm that optimally manages each area's power flow and provides a consensus framework. All clusters have controllable assets (DERs) to help track the cluster reference setpoints. The cluster setpoints are optimally calculated to balance the local objectives and the global setpoint tracking. The local control setpoints are optimally changed for each cluster to reach the global control objective, which is set based on the optimization framework.

### 5.3.1 Use-cases for SOC based set-point generation

Table 5.1 presents 10 cases of the ADMM based set-point sharing. The test cases assume three constant clusters with BESS kW rated capacities of 70, 25, and 50 kW. The total BESS storage capacity is 225, 75, and 150 kWh. The storage ratings are arbitrarily assumed to demonstrate the ADMM based set-point sharing with different SOC levels of each cluster. Case 1-5 presents the case with SOC management while tracking area set-point. Case 6-10 illustrates SOC and tie-flow management and area reference tracking.

Table 5.1: Test cases illustrating ADMM based area set-point sharing

Case	Area Error	SOC			Tieflow			Setpoints			Area Error (With Control)
		Cluster 1	Cluster 2	Cluster 3	Cluster 1	Cluster 3	Cluster 3	Cluster 1	Cluster 2	Cluster 3	
1	100	0.5	0.5	0.5	-	-	-	45.8	14.52	37.61	2
2	100	0.25	0.5	0.5	-	-	-	-16	25	50	41
3	100	0.1	0.5	0.5	-	-	-	-75	25	50	100
4	100	0.1	0.1	0.5	-	-	-	-75	-25	50	150
5	100	0.8	0.1	0.3	-	-	-	75	-25	50	0
6	100	0.5	0.5	0.5	30	-20	10	49.2	-0.1	29.5	21.4
7	100	0.25	0.5	0.5	30	-20	10	-11.8	19.9	49.6	42.2
8	100	0.1	0.5	0.5	30	-20	10	-75	25	50	100
9	100	0.1	0.1	0.5	30	-20	10	-75	-25	50	150
10	100	0.8	0.1	0.3	30	-20	10	58	-25	37.3	29.7

- Equal SOC Case: Case 1 and Case 6 assumes equal SOC level for all clusters. Case 1 accurately tracks the area reference with an error of only 2kW. Since the tie-flow contradicts the dispatch set-points for each cluster, the area reference tracking is compromised while minimizing the overall tie-line flow error. When tie-flow management is applied, the area error increases to 21.4 kW, whereas the total tie-flow error reduces from 27 kW to 19.5 kW.
- Low SOC Case: The SOC level of cluster 1 reduces to 0.25 for Case 2 and Case 7. Hence, cluster 1 is assigned a set-point to charge at a lower rate while clusters 2 and 3 are discharging at full capacity. The area error increases to 41 kW for case 2. Since the weights for SOC management are higher than tie-flow management for cluster 1, the area error increases only by a small magnitude to 1.2 kW, and no significant difference is observed in the tie-flows.
- Extremely low SOC Case (Cluster): The SOC level of cluster 1 reduces down to the lower threshold of 0.1. Hence, cluster 1 is assigned a set point to charge at total capacity. The functionalities of area reference tracking are disabled for cluster 1. To minimize the impact of cluster 1 charging at the rated capac-

ity, cluster 2 and cluster 3 are assigned the set-points to discharge at the full capacity.

- Extremely low SOC Case (Grid): The SOC level of cluster 1 and cluster 2 reduces to 0.1. Also, the overall storage level of the grid is below 25% for Case 4. Hence, clusters 1 and 2 are set to charge at the rated capacities. The impact of the high charging on the area reference is minimized by cluster 3 by discharging at full capacity. Since the tie-flow management is automatically disabled (because of lower priority), there is no variation in the tie-flows of case 4 and case 9.
- Unbalanced SOC: The SOC level of cluster 1 is 0.8 (overly-charged), cluster 2 is 0.1 (lower threshold), and cluster 3 is 0.3 (normal operating range). All clusters track the area reference accurately without tie-flow management (Case 5). With Tie-flow minimization (Case 10), the area error increases to 29.7 kW, and the tie-flow error reduces from 34 kW to 22.7 kW.

With the same system configuration (BESS ratings and 3 clusters), the effect of area control was quantified through 1000 random scenarios of area set-points and SOC values of three clusters. Figure 5.3 to Figure 5.4 shows the results from area control without Tie-line flow minimization. System SOC significantly impacts the BESS support capabilities. The cluster set-point restores the state of charge whenever the BESS is depleted or over-charged. Figure 5.3 shows the variation in the area error for different SOC levels of the system. The system SOC level suggests the average SOC of all clusters. The area error is significantly reduced for the cases with the system SOC between 0.3 and 0.7. The area error gradually increases for the SOC below 0.3 and beyond 0.7. The operational bandwidth for tracking the area reference is between 0.2 and 0.8. Hence, the clusters start SOC restoration for any cases with system SOC below or above 0.2. As a result, the area error increases for these cases.

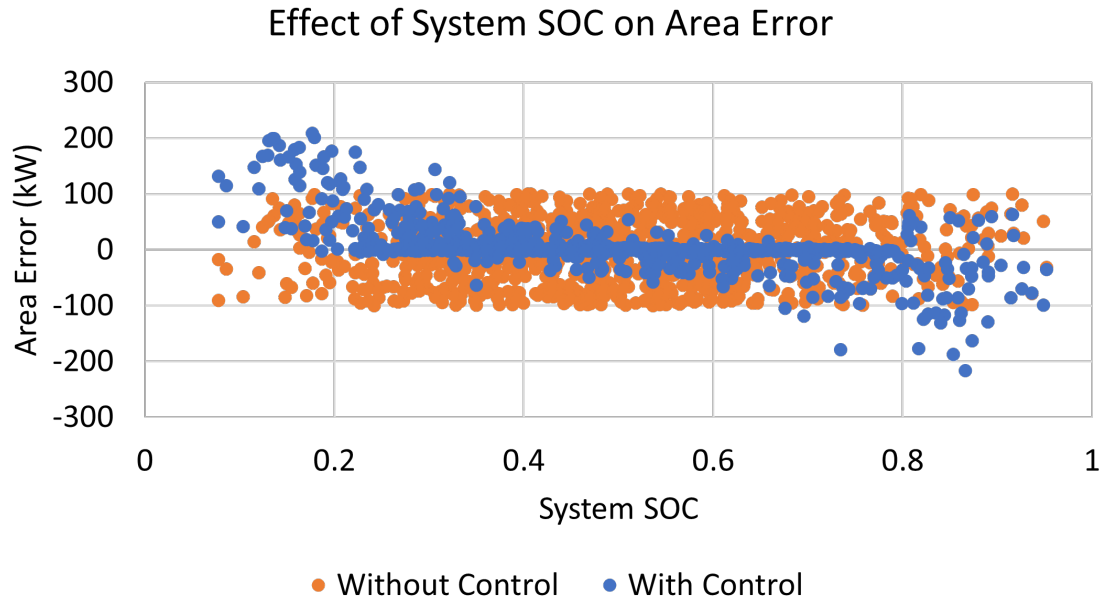


Figure 5.3: Effect of system SOC on area error

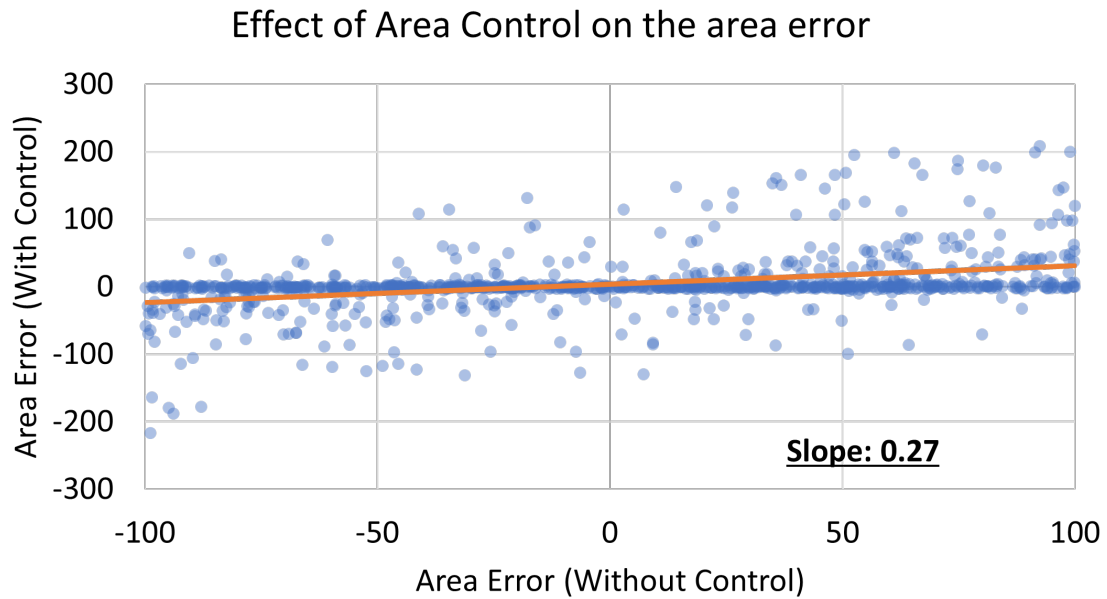


Figure 5.4: Effect of area control on area error

Figure 5.4 shows the effectiveness of area control in reducing the area error. The slope of the regression line indicates 73% reduction in the area error. The higher density of the points near  $y = 0$  shows the effectiveness of the area control in reducing

the area error. The reduction in area error is further quantified through the error distribution plots. Figure 5.5 shows the error distribution without area control. Since the scenarios are randomly generated, the 100 scenarios are equally distributed for the area errors between -100 to 100 kW. Every bin of 10kW width has anywhere between 40 to 60 scenarios. The figure 5.6 shows the reduction in area error with the area control.  $>65\%$  cases have shifted to the bins with errors between -10kW to 10 kW. Hence, the proposed approach effectively reduces the error below 10 kW for  $>65\%$  of the cases.

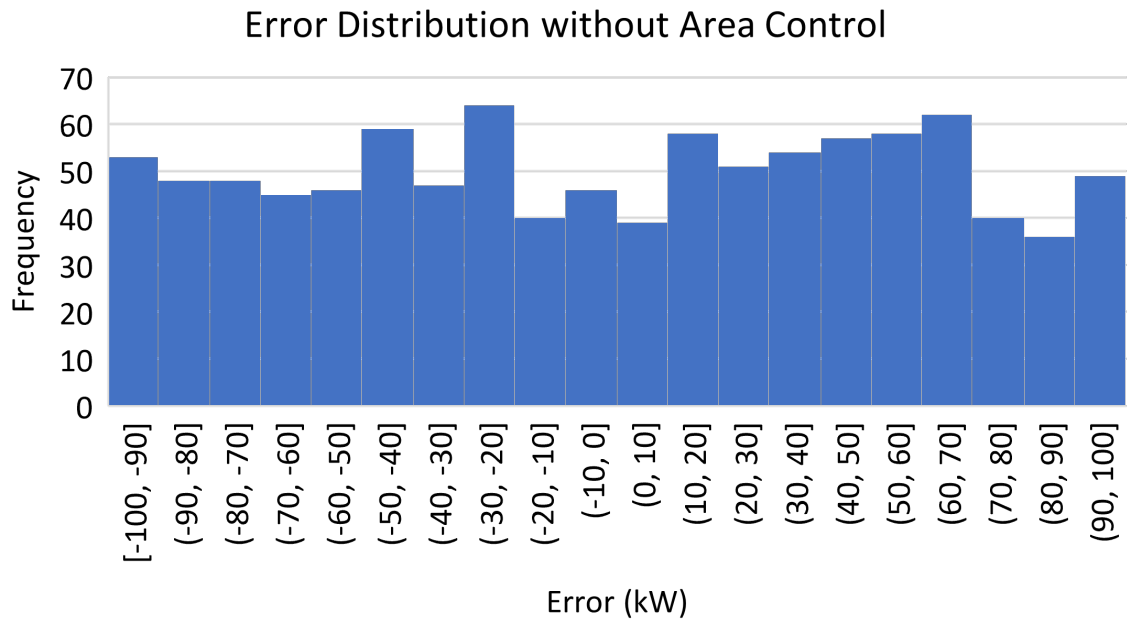


Figure 5.5: Error distribution without area control

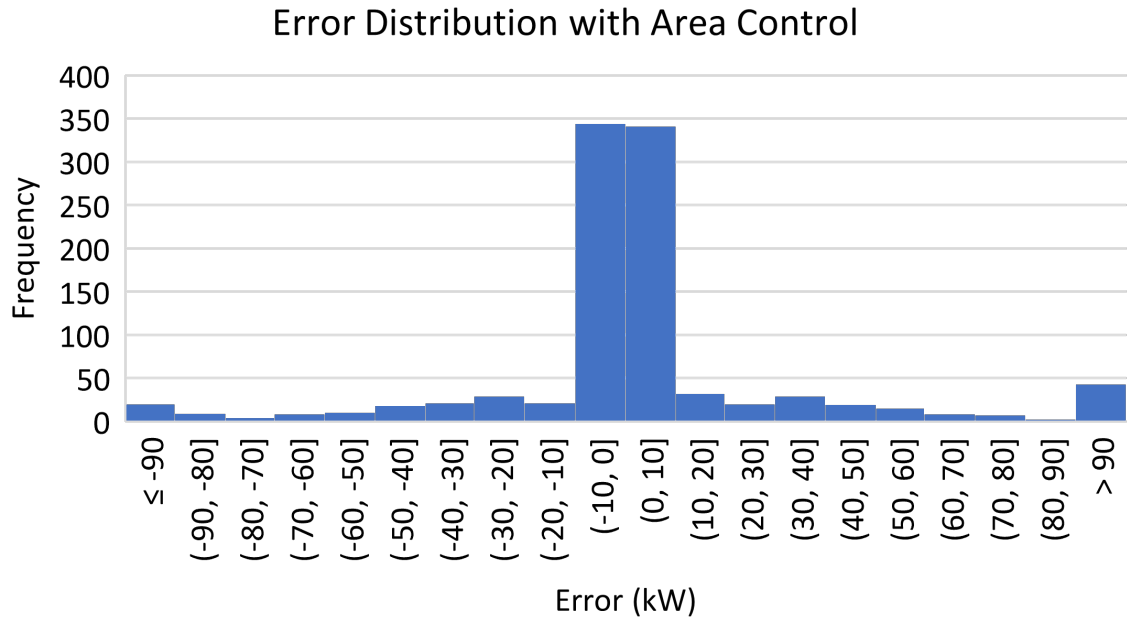


Figure 5.6: Error distribution with area control

Figure 5.7 to 5.8 shows the results from area control along with the tie-line flow minimization. An additional objective in the optimization is expected to impact the efficiency in reducing the area error. Here, the spectral clustering approach is expected to identify the balanced clusters, whereas the area controller may help maintain the load and generation balance within the clusters by minimizing the netload. Figure 5.7 shows the variation in the area error for different SOC levels of the system. The area error is reduced for the cases with the system SOC between 0.3 and 0.7. However, the reduction in the area error is not as efficient as in use-case 1. The area error gradually increases for the SOC below 0.3 and beyond 0.7. The operational bandwidth for tracking the area reference is between 0.2 and 0.8. Hence, the clusters start SOC restoration for cases with system SOC below 0.2 or above 0.2. For the boundary cases, the tie-line flow minimization is automatically disabled by the reduced weights in the objective function, and hence the area error is comparable to use case 1.

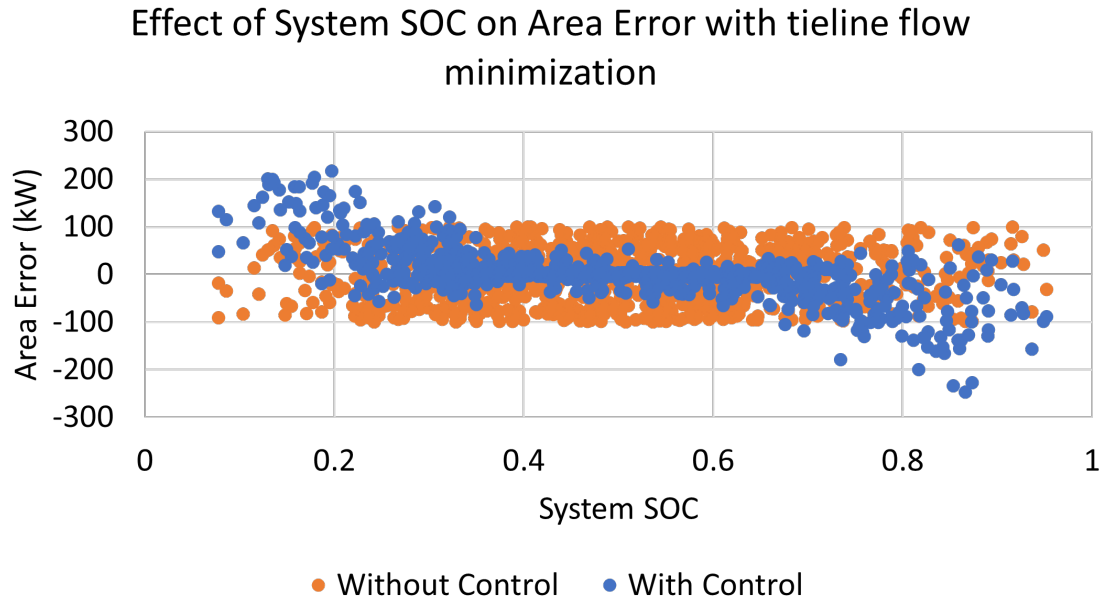


Figure 5.7: Effect of system SOC on area error with tie-line flow minimization

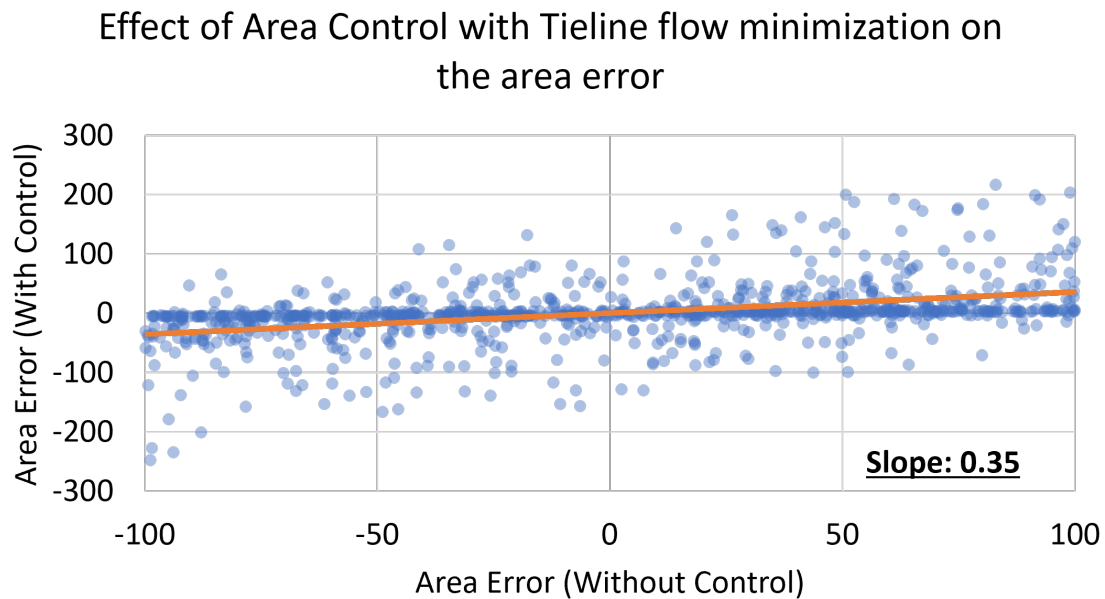


Figure 5.8: Effect of area control with tie-line flow minimization on the area error

Figure 5.8 shows the effectiveness of the area control in reducing the area error along with the tie-line management. The slope of the regression line indicates a 65% reduction in the area error. The reduction in area error is further quantified through

the error distribution plots. Figure 5.9 shows the reduction in area error with the area control.  $>50\%$  cases have shifted to the bins with errors between  $-10\text{kW}$  to  $10\text{kW}$ . More than  $80\%$  cases show the area error reduction between  $-50\text{kW}$  and  $50\text{kW}$ .

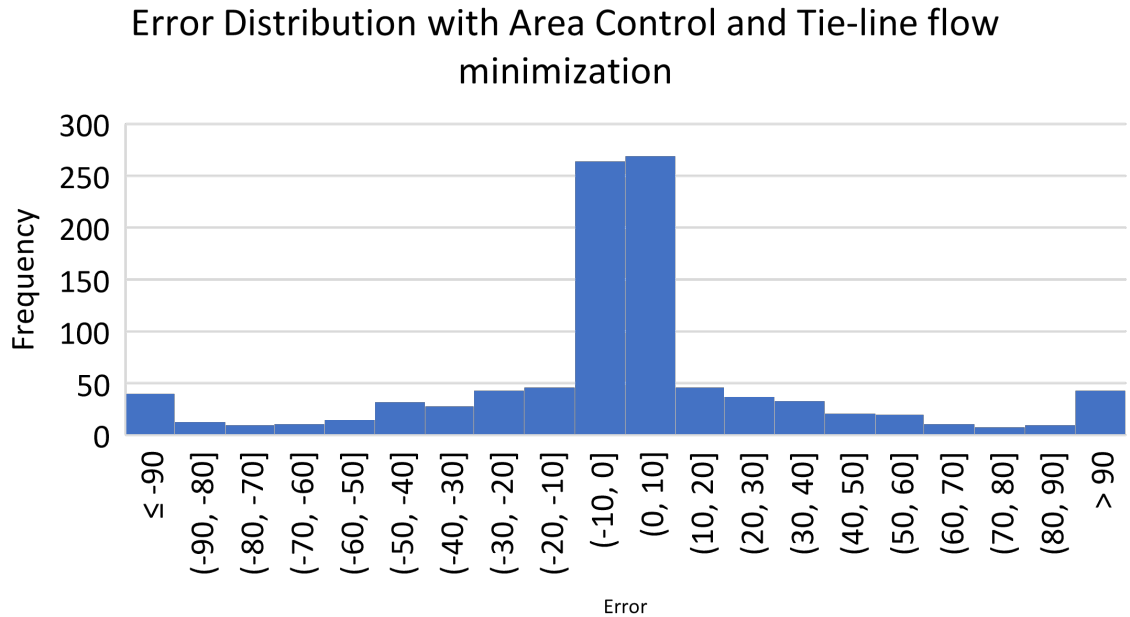


Figure 5.9: Error distribution with area control and Tie-line flow minimization

Figure 5.10 and figure 5.11 shows the distribution of the tie-line flow for use case 1. The average tie-line flow without the net-load minimization is  $47\text{ kW}$ . With the net-load minimization, the average tieflow gets reduced to  $41\text{ kW}$ . The reduction tie-line flow can be improved by increasing the corresponding weight of the local objective function in equation 5.11. However, added objective to minimize the tie-flow would impact the area error. Also, the distribution grid's re-clustering will identify the balanced clusters, if required. The proposed approach is intended to maintain the balance among the clusters while reducing the area error.

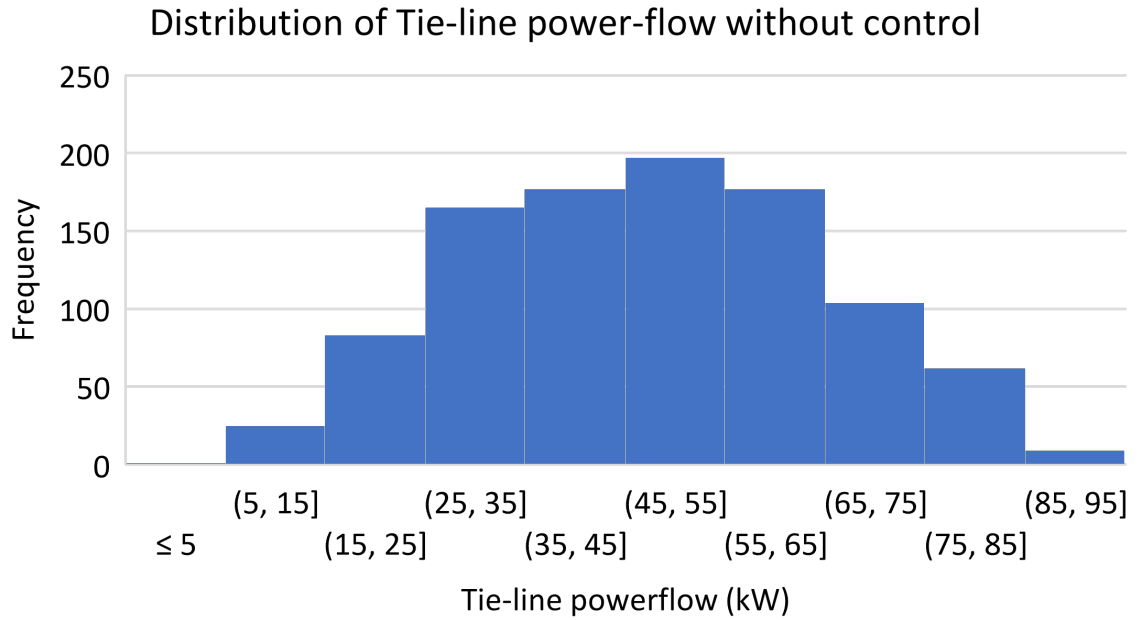


Figure 5.10: Distribution of tie-line flow without control

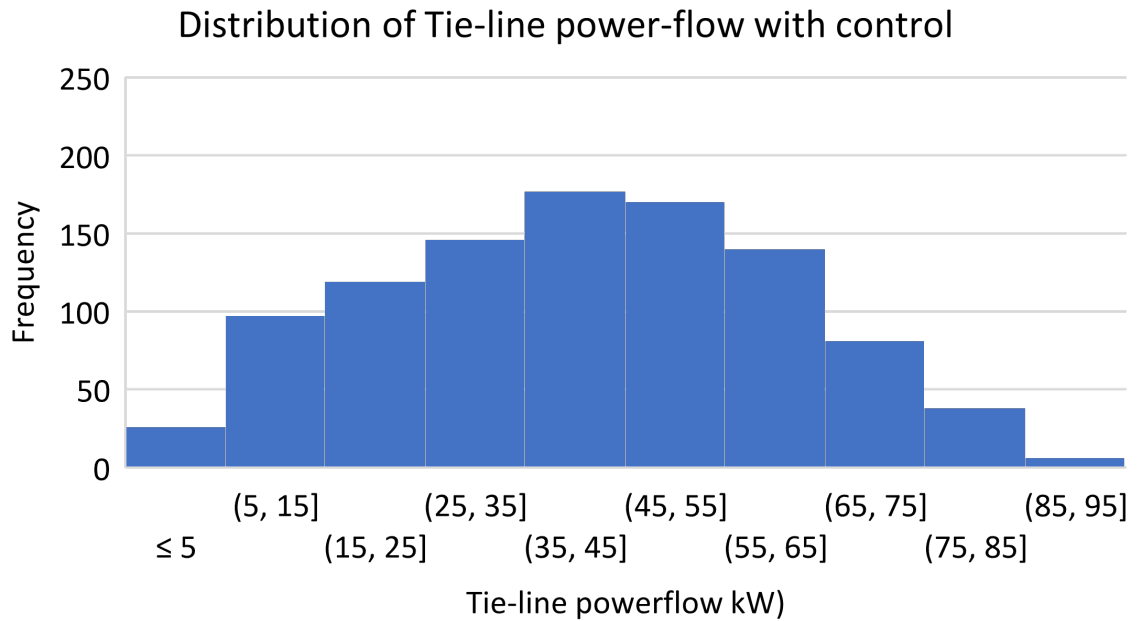


Figure 5.11: Distribution of tie-line flow with control

#### 5.4 Reference set-point tracking

The ADMM based sharing algorithm provides the reference for each cluster based on the area error set-points. The cluster reference is calculated at a higher time res-

olution than the cluster control set-points to avoid the haunting among the controls. The cluster control set-points are calculated to the least square estimation approach for every cluster based on the cluster references. The objective function of the least square estimation is given by:

$$\min U = \sum_{t=T-\Delta t}^T \frac{1}{2} (P_{nl}(t, k) * x(t, k) - P_{nl}^{ref}(t, k))^2 \quad (5.15)$$

Every BESS within the cluster is charging or discharging at a different rate. If the cluster control time resolution is  $Tc$  and the ramp-rate limitations for BESS  $bess(i)$  for cluster  $k$  is  $\zeta_{bess(i)}$ , the total ramp rate limitations for the cluster  $k$  is given by:

$$\zeta_c(k) = \sum_{i=1}^N \zeta_{bess(i)} \quad (5.16)$$

Based on the ramp rate limitations of the cluster, the constraint of the lease square estimation is formulated as

$$\frac{(-\zeta_c(k) - P_{nl}(t-1) + P_{nl}^{ref}(t))}{P_{nl}(t-1, k)} \leq x \leq \frac{(\zeta_c(k) - P_{nl}(t-1) + P_{nl}^{ref}(t))}{P_{nl}(t-1, k)} \quad (5.17)$$

Based on the value of optimization coefficient  $x$ , the change in the cluster dispatch is calculated as:

$$dp(t) = \frac{1}{\Delta t} \sum_{t=T-\Delta t}^T P_{nl} * x(t) - P_{nl}(t-1) \quad (5.18)$$

$$Pset(t) = Pbess_{measured}(t-1) + dp(t) \quad (5.19)$$

The reference set-point tracking is illustrated on a small cluster. The cluster is assumed to have a rated kW support capacity of 100 kW and a total ramp rate limitation of 10 kW/s. The total storage within the cluster is assumed to be 300kWh. The initial SOC is set to 0.5 to understand the effect of the control on the SOC of the storage. The proposed approach is analyzed for two use cases- Net-load balance and Dynamic set-point tracking. To better understand the impact of the control time

resolution on the reference tracking, the three-time intervals - 5s, 30s, and 60s are analyzed for each use case.

- Net-load Balance: The use case demonstrates the local load support capability of the control architecture. The cluster net-load reference is zero, indicating a perfect balance of load and generation within the cluster. Figure 5.12 shows the tracking performance of the cluster control simulated for  $>2.5$  hours. The net load without control shows both PV and load intermittencies within the cluster. High intermittencies between 0 and 2000 seconds indicate the tripping of PVs. The control at lower time resolution offers granular tracking, especially during the intermittencies. The table 5.2 shows the root mean square error for the zero reference tracking. For 5-second control time-resolution, the RMSE reduces to 11.26 kW, indicating 71% improvement compared to the net load without control. The SOC variation is similar for all control time resolutions (Figure 5.13).

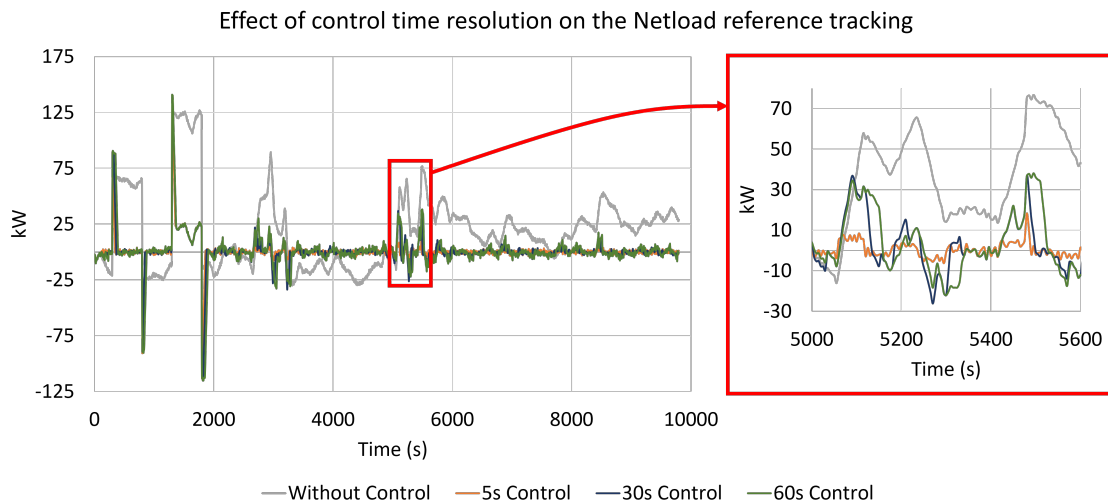


Figure 5.12: Effect of control time resolution on the Net-load reference tracking

Table 5.2: Effect of control time-resolution on the tracking error

Use Case 1		
Without Control	39.6 kW	
Time Resolution	RMSE With Control	% Improvement
5s	11.3 kW	71.5%
30s	14.5 kW	63.4%
60s	17.7 kW	55.1%

Use Case 2		
Without Control	39.3 kW	
Time Resolution	RMSE With Control	% Improvement
5s	18.2 kW	53.7%
30s	22.4 kW	43.0%
60s	26.5 kW	32.4%

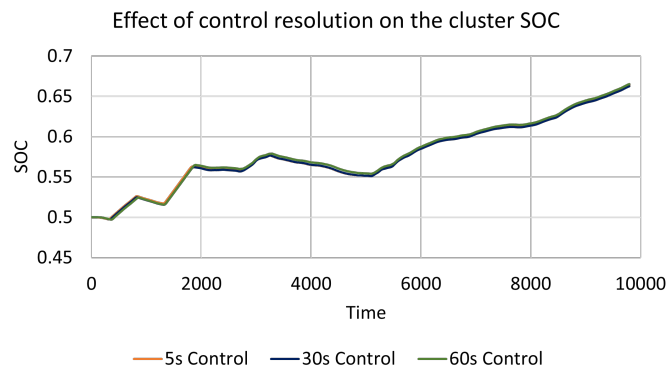


Figure 5.13: Effect of control resolution on the cluster SOC

- **Dynamic setpoint tracking:** This use case demonstrates the tracking capability of dynamically varying external setpoint. The cluster set-load reference is generated every 500 seconds based on the local net-load envelope. The figure 5.14 shows the tracking performance of the cluster control simulated for >2.5 hours. The setpoint changes from 0 to 75 kW at 5500s. It takes 220 seconds for the cluster BESS to change the dispatch from -80kW to 50 kW. The higher setting time is primarily because of the net load, which gradually decreases from 70 kW to 20 kW. Table 5.2 shows the root mean square error for the set-point tracking.

For 5-second control time-resolution, the RMSE is 18.19 kW and increases for the control at lower time resolution. The SOC variation is similar for all control time resolutions.

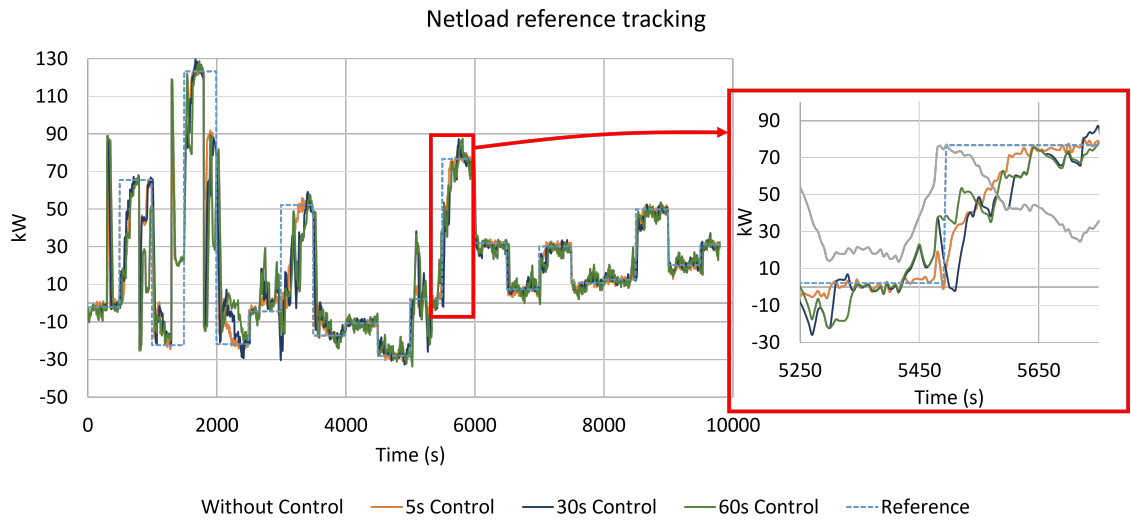


Figure 5.14: Effect of control time resolution on netload reference tracking

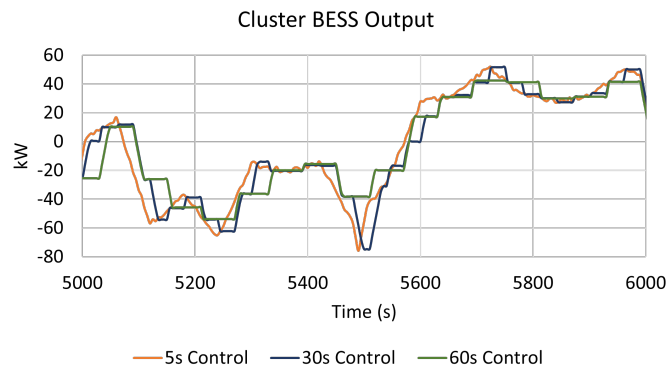


Figure 5.15: BESS output for control at different time resolution

## 5.5 Implementation: IEEE 123 bus system

The proposed approach of set-point tracking and ADMM based area controller set-point sharing is demonstrated on IEEE 123 bus system with DERs. The DER ratings and locations and the load and PV profile are discussed in chapter 4. The proposed control is implemented in an OpenDSS based co-simulation environment.

The ADMM based area control and set-point tracking algorithms are implemented as a Matlab function. The python based controller script executes the proposed algorithm periodically. The cluster set-point tracking is performed at a 5-second resolution, and the area control-based set-point sharing is performed every 5 minutes.

The proposed approach is demonstrated through following case studies.

- Use case 1: Dynamically varying area set-points:
- Use case 2: Net-load minimization:

#### 5.5.1 Use case 1: Dynamically varying area set-points.

Here, the set-points are provided to the area controller for tracking. Figure 5.16 shows the feeder-head power-flow without control and the set-points to track at the feeder-head. The proposed approach shares the set-points among the clusters based on the BESS state of charge and tie-line flows. The cluster control is implemented for static and dynamic clusters. Figure 5.16 shows the feeder-head power-flow tracking the set-points. Figure 5.17 compares the tracking error for both- constant and dynamic cluster configuration. The RMSE tracking error for dynamic cluster control is 72 kW, and for the constant cluster, control is 73kW. The cluster control reduces the overall error from 238.8 kW to 73 kW. Table ?? summarizes the tracking error at the cluster level for both static and dynamic control. Figure 5.19 and figure 5.20 shows the tie-line flow for both control strategies. The tie-line flow is lower for dynamic clusters because of varying cluster configurations.

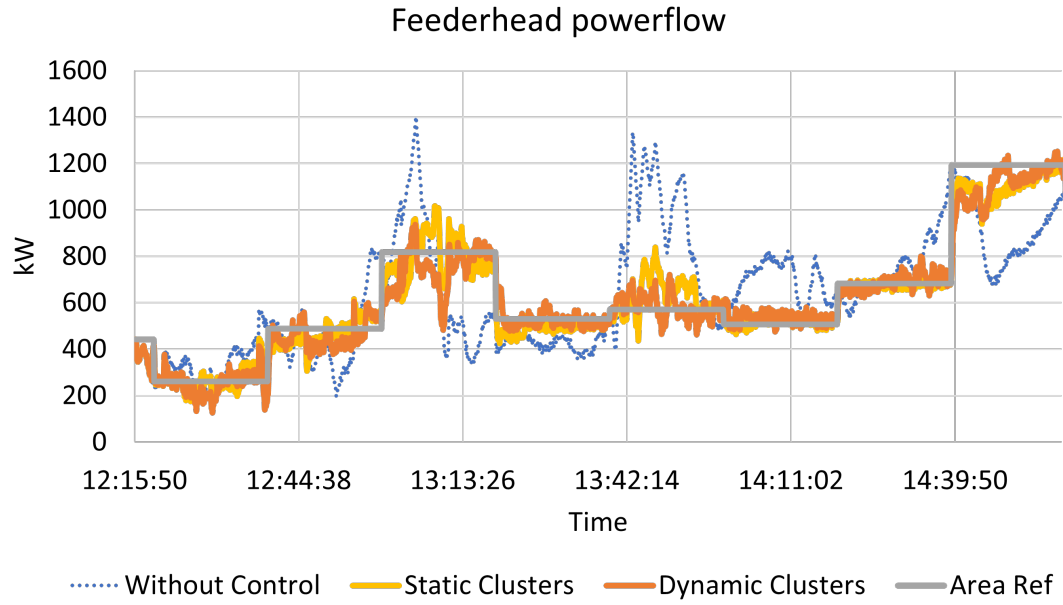


Figure 5.16: Tracking of area controller set-point at feeder-head

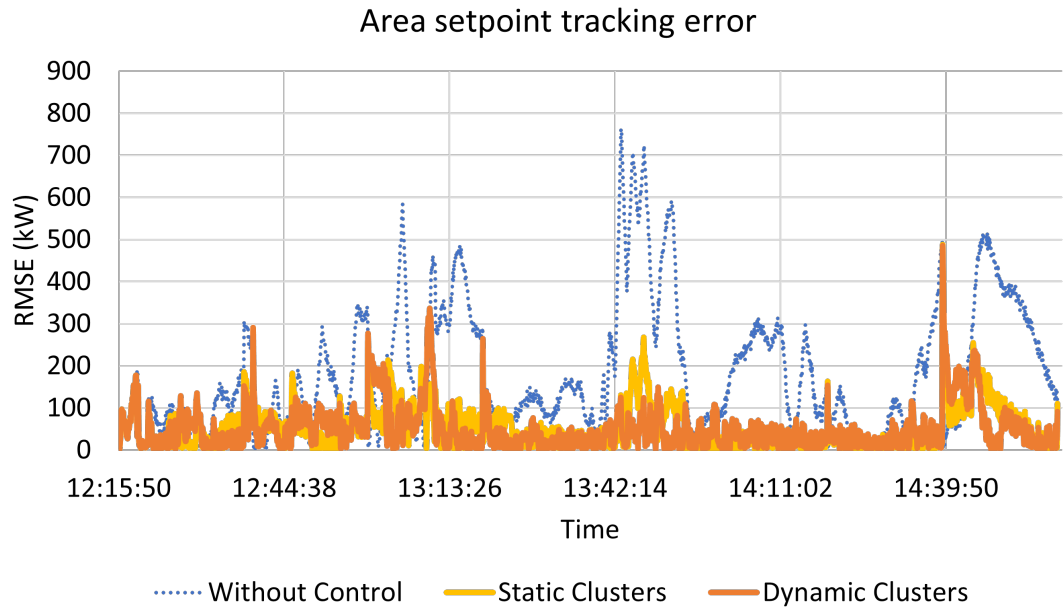


Figure 5.17: Tracking error for static and dynamic cluster control

Table 5.3: Tracking error at cluster level

	Constant Cluster	Dynamic Cluster
Cluster1	30.0	37.4
Cluster2	14.0	16.9
Cluster3	10.2	19.7
Cluster4	31.0	28.8
Cluster5	30.4	37.4
Cluster6	30.2	9.4
Feeder-head	73.1	72.6

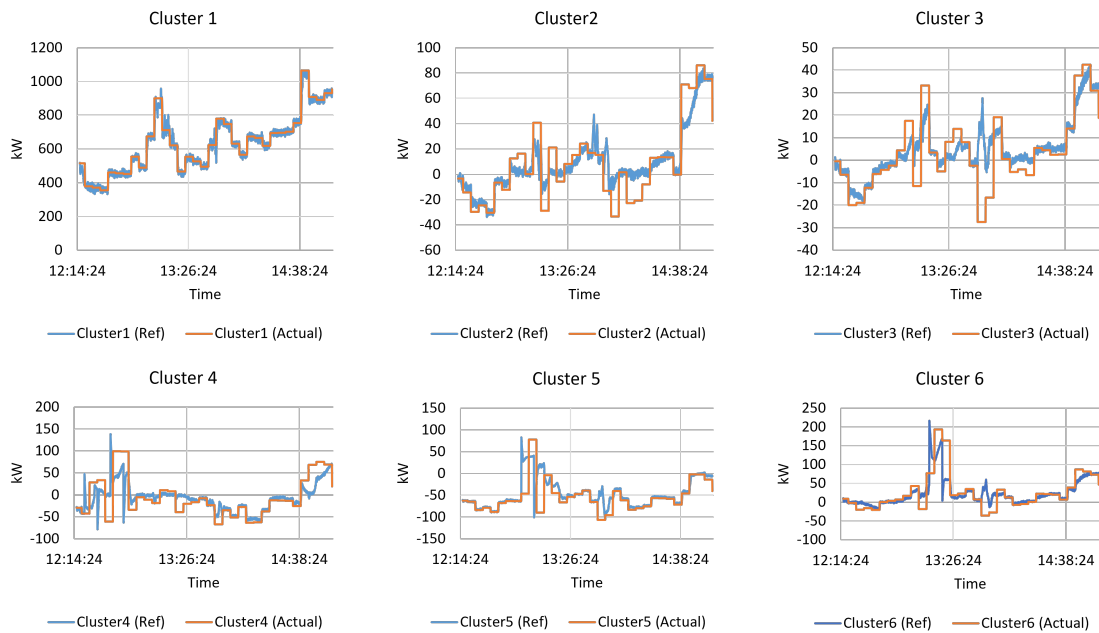


Figure 5.18: Area set-point sharing at tracking at cluster level

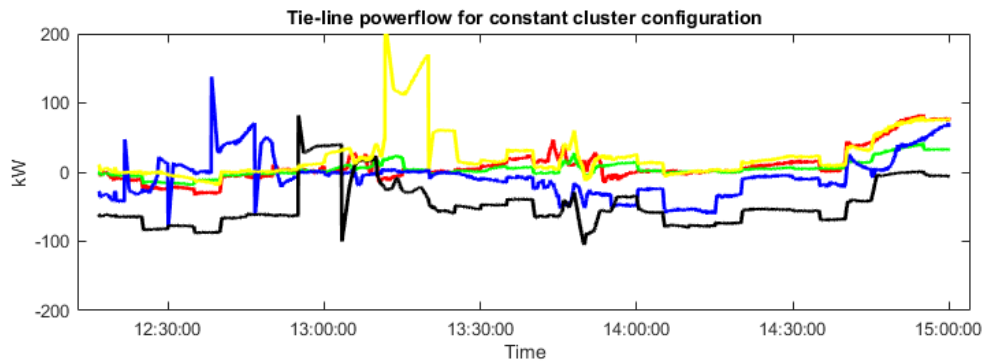


Figure 5.19: Tie-line power-flow for constant cluster configuration

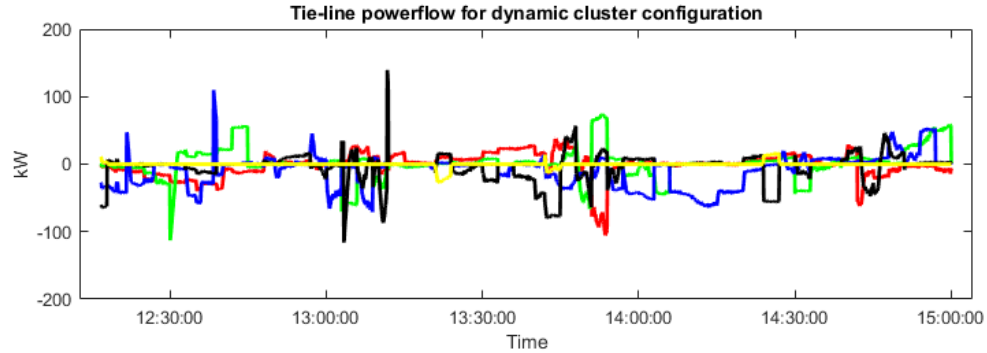


Figure 5.20: Tie-line power-flow for dynamic cluster configuration

### 5.5.2 Use case 2: Net-load minimization

Here, the feeder-head reference is set to zero. The use case aims at supporting the loads on the feeder through local DER generation. Here, the use case is intensive in terms of BESS's support requirements. The use case also establishes the groundwork for the islanded operation through cluster control discussed in chapter 7. Here, the BESS is required to support the dedicated clusters' local load. The area controller distributes the set-points to each cluster based on the approach discussed in this chapter. By supporting the loads within the clusters, the net load of the feeders tracks the zero reference. Figure 5.21 shows the overall of the feeder tracking the zero reference. Since the BESS KW requirement is substantially high for net-load minimization purposes, the SOC depletes over time, limiting the use case demonstration to only a few hours. Figure 5.22 shows the envelope of BESS state of charge. One of the clusters has a higher PV generation than the load. Hence, the BESS belonging to that cluster charges to make net-load at cluster level equal to zero. 70% is set as an upper threshold, after which the BESS from the cluster with additional generation starts contributing at the feeder level in reducing the overall tracking error.

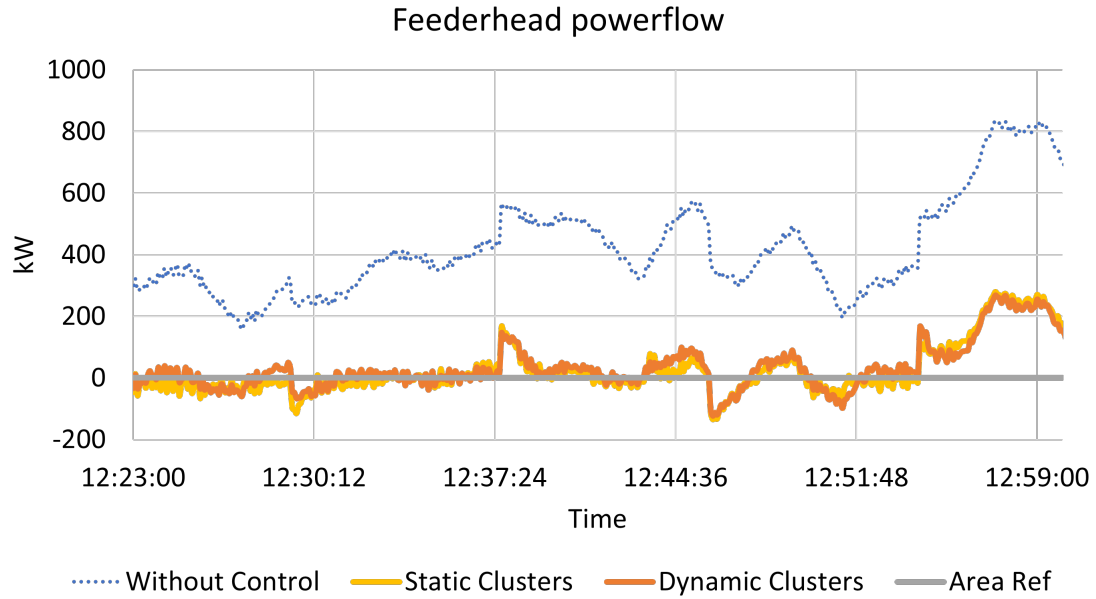


Figure 5.21: Feeder head powerflow for net-load minimization

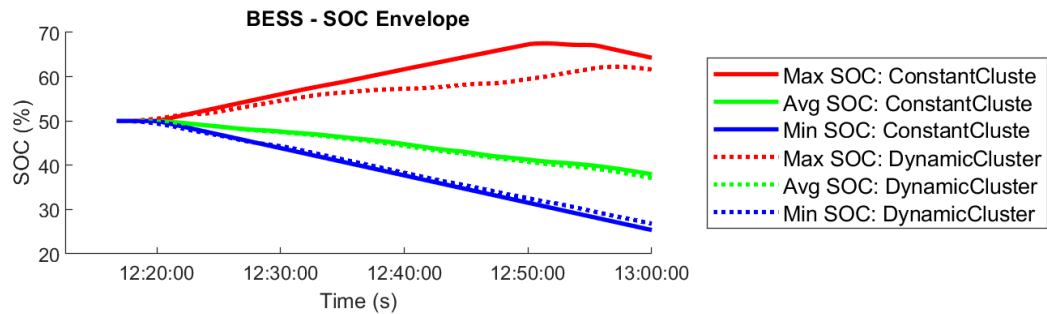


Figure 5.22: Variations in BESS SOC during net-load minimization application

## 5.6 Chapter Summary

The chapter proposes an ADMM based sharing approach for distributing the feeder-head setpoints provided by the area controller among the cluster. Along with the tracking error at the feeder-head, the cluster SOC level and the tie-line power flows are also included in the local objective function of the ADMM based sharing optimization. The chapter also proposes modifying the cluster control approach presented in the previous chapter to track the cluster reference setpoints. The proposed approach is implemented on IEEE 123 bus system for two use-cases: Area controller reference

setpoint tracking and Feeder net-load minimization.

CHAPTER 6: Model predictive control approach for DER clusters in power distribution system

6.1 Introduction

Model predictive control is often used to control dynamic systems where predictions can further improve the tracking accuracy. The previous chapter proposed an approach of ADMM based sharing of the set-points and a least square estimation-based approach to track the set-points. The least-square estimation-based approach is further improved in this chapter to work as an optimizer for the model predictive control. Figure 6.1 shows the complete control architecture for the cluster-based control along with the implementation of the model predictive control.

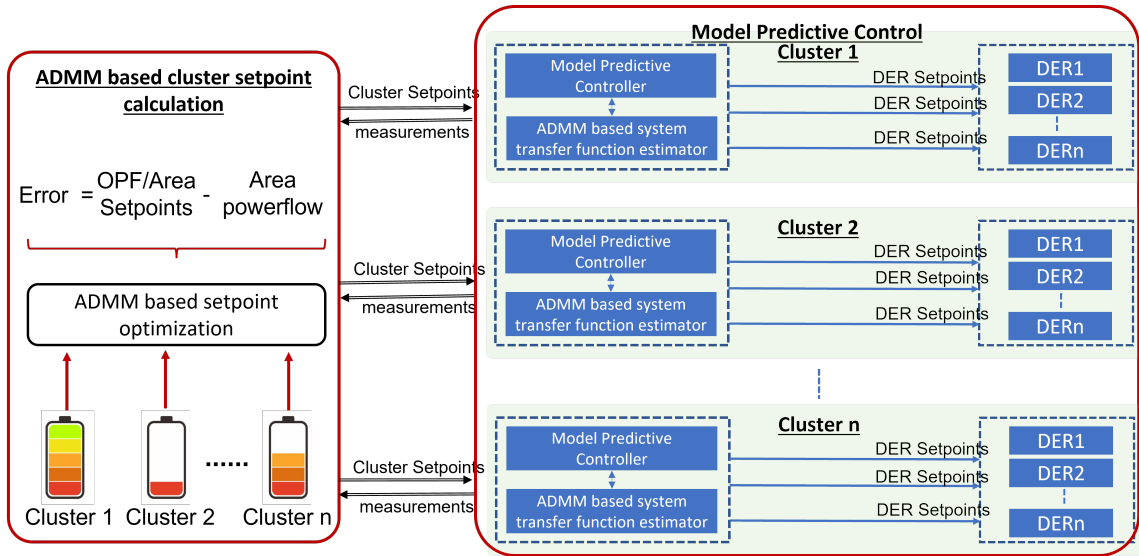


Figure 6.1: Cluster control architecture

Section 6.2 introduces the model predictive control application for controlling the cluster net-load. Section 6.3 discusses an ADMM based approach for estimating the plant model at the given operating state based on the measurements. Section 6.4

provides the theoretical formulation of the MPC optimizer. Section 6.5 discusses the results of implementing the complete control architecture on the 650 bus system.

## 6.2 Model Predictive Control

Model predictive control is a widely used advanced control technique for multiple variable systems. If a dynamic model of the system is available, optimized input variables can be calculated based on past measurements and predict their impact on the output.

The input variables to MPC are classified into three types:

- **Manipulated Variables:** Manipulated variables are the input variables to the system that can be changed. In cluster control applications, the BESS set-points are the manipulated variables.
- **Measured Disturbance:** The system inputs that can not be altered are the measured disturbance. The critical load measurements may be available from the field; however, they are not controlled externally through any set points. Hence the measured load can also be considered as the measured disturbance.
- **Unmeasured Disturbance:** Not all the loads on the system are measurable. Also, the losses in the distribution system can not be measured. Since direct measurements are not available for these variables, they are known as unmeasured disturbances.

The output variables are also known as the control variables. The control variable captures the interaction between the manipulated variables and the system disturbances. In the current work, the cluster net-load is considered as the control variable in the proposed application.

Figure 6.6 shows the MPC based cluster control architecture. The MPC-based control framework is primarily comprised of two components: System Identifier and

Optimizer. The system identifier is responsible for estimating the system's state based on the measurements. An optimizer calculates the optimum set-point values for the control of the clusters. The system model estimated by the system identifier is used to predict the system behavior and optimize the future set-points based on the predictions. The following section discusses the formulation of system identifiers and optimizers in detail for the cluster control application.

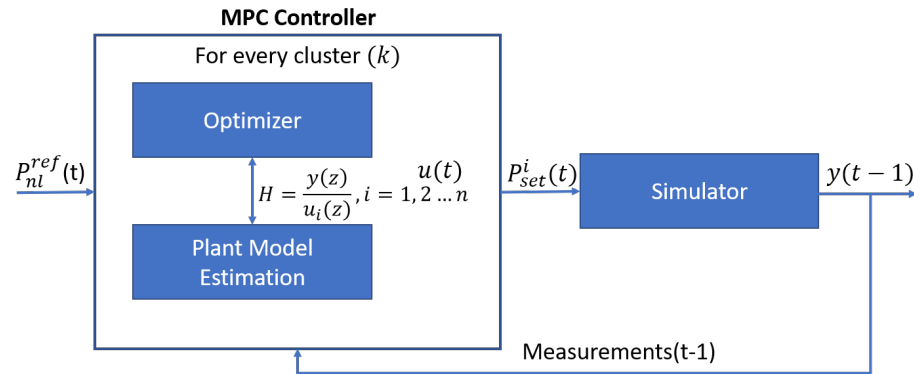


Figure 6.2: MPC based cluster control

### 6.3 Theoretical Formulation: Plant Model Estimator

The success of the MPC framework depends on the accuracy of the plant model. An inaccurate model or unstable model can worsen the system's operating condition. The predictions are performed using a dynamic model. Although a distribution system is non-linear, modeling a non-linear system is analytically and computationally intensive. Hence, the measurements are used to linearize the system operation at the specific operating condition. MPC approaches typically prefer the line, empirical models as a multi-variable version of the step response or difference equation models.

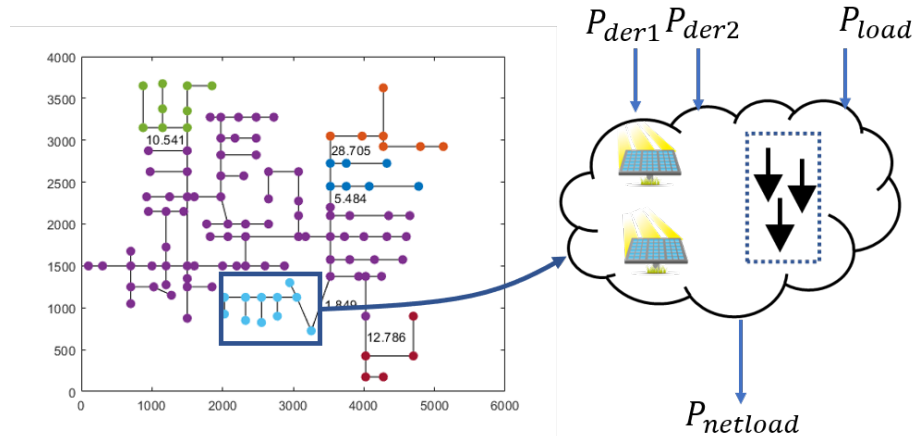


Figure 6.3: Representation of the cluster as a system

Current research proposes an ADMM based estimation of the transfer functions. Chapter 5 proposed the application of ADMM based approach for solving the sharing problem. The same approach is used for solving a consensus problem in this chapter. The figure 6.3 shows the cluster as a local system with inputs and outputs. The net load within the cluster is a linear combination of load, PV, losses, and BESS output. BESS and PVs are inverter-based resources. Hence, all inverter-based resources contribute to the overall dynamics of the system. The measurements are available for all PVs, storage, and measured loads. Hence the cluster system can be modeled as a multiple input single output system. The inputs of the MISO system are classified into a manipulated variable (all BESS), measured noise (Load and PV), and unmeasured noise (losses and unmeasured loads). Considering the futuristic scenario of the potential field application, it is fair to assume that the measurements from all loads are available. Hence, all PVs and loads can be aggregated as the total measured noise on the system. The set-points provided to the individual BESS acts are the only manipulated variables within the clusters.

A MISO system with inputs  $u_1, u_2$ , and  $u_3$  and output  $P_1$  can be represented as

$$\begin{bmatrix} P_1(z) \end{bmatrix} = \begin{bmatrix} G_{11}(z) & G_{12}(z) & G_{13}(z) \end{bmatrix} \begin{bmatrix} u_1(z) \\ u_2(z) \\ u_3(z) \end{bmatrix} \quad (6.1)$$

Here  $G(z)$  are the transfer functions mapping the individual inputs to the output.

The individual transfer functions can also be represented as:

$$G_{11}(Z) = \frac{P_1(z)}{u_1(z)} = \frac{b_1^1 z^{-1} + b_2^1 z^{-2} + \dots + b_k^1 z^{-k}}{1 + a_1^1 z^{-1} + a_2^1 z^{-2} + \dots + a_k^1 z^{-k}} \quad (6.2)$$

$$G_{12}(Z) = \frac{P_1(z)}{u_2(z)} = \frac{b_1^2 z^{-1} + b_2^2 z^{-2} + \dots + b_k^2 z^{-k}}{1 + a_1^2 z^{-1} + a_2^2 z^{-2} + \dots + a_k^2 z^{-k}} \quad (6.3)$$

$$G_{13}(Z) = \frac{P_1(z)}{u_3(z)} = \frac{b_1^3 z^{-1} + b_2^3 z^{-2} + \dots + b_k^3 z^{-k}}{1 + a_1^3 z^{-1} + a_2^3 z^{-2} + \dots + a_k^3 z^{-k}} \quad (6.4)$$

Equation 6.2-6.4 can also be represented in the least square format as follows:

$$\begin{bmatrix} L_1 & M_1 \end{bmatrix} \begin{bmatrix} a^1 \\ b^1 \end{bmatrix} = \begin{bmatrix} B_{11} \end{bmatrix} \quad (6.5)$$

$$\begin{bmatrix} L_2 & M_2 \end{bmatrix} \begin{bmatrix} a^2 \\ b^2 \end{bmatrix} = \begin{bmatrix} B_{21} \end{bmatrix} \quad (6.6)$$

$$\begin{bmatrix} L_3 & M_3 \end{bmatrix} \begin{bmatrix} a^3 \\ b^3 \end{bmatrix} = \begin{bmatrix} B_{31} \end{bmatrix} \quad (6.7)$$

$a$  : is vector of denominator coefficients ,  $a^1 = a^2 = \dots = a^4 = z$

$b$  : vector of numerator coefficients

$L$  : is matrix of previous samples of  $P_m$

$M$  : is matrix of current and previous samples of  $u_n$

For a MISO system, the denominator of all transfer functions need to be equal. Hence, the objective here is to make  $a^1 = a^2 = \dots = a^4 = z$ . The objective function for the global consensus problem is represented as:

$$\underbrace{Min}_{a^1, \dots, a^q, z} \sum_{q=1}^2 \frac{1}{2} \left\| \begin{bmatrix} L^q \\ a^q \end{bmatrix} - \left( \begin{bmatrix} B^q \\ \sum_{i=1}^2 \begin{bmatrix} M^q \\ b^q \end{bmatrix} \end{bmatrix} \right) \right\|^2 \quad (6.8)$$

$$\text{subject to } a^q - z = 0 \quad (6.9)$$

Here,  $z$  is the global consensus solution, that is obtained when the local estimates of all local processors denoted by  $a^q$  reach the same value. The ADMM estimation method uses Augmented Lagrange multiplier approach

$$L_\rho = \sum_{q=1}^2 \frac{1}{2} \left\| \begin{bmatrix} L^q \\ a^q \end{bmatrix} - \left( \begin{bmatrix} B^q \\ \sum_{i=1}^2 \begin{bmatrix} M^q \\ b^q \end{bmatrix} \end{bmatrix} \right) \right\|^2 + w_q^T (a^q - z) + \frac{\rho}{2} \| (a^q - z) \|^2 \quad (6.10)$$

Here,  $a$  and  $z$  are the vectors of the primal variables,  $w$  is the vector of the dual variables.

As discussed in chapter 5, an iteration  $(k+1)$  of ADMM based optimization consists of three steps. The fourth step is added here to update the numerators of the transfer function based on the updated denominators (global variables):

1. Local variable update  $a^{i(k+1)}$ : Updating local variables  $a^{i(k+1)}$ , where  $i = 1, 2, \dots, N_{bess}$  are calculated in parallel.
2. Global variable update  $z^{(k+1)}$ : Requires all updated local variables to calculate

the mean  $z^{(k+1)}$  using equation 6.11

$$z^{(k+1)} = \frac{1}{N_{bess}} \sum_{i=1}^{N_{bess}} a^{i(k+1)} \quad (6.11)$$

3. Dual variable update  $u^{(k+1)}$ : Calculated based on the difference of local variables ( $a^{(k+1)}$ ) and the updated global variable  $z^{(k+1)}$ , as shown in the equation 6.12

$$u^{(k+1)} = u^{(k)} + a^{(k+1)} - z^{(k+1)} \quad (6.12)$$

4. Numerator variable update  $b^{(k+1)}$ : This is an additional step to the ADMM approach. Based on the changes in the denominator coefficients, the numerical variables are re-calculated using the least square approach (Equation 6.13).

$$[M^q][b^q] = [B^q] - [L^q][a^q] \quad (6.13)$$

The approach for the transfer function estimation is validated through the following steps:

- Generate a random  $n^{th}$  order stable system with  $N$  inputs and 1 output in MATLAB.
- Simulate the system with a series of training data with small perturbations.
- Use the output and the input data-set to generate the transfer function of  $m^{th}$  order using the proposed ADMM based approach.
- Validate the step response of the estimated and the simulated system.
- Validate the response of the system with the training data-set.

The validation was performed over a 3rd order system with 3 inputs and 1 output using the above approach. Figure 6.4 compares the actual and the estimated system. The transfer function coefficients of the estimated system and the actual system matches with fair accuracy. The step response and the system response to the training data match with high accuracy.

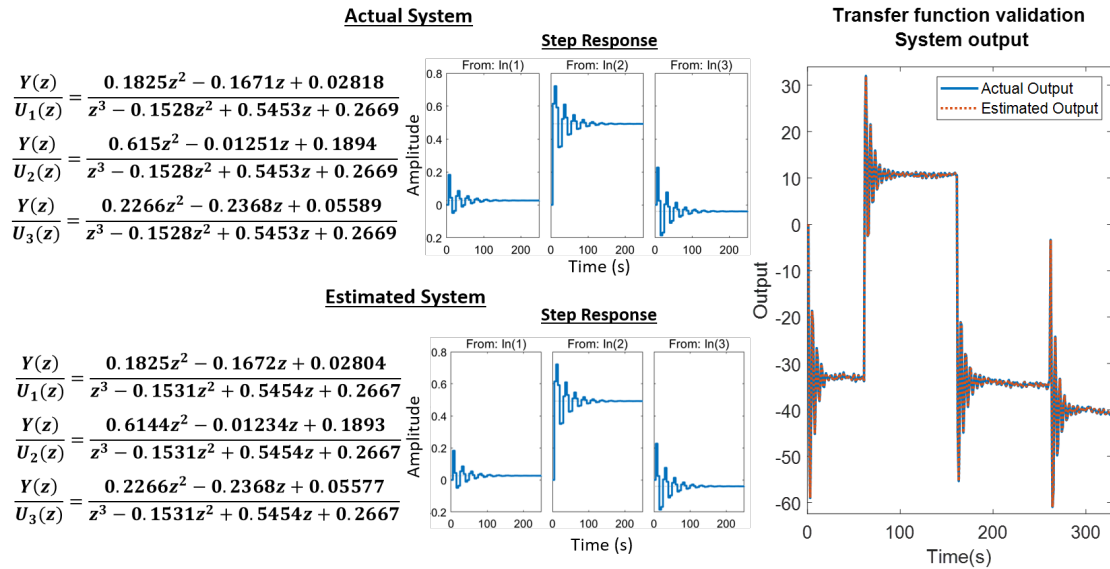


Figure 6.4: Validation of estimated transfer function against the actual system of same order.

An exact order of the distribution system is not known. Hence, a validation is performed for a 10th order system against the 3rd order estimated system. Figure 6.5 compares the step response and the response to the training data for 10th order system and the estimated 3rd order system. The step response does not capture all the oscillation; however, the magnitude and the settling time of the actual and estimated system are the same. The system output of the reduced-order system does not capture the smaller intermittencies in the output. However, the overall output profile closely matches the actual system.

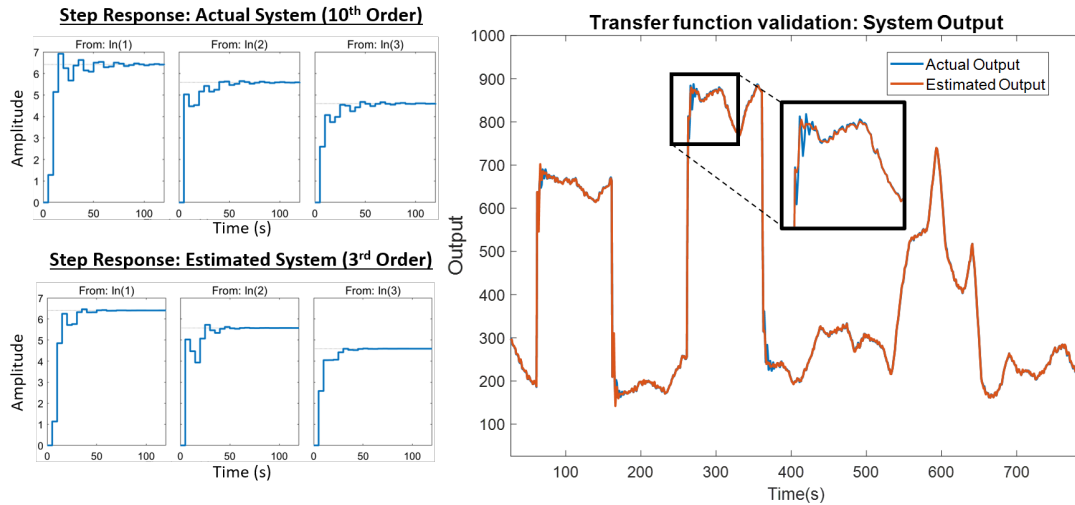


Figure 6.5: Validation of estimated transfer function against the actual system of higher order.

The validation cases prove the system estimation accuracy at a given operating point. If the control is performed at a higher time interval, the transfer functions are expected to capture the dynamics from the distribution system.

#### 6.4 Theoretical Formulation: Optimizer

An optimizer calculates the set-points for the actual system. An optimization for the set-points is performed based on the historical values and the predicted response of the system based on the system model. Figure 6.6 shows the optimizer modelled for the cluster control.

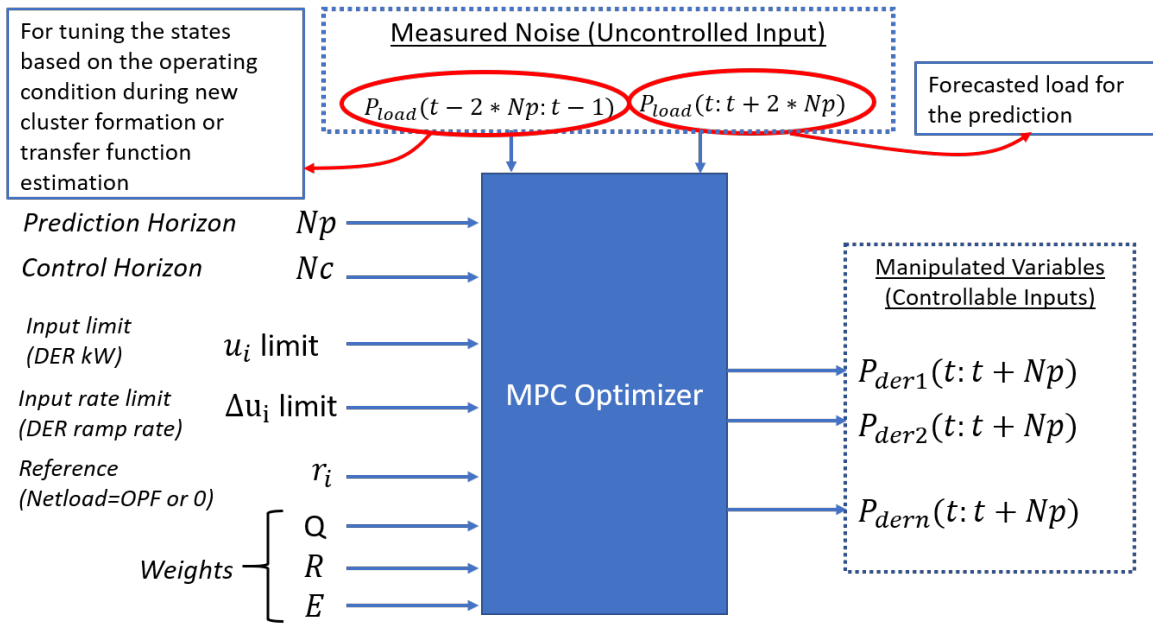


Figure 6.6: MPC Optimizer

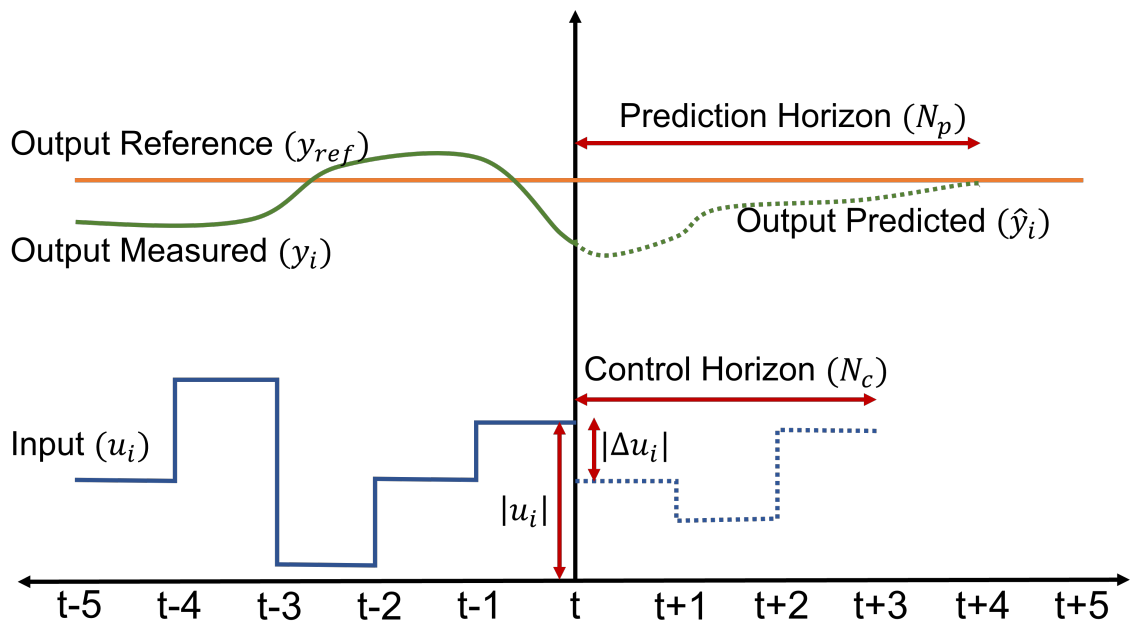


Figure 6.7: Relevance of MPC configuration parameters

The optimizer is configured for the following parameters (also represented in Figure

6.7).

- Prediction Horizon- the future time intervals considered by the optimizer to determine the manipulated variable's setpoints.
- Control Horizon- the setpoints calculated for the future time steps based on the predicted state of the system. The control horizon is kept less than the predicted horizon.
- Input Limit: The constraint limiting the magnitude of the manipulated variable
- Input Rate Limit: The constraint limits the change of the manipulated variable.
- Input Penalty (R): The weight associated with the magnitude of the manipulated variable in the optimizer cost function.
- Input Rate Penalty (E): The weight associated with the variation in the manipulated variable at each time-step in the cost function.
- Output Penalty (Q): The weight associated with the tracking error of the system output.

The reference signal  $r_i$  is provided by the area controller. The input limit is provided based on each BESS's kW rating and ramp rate constraint. If the optimizer calculates the set-point for every control time-step, a smaller value for the  $N_c$  is preferred to reduce the computational burden.

For cluster control application, the objective function for the optimizer can be formulated as:

$$J = \min_{x_N, u_N} \sum_{i=t-N}^t [y(t) - r(t)]^T \cdot Q \cdot [y(t) - r(t)] + \sum_{i=t-n-N}^{t-n} U^T(t) \cdot R \cdot U(t) + \sum_{i=t-n-N}^{t-n} \Delta U^T(t) \cdot E \cdot \Delta U(t)$$

subject to

$$x(t+1) = Ax(t) + Bu(t), t = 0, 1, \dots, N_p - 1$$

$$y(t) = Cx(t), t = 0, 1, \dots, N_p$$

$$y_{min} \leq y(t) \leq y_{max}, t = 0, 1, \dots, N_p$$

$$u_{min} \leq u(t) \leq u_{max}, t = 0, 1, \dots, N_c$$

$$\Delta u_{min} \leq \Delta u \leq \Delta u_{max}, t = 0, 1, \dots, N$$

The objective function consists of 3-sub objectives: Tracking error minimization, Input minimization, and Input rate minimization. A cluster with 2 BESS is used to understand each sub-objective and the effect of weights associated with each sub-objective.

1. Tracking error minimization: The  $r(t)$  is the reference signal provided externally. The area controller provides the reference signal for each cluster. The sub-objective is enforced through the output penalty weight ( $Q$ ). Figure 6.8 shows the tracking performance for different values of  $Q$ . Table 6.1 quantifies the effect of  $Q$  on the tracking error. The tracking is optimal for the  $Q > 5$ . No significant improvement is observed for  $Q > 5$ .

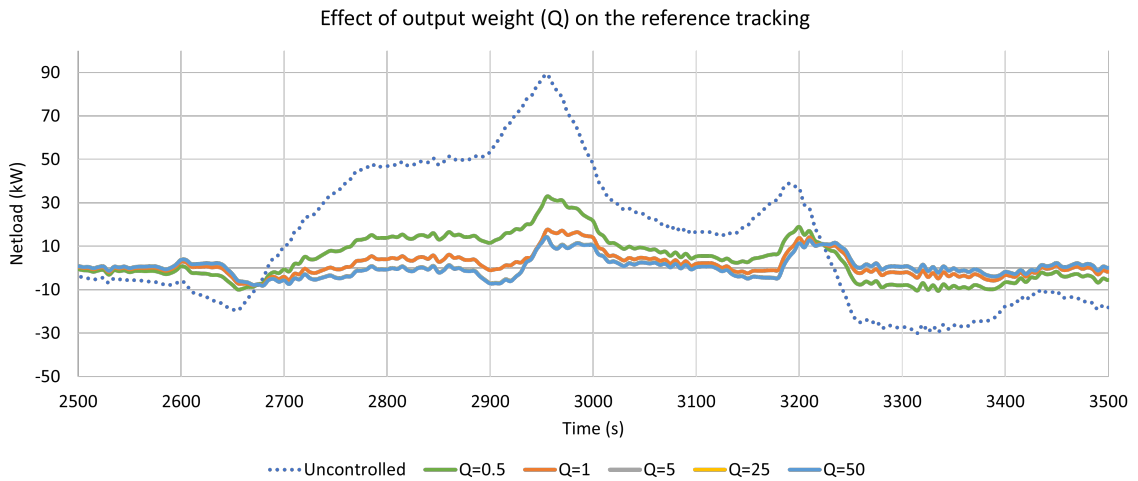


Figure 6.8: Effect of output weight ( $Q$ ) on the reference tracking

Table 6.1: Effect of output weight (Q) on the reference tracking

Q	Error
-	34.2
0.5	11.16
1	5.51
5	4.55
25	4.55
50	4.55

2. Input minimization: The BESS setpoints are the inputs provided for the net-load management. The number of input signals varies based on the controllable DERs within each cluster. MPC framework determines the optimal inputs for each DERs within the clusters. The input penalty weight R is used to penalize the setpoints of each DER. The prioritization of the DERs can also be done by manipulating the input weights associated with a specific DER. Figure 6.9 and figure 6.10 shows the effect of input weights on tracking performance and the SOC level of the storage. Table 6.2 quantifies the effect of R on the tracking error and BESS utilization. The higher weight of the input penalty coefficient would reduce the output/setpoint from the DERs and thereby increase the tracking error. However, the higher weight of Q reduces the depletion of the storage capacity.

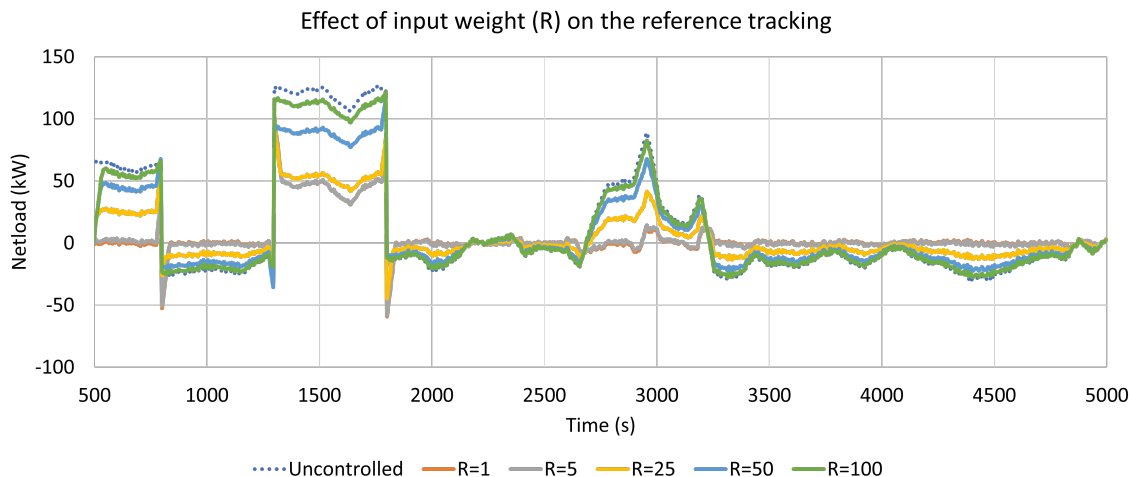


Figure 6.9: Effect of input weight R on the reference tracking

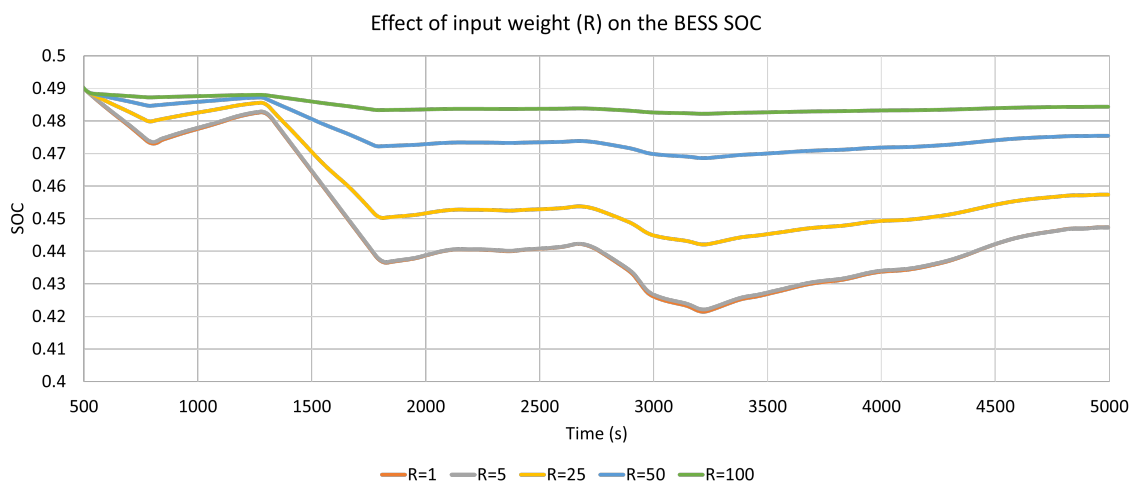


Figure 6.10: Effect of input weight (R) on the BESS SOC

3. Input rate minimization: This sub-objective aims at reducing the variations in set-points of each BESS. The lower variations in the BESS output increase the system stability. Figure 6.11 and 6.12 shows the effect of  $E$  on the tracking error and output variations of the BESS. Table 6.3 quantifies the effect of  $E$  on the tracking error. The input rate penalty weights do not significantly impact

Table 6.2: Effect of input weight (R) on the reference tracking and BESS SOC

R	Error	Minimum SOC
-	34.2	-
1	4.55	0.42
5	4.6	0.42
25	14.46	0.44
50	25.27	0.46
100	31.42	0.48

the tracking error; however, it improves the management of individual DERs to meet the overall goal (Figure 6.12).

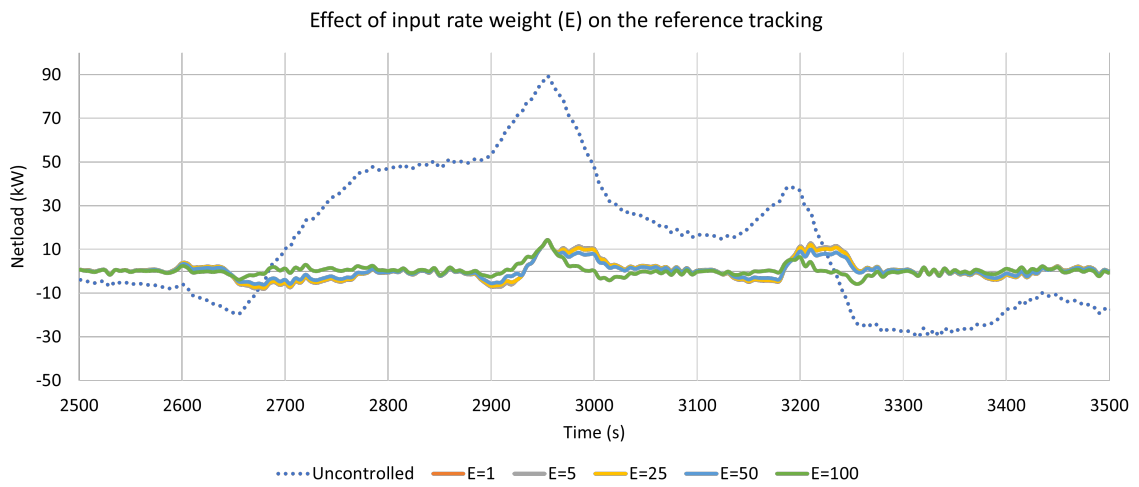
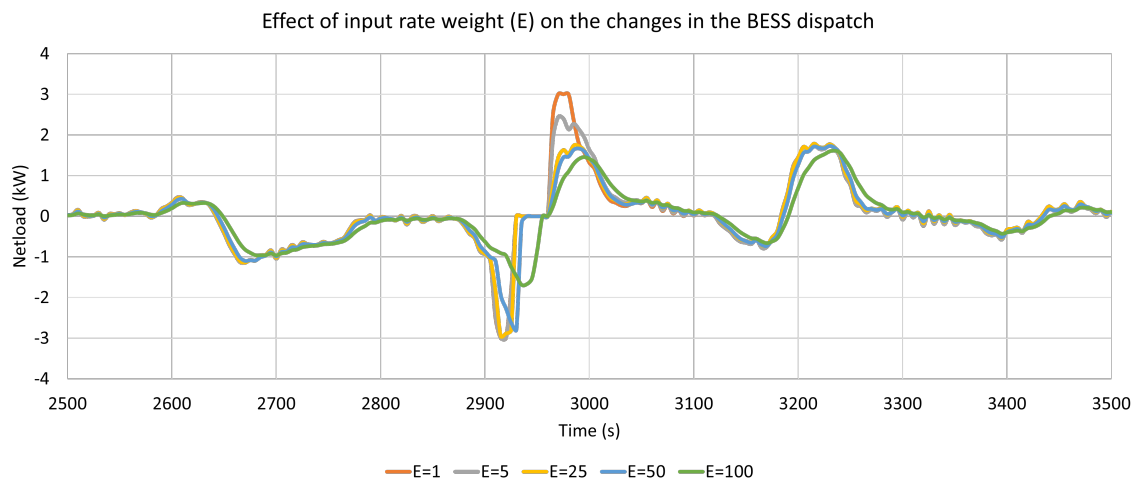


Figure 6.11: Effect of input rate weight on the reference tracking

Table 6.3: Effect of input rate weight ( $E$ ) on the reference tracking and BESS dispatch

$E$	Error	Max(dp)
-	34.2	-
1	4.55	3
5	4.54	3
25	4.29	2.94
50	3.56	2.79
100	2.48	1.68

Figure 6.12: Effect of input rate weight ( $E$ ) on the changes in BESS dispatch

The PV and load forecast contribute to the accuracy of MPC-based tracking. The figure 6.13 shows three simple models predicting the disturbance. The research does not focus on the short-term forecast but utilizes the short-term forecast for MPC control. PV intermittencies are more compared to the load intermittencies. Hence, for a system with high DER penetration, an accurate DER forecast itself would improve the system's accuracy. In the absence of the forecast, the previous measurement values can also be extrapolated to get the magnitude of the disturbance (Figure 6.13). Figure 6.14 shows the output for different disturbance models. The tracking error is minimum for the forecast model. The disturbance model extrapolating the trend has the highest error because of PV intermittencies. The RMSE for the case of

each disturbance is summarized in the table 6.4.

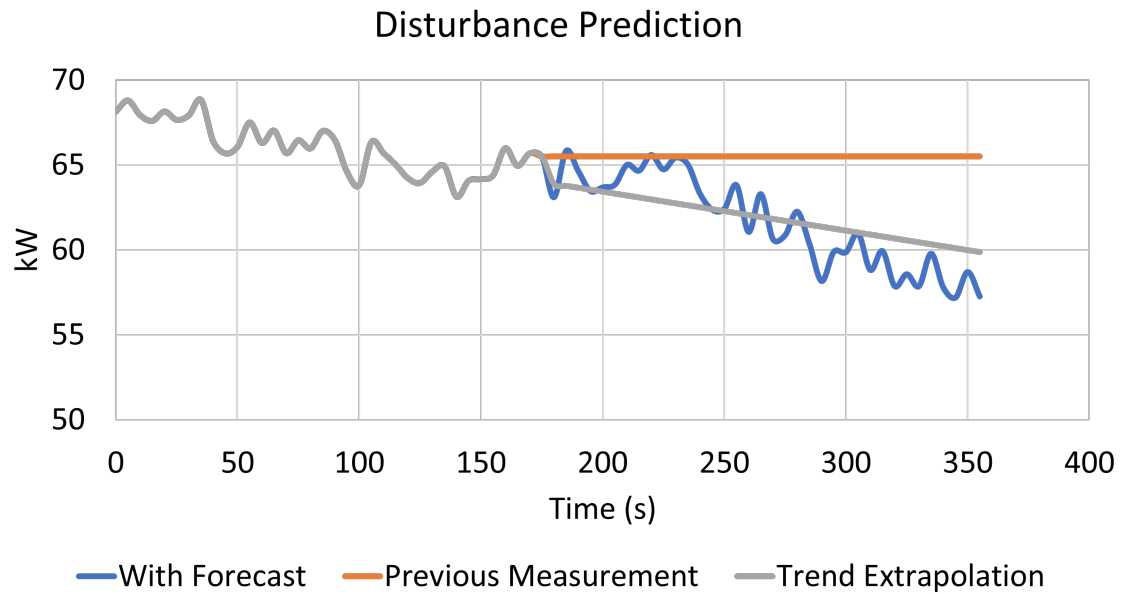


Figure 6.13: Short term feeder load forecast

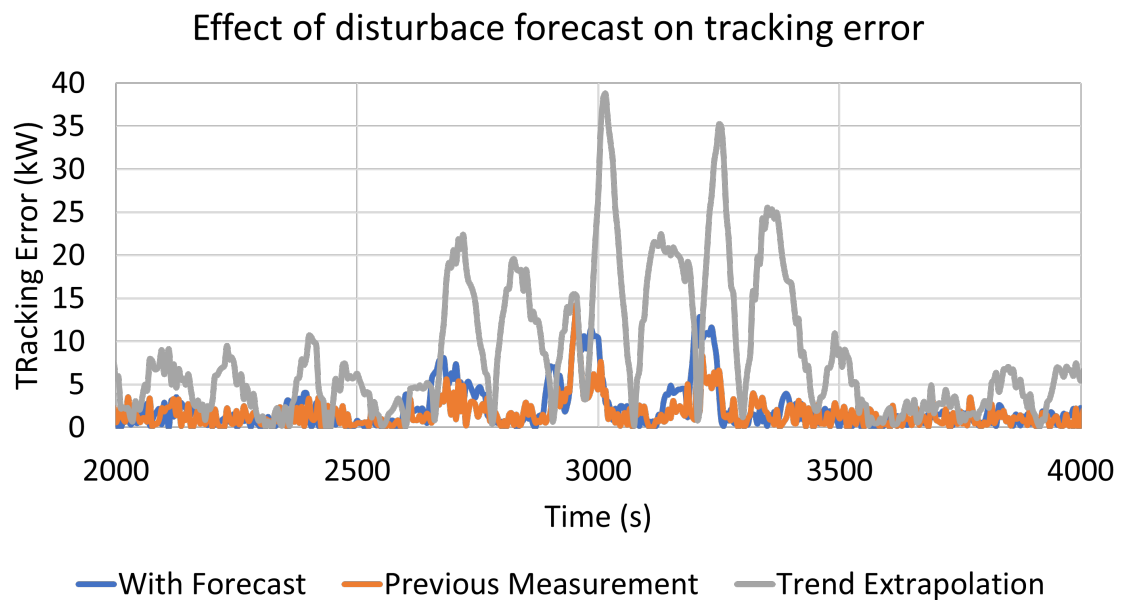


Figure 6.14: Effect of load forecast on the tracking error

Table 6.4: Tracking Error for different disturbance models

Error Without Control: 47.3 kW		
Case	Error	%Reduction
With Forecast	17.42	63.15
Previous Measurement	20.15	57.37
Trend Extrapolation	23.07	51.18

### 6.5 Implementation: 650 bus system

Earlier, the cluster control was implemented on IEEE 123 bus system with 15 DERs (PV + Energy Storage). Here PVs are assumed to be uncontrollable, and hence, the MPC-based approach leverages the flexibility of energy storage for the cluster level control. Hence for every cluster, the uncontrolled disturbance is the aggregated load and PV generation. Since the state-of-art short-term PV forecasting algorithms can predict the PV generation based on irradiance with a good amount of accuracy, the forecasted cluster net-load consists of load forecast based on 5 minutes moving average (figure 6.15) scaled down to local cluster level load and actual PV generation in the cluster. The evaluation of the model predictive control approach is performed by analyzing the following two use cases with a fixed cluster configuration.

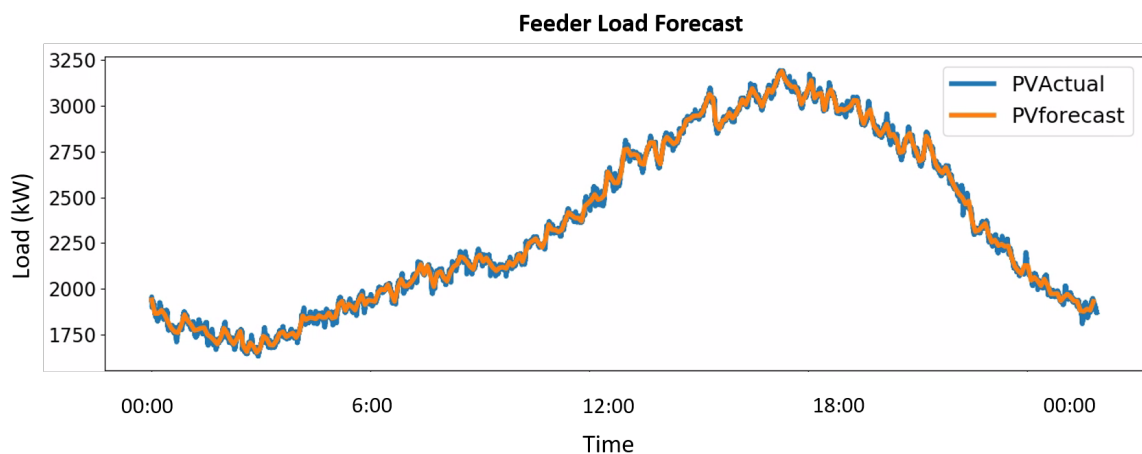


Figure 6.15: Feeder Netload forecast

Table 6.5: DER Ratings for 650 bus system

DER Type	kW Rating	kWh Rating	Total Count	Total kW	Total kWh
PV	30		31	930	
PV	60		23	1380	
PV	180		22	3960	
PV	500		3	1500	
PV	1000		1	1000	
BESS	45	135	22	990	2970
BESS	125	375	3	375	1125
BESS	250	750	1	250	750
Total			106	10385	4845

In this chapter, the fully integrated framework with all the algorithms viz., area controller, ADMM based transfer function development and the cluster control using MPC is demonstrated on a 650 bus system. The DER ratings for IEEE 650 bus system is summarized in table 6.5. This section will now show implementation and use cases with this fully integrated framework with two metrics, the area and cluster error and b) computationally able to run in less than 1 minutes.

**Implementation and Use cases:** The information of the distribution feeder is included in Figure 6.16 for illustration purpose. The PV and load profile is shown in Figure 6.17.

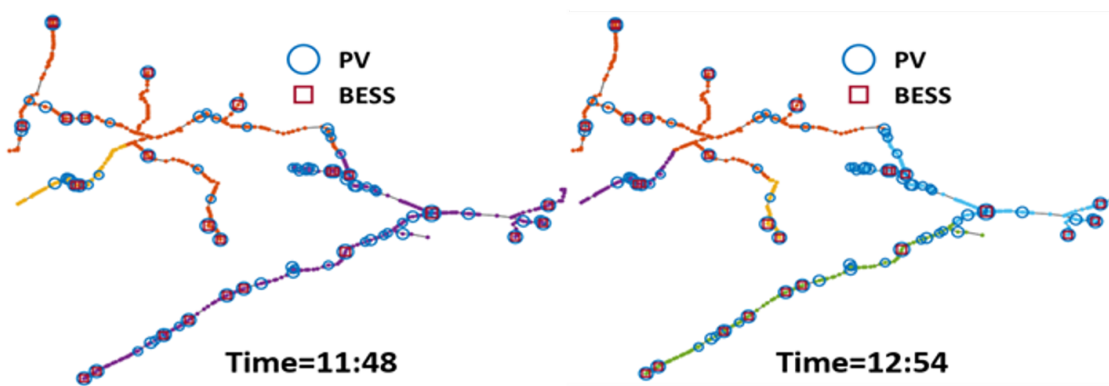


Figure 6.16: Dynamically varying clusters for 650 bus system

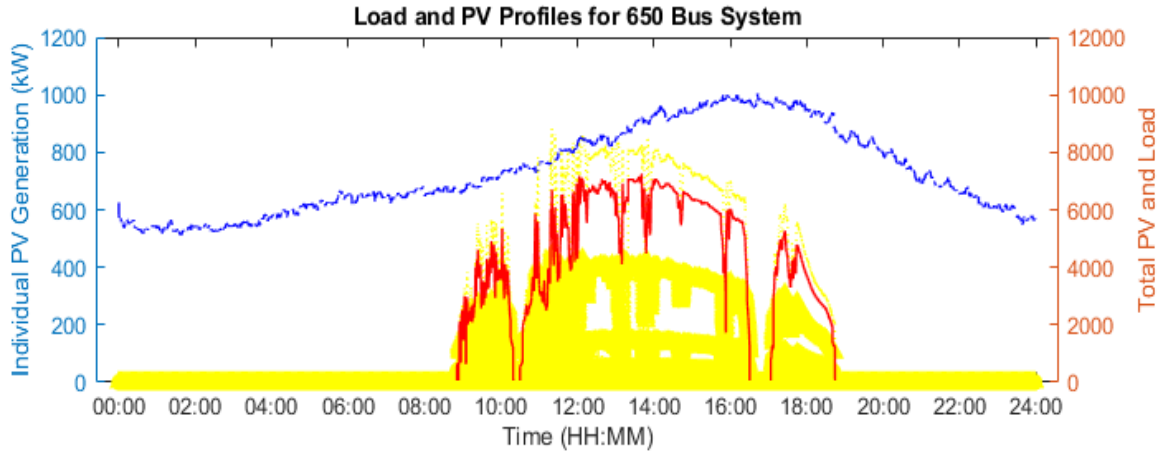


Figure 6.17: Load and PV generation on the 650 bus feeder

### 6.5.1 Use case 1: Area Control with Set-point Tracking

The first study was to have the area controller tracks the feeder head power reference in the form of area reference. Figure 6.18 presents the tracking ability of the area controller (marked as dynamic clusters with control). It is noted that the area controller not only tracks the the set-point well, but also delivers appropriate cluster set-points. We have also tested the algorithm with dynamically changing cluster formations of DER clusters. The integration of dynamically changing active power cluster algorithm shows that with dynamic clusters (blue plot), the integrated framework provides better tracking ability as opposed to static clusters and without control.

Table 6.6: Average Error: Use case 1

Cluster ID	Without Control	With Control	% Error With Control
Cluster 1	514.4 kW	232.7 kW	1.41%
Cluster 2	60.4 kW	16.3 kW	1.3%
Cluster 3	81.7 kW	17.8 kW	1.7%
Cluster 4	104.6 kW	36.0 kW	2.35%
Cluster 5	69.5 kW	23.4 kW	1.87%
Cluster 6	59.6 kW	14.5 kW	1.54%
Feeder-head	668.6 kW	232.7 kW	1.21%

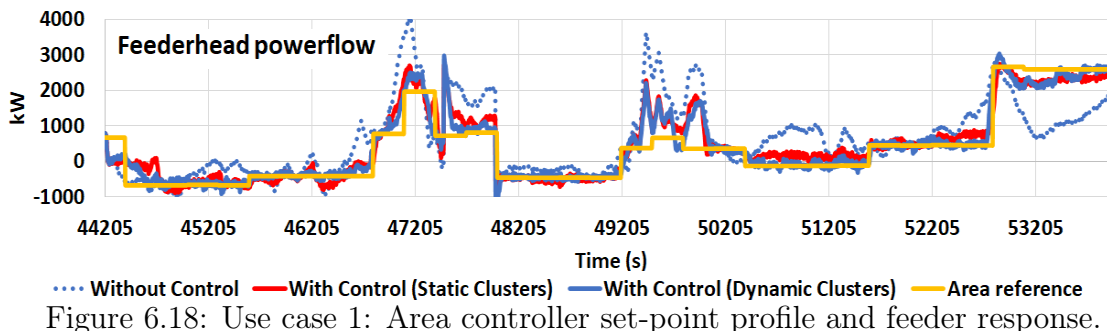


Figure 6.18: Use case 1: Area controller set-point profile and feeder response.

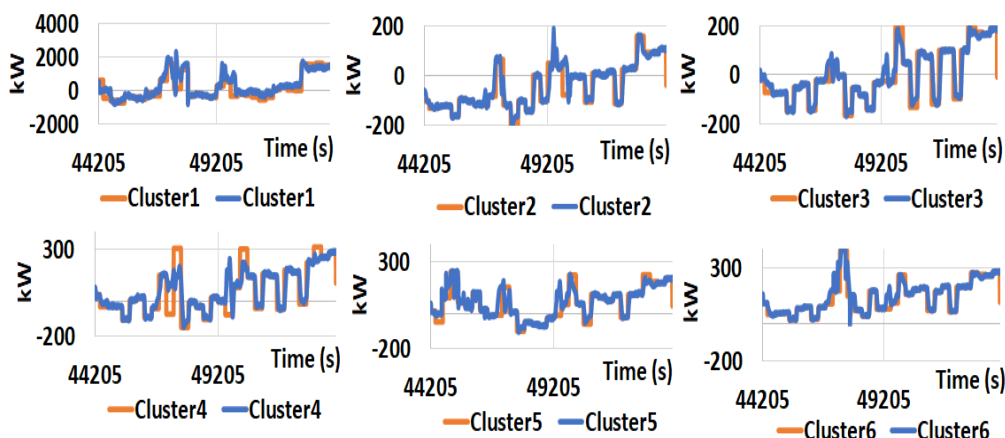


Figure 6.19: Use case 1: Cluster Set-point Tracking.

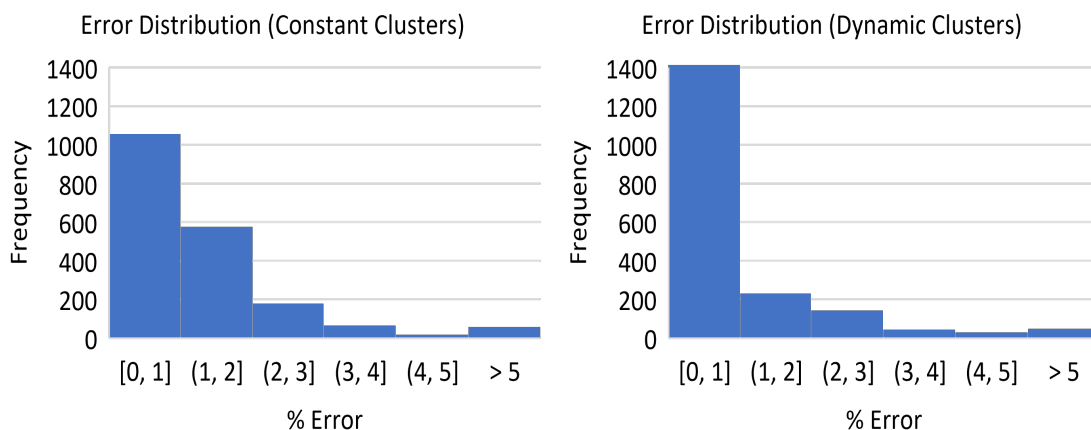


Figure 6.20: Frequency of error distribution between static and dynamic cluster based overall architecture.

It also ensure that the cluster netload is close to zero based on the given battery capacity. As it can be seen from figure 6.19, the MPC ADMM framework was able to track the cluster set-points (set by the area controller) well. Table 6.6 illustrates the overall % error with and without area control. It can be seen that the maximum %

error is less than 3. The frequency of error distribution for various tests are illustrated in figure 6.20. It can be seen that with dynamic cluster, the % error is shifted more to below 1.

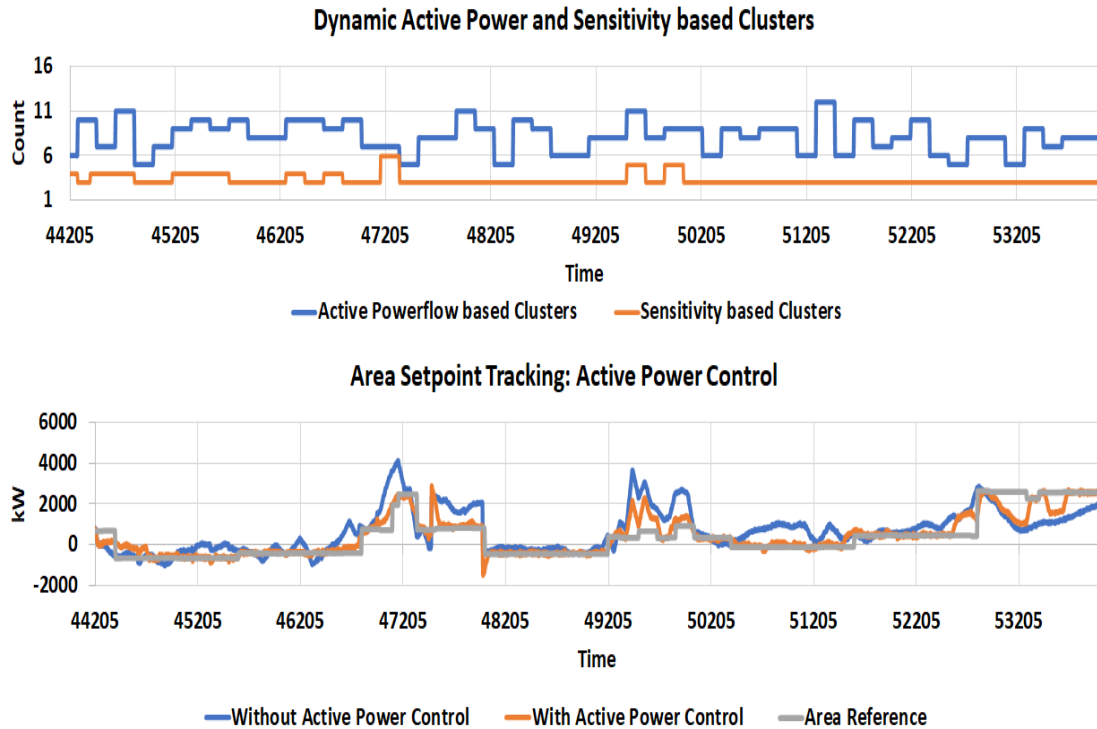


Figure 6.21: Area controller set-point profile and feeder response.

### 6.5.2 Use case 2: Active and Reactive Power Control

The second test (out of all the integration test) we are going to illustrate is to show the ability of the overall framework to perform and active power (P) and reactive power (Q) tracking. Figure 6.21 illustrates the cluster counts that is changing dynamically with time. This shows that the cluster formation is stable and both clusters (active power and reactive power- sensitivity based clusters) are changing with time. It can also be seen that the active power control tracks the set point better and accurately as opposed to controller without active power.

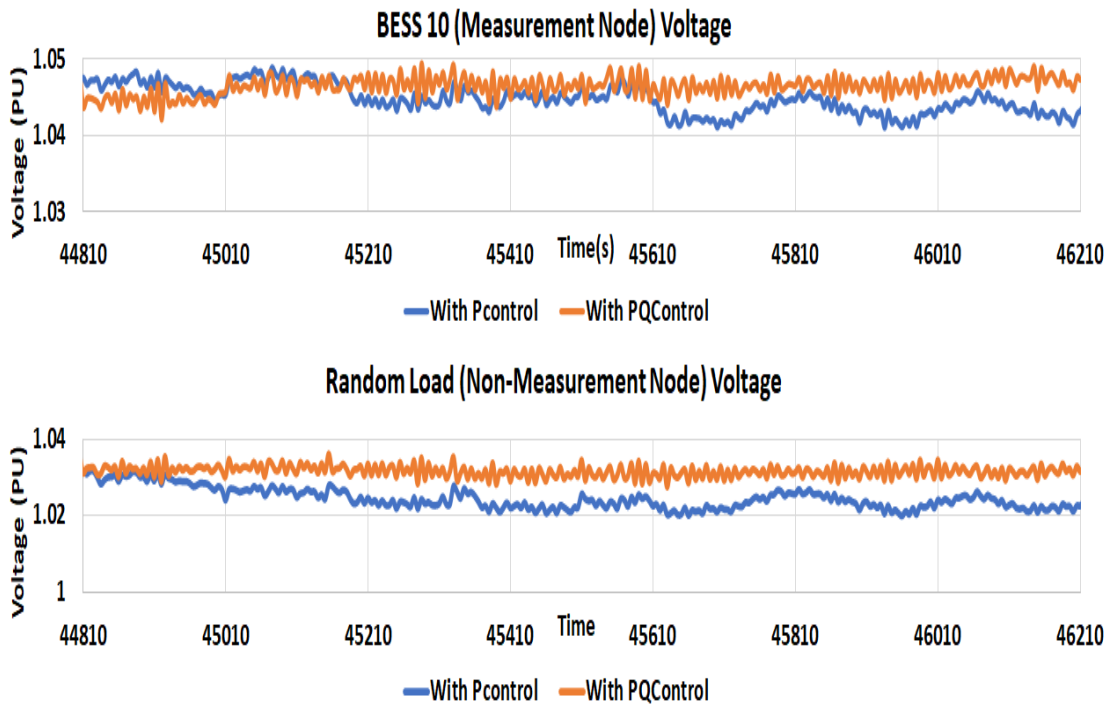


Figure 6.22: Voltage variations for measurement and non measurement node of 650 bus system

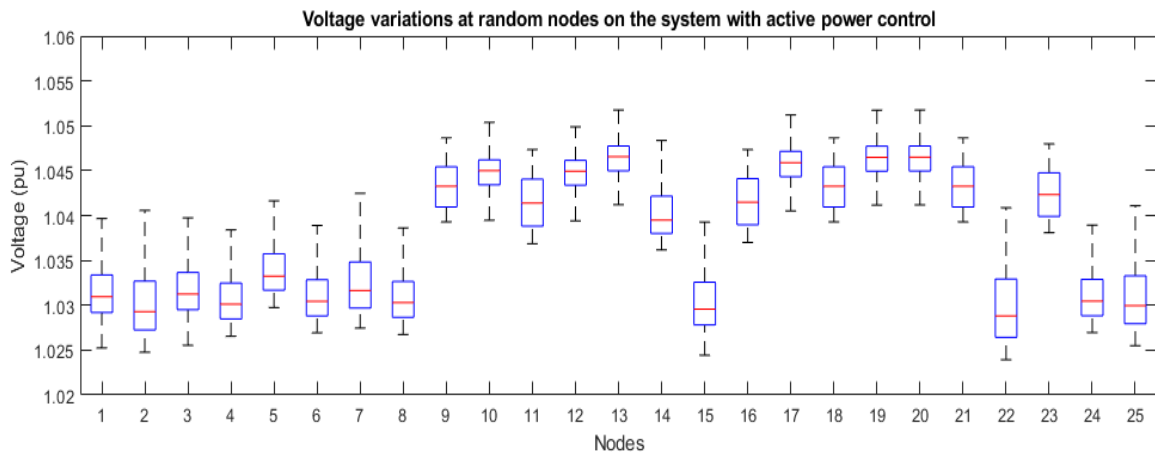


Figure 6.23: Voltage variations for 25 random system nodes with active power control

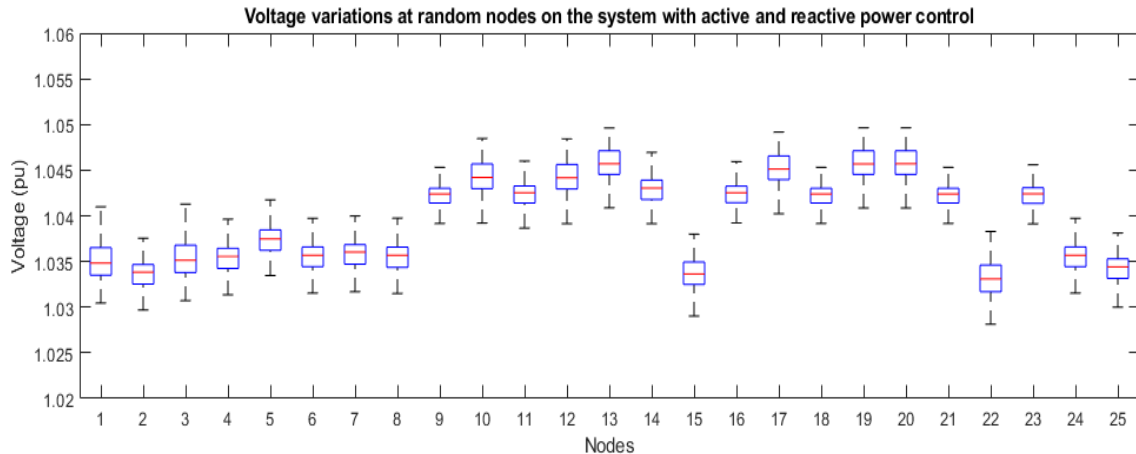


Figure 6.24: Reduction in the voltage variations for 25 random system nodes with active and reactive power control.

The goal of the reactive power set-point along with sensitivity based clustering is to track the  $Q$  such that the voltage profile, especially of most important nodes (DERs, regulator points and PCC) are flat as possible. Figure 6.22 illustrates two voltage profiles (one on a battery point- BESS 10) and another random load point. It can be seen that the profile is smooth with the proposed algorithm when compared to no reactive power clustering and support.

Figure 6.23 represents the voltage variations for 25 random system nodes with active power control. It can be seen that the voltage band error is between 1.055 and 1.02. Figure 6.24 represents the voltage variations for 25 random system nodes with active power and reactive power control. It can be seen that the voltage band error is between 1.05 and 1.027. This illustrates that the voltage profile has a tighter bandwidth with the proposed architecture.

The frequency of the error distribution with the active and reactive power control is illustrated in figure 6.25. It can be seen that the error for majority of instances is still constrained to less than 5% with the added reactive power control.

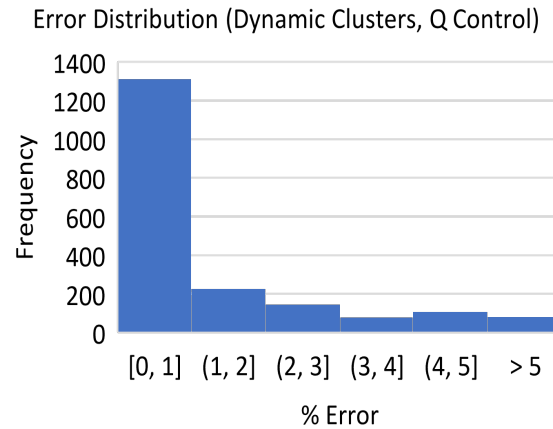


Figure 6.25: Frequency of error distribution between static and dynamic cluster based overall architecture.

### 6.5.3 Computational time and overall integration time frame

The overall integration framework is illustrated in figure 6.26. it can be seen that the complete architecture modules can be executed within 20 seconds (sequentially) time frame. However, not all modules are executed at every time step. The cluster control is the only module that runs at the 5 second time interval. The computational time for the cluster control module and parallel execution of processes to calculate the set-points for each cluster and corresponding DERs is between 2-4 seconds. Hence, the current architecture is implementable on the real-time systems at a control resolution of 5 seconds. Currently, we are running the complete framework in the standard PC with i7-7700 processor @3.6GHz and 16 GB RAM.

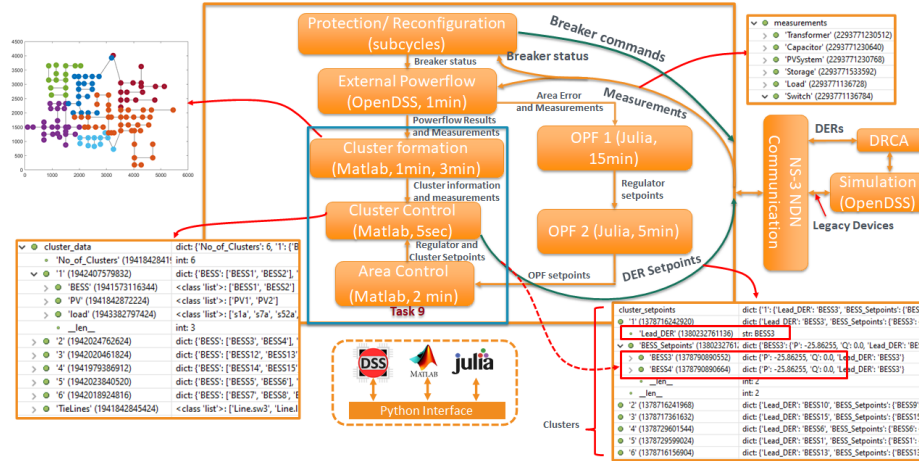


Figure 6.26: Overall integration framework with timing.

## 6.6 Chapter Summary

The chapter implemented the model predictive control approach to improve the tracking performance of the clusters. An approach was proposed to estimate the system state using the ADMM based optimization. The approach successfully identifies the systems of similar or higher order. A complete control framework is implemented on a 650 bus system. Implementation of the control framework on the 650 bus system proves the scalability of the approach.

## CHAPTER 7: Resiliency Management of power distribution system with DERs

### 7.1 Introduction

Chapter 1 introduces the requirement of a critical load management system. The primary goal of the critical load management system is to provide uninterrupted power to the critical loads on the system. From a utility's perspective, maximizing the support to both-critical and non-critical assets on the grids would further increase the overall grid resilience. Chapter 4-6 proposes the cluster-based control strategies to locally support the load on the distribution grid for multiple applications. The current chapter proposes an approach to improve the resilience of the distribution grid through cluster control of DERs and optimized load management.

Section 7.2 introduces the metrics to quantify the system resilience for the critical loads. Section 7.3 discusses the adaptability of the proposed cluster control approach for a re-configured grid during the system disturbance. Section 7.4 proposes an approach for managing the loads within the cluster through DER support in an islanded operating condition during a grid outage. Finally, the proposed load management approach is implemented on the IEEE 123 bus system along with the cluster control of DERs in section 7.5.

### 7.2 Resiliency Metrics

Presidential policy directive (PPD-21) designates the power grid as critical infrastructure and defines resilience as: "The term 'resilience' means the ability to prepare for and adapt to changing conditions and withstand and recover rapidly from disruptions. Resilience includes the ability to withstand and recover from deliberate attacks, accidents, or naturally occurring threats or incidents." The resilience of the power

grids differs from the reliability in terms of the operating state. Reliability of the grid is quantified for the normal operating conditions, whereas the grid's resilience is quantified for the grid to operate during disruptive events capable of creating outages.

Currently, the metrics quantifying resiliency are under development. The power grid industry still lacks the universally recognized and accepted standards to quantify resiliency. Hence, the current work derives the consequence-based resilience metrics, as proposed in [104].

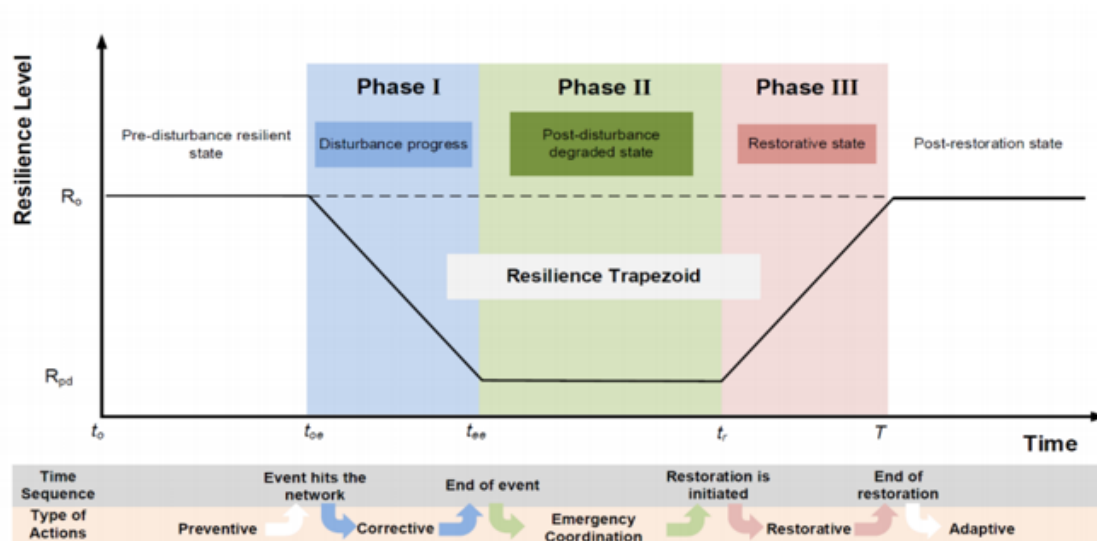


Figure 7.1: Representation of the system resilience level during the disturbance [105]

Figure 7.1 shows the resilience of the system during the disturbance, as implied by IEEE-PES task force on Resilience framework, Methods and, Metrics for Electricity Sector [105]. A typical disturbance event is classified into three phases- Disturbance progress, post-disturbance degraded state, and restorative state. The metrics discussed in the current chapter represent the system's resilience level based on the consequence-based resilience metrics. Here, the resilience during a grid outage event is calculated through the relative comparison against the normal operation condition. The cause of the outage is out of the study scope. The resiliency of the distribution

grid during the loss of service, irrespective of the cause of the outage, is quantified in terms of loss of loads, economic loss, and social discomfort.

### 7.2.1 Loss of loads

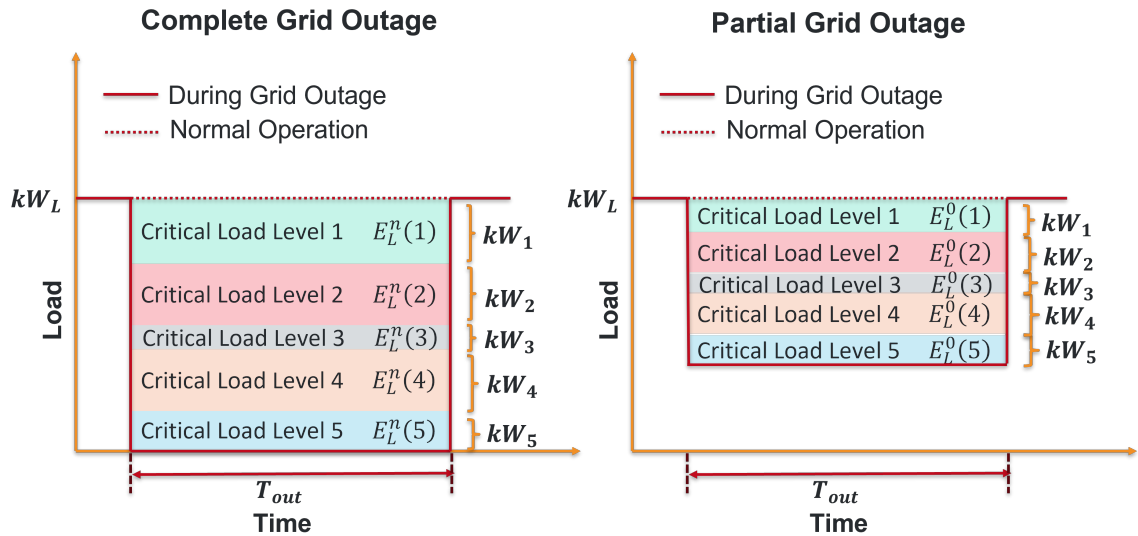


Figure 7.2: Overall integration framework with timing.

Loss of load metrics is widely used to quantify the system resiliency. Here, the loss of load is extrapolated for the outage period and compared against the energy served during the normal operation condition. Figure 7.2 represents the scenario where an outage affects the part or the complete load on the grid. Here, if  $E_{grid}^n$  is the energy served during normal operation and  $E_{grid}^o$  is the energy un-served during the grid outage, the resiliency is quantified as shown in the equation 7.2

$$R_l = 1 - \frac{E_{grid}^o}{E_{grid}^n} \quad (7.1)$$

The value of the  $R_l$  ranges between 0 and 1. 0 represents the complete loss of load during an outage, whereas 1 represents a resilient grid capable of overcoming the grid outage. Depending on the type of load being served at each metering point, the

criticality level of the load varies. Utilities may categorize the loads on the distribution grid based on customer data and assign an appropriate critical level. The loss of load calculation can be further applied for each critical load level to identify the impact on each category. Current work assumes 5 critical levels (levels 1 to 5) for the loads. Here the level 5 loads are considered the most critical loads on the system.

$$R_l(C) = 1 - \frac{E_{grid}^o(C)}{E_{grid}^n(C)} \quad (7.2)$$

where  $C = 1, 2, 3, 4, 5$

### 7.2.2 Economic loss

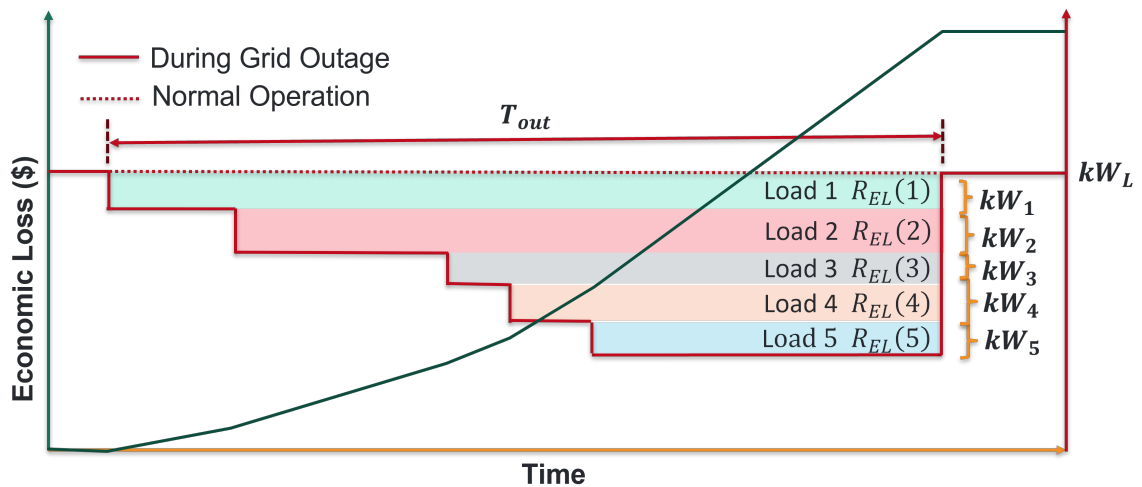


Figure 7.3: Economic loss during an outage

The economic consequences during a grid outage are experienced by both-Utility and the customers. From the utility's perspective, the economic consequence includes the loss of revenue and the cost of grid repairs and recovery. The economic loss for the customer varies based on the type of services being offered by the customer. This may account for but is not limited to loss of assets, business revenue, and business interruption. The different types of economic losses are aggregated in the current

work and represented by assigning an economic loss factor  $\epsilon$  to each load on the system. For an outage duration  $T_{out}$ , the economic loss ( $R_{EL}$ ) for the load  $i$  is given by equation 7.3. For a distribution feeder outage affecting  $N$  customers, the total economic loss is the aggregated economic loss of all load on the system (Equation 7.4). It is to be noted here that the economic loss may or may not correlate with the criticality level of the load. For example, the economic loss for a grocery store may be higher; however, the criticality level for a healthcare facility like a clinic may be high compared to the grocery store.

$$R_{EL}(i) = \epsilon(i) * P_{kw}^i * T_{out}(i) \quad (7.3)$$

$$R_{EL} = \sum_{i=1}^N \epsilon(i) * P_{kw}^i * T_{out}(i) \quad (7.4)$$

### 7.2.3 Loss in social discomfort

The social discomfort aspect of grid resilience is not easily quantifiable. The social discomfort during the grid outage varies for every customer and depends on the weather condition. For example, the social discomfort experienced by a nursing home may be significantly higher compared to a mid-aged residential customer. Also, the social discomfort may be lower during moderate temperatures than in extreme temperatures (extreme summer and winter). During extreme weather conditions, the social discomfort may increase non-linearly with outage duration. Hence, during the system-wide events due to significant loss of generation, utilities plan rotating outages to reduce the outage duration at specific locations. In the absence of a well-established model quantifying social discomfort, the current work proposes a linear model where every load on the distribution grid is assigned a social discomfort factor  $\psi$ . For an outage duration  $T_{out}$ , the total social discomfort ( $R_{SD}$ ) for the load  $i$  is given by equation 7.5. The total social discomfort caused to all customers during the grid outage

can be aggregated as shown in the equation 7.6.

$$R_{SD}(i) = \psi(i) * T_{out} \quad (7.5)$$

$$R_{SD} = \sum_{i=1}^N \psi(i) * T_{out}(i) \quad (7.6)$$

### 7.3 Situational awareness based cluster formation

The major disturbances may result in partial loss of the distribution grid, loss of distributed energy resources, or may react through an automated reconfiguration. The proposed clustering approach in chapter 3 is further improved to adapt to each of these disturbances. This section demonstrates the adaptability of the distribution grid clusters to the varying grid conditions. The proposed controller monitors the variations in the switch positions, DER outputs, and feeder-head power flow. If a change in the switch position is detected, a re-clustering flag is triggered. An external power flow is performed by mapping the switch position and the most recent measurements from loads and DERs. The variations in the grid conditions are reflected in the power flow, which is then considered for the re-clustering of the distribution grid.

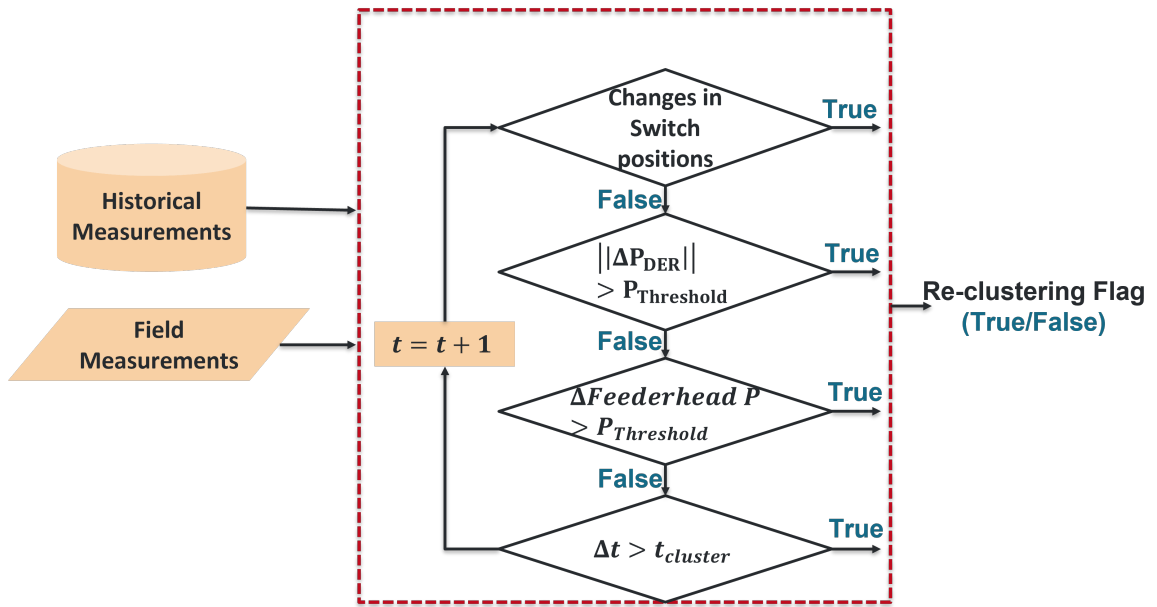


Figure 7.4: Situational awareness based cluster formation

### 7.3.1 Partial outage of the distribution feeder

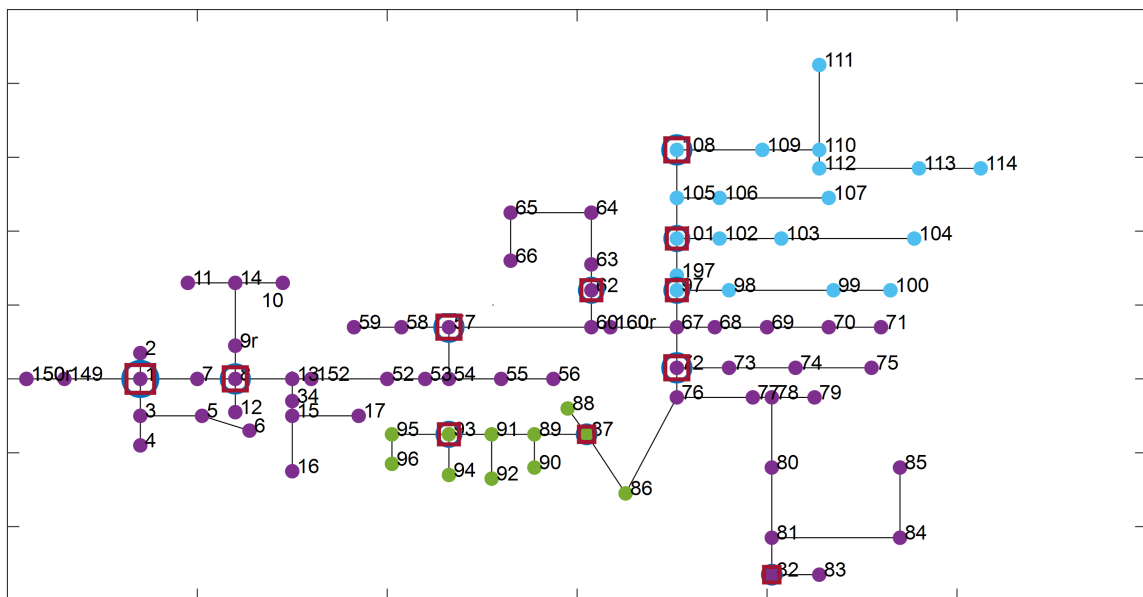
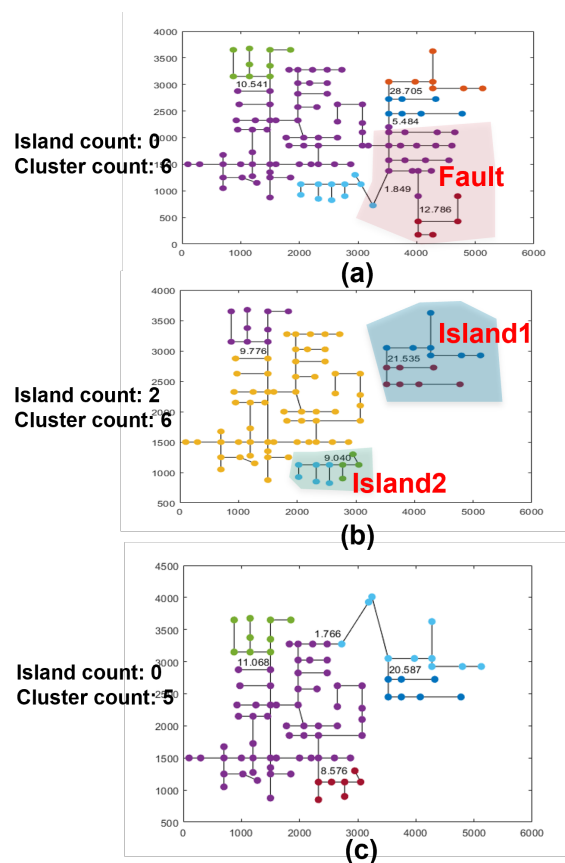


Figure 7.5: Adaptability of the clustering approach during partial outage scenario

The partial outage on the grid typically occurs due to local faults and the resulting response from the protection devices. Routine maintenance may often require an outage on the distribution grid. Under such operation conditions, the proposed clustering approach is required to accommodate the partial grid outage. Typically, the power-flow results show zero power-flowing through the lines affected by the partial outage. Hence, the adjacency matrix, diagonal matrix, and the resulting Laplacian matrix would be singular. The automated cluster detection algorithm would fail since the singular matrix only has 0 as the eigenvalue. To overcome matrix singularity due to partial outage, the branches with power flow lower than the threshold are ignored during the graph formation. Then nodes connecting the branches with non-zero power flow are re-numbered to create the reduced Laplacian consisting of only active elements. The clustering is then performed over the reduced Laplacian. Figure 7.5 shows the cluster formation during the partial outage on the grid.

### 7.3.2 Grid re-configuration

The grid reconfiguration during the disturbances is performed to connect the healthy part of the affected feeder to the operational zone of the same feeder or an adjacent feeder. When an adjacent feeder is connected, a new node and branch is added to the clustering approach. The algorithm ensures the addition of the additional nodes and branches to the system during the reconfiguration. The figure 7.6 shows the cluster formations on IEEE 123 bus system during the grid-reconfiguration scenario.



### 7.3.3 Switch location based clusters

Major interruptions often occur during severe weather conditions. The cluster control approach can further help grid operators prepare for any possible grid disturbances during severe weather events. Constraining the clusters based on the switch locations and maintaining the net-load balance through cluster control (discussed as a use-case 2 in the chapter 5) ensures that the load within the cluster is locally satisfied. Also, this reduces the power flow through the switches considerably, which may later help in the seamless operation of switches or breakers upon the requirement. Also, if the local storage is equipped with grid forming functionalities, the net-load balance through cluster control may help in the seamless transition of inverters from grid following to grid forming modes. Figure 7.7 shows the clusters on IEEE 123 bus system constrained by the switch positions. The following additions are made to the proposed two-layer spectral clustering approach to ensure that the clusters are formed based on the switch location.

- The power flow through the switch is set to the threshold value
- Minimum number of clusters is set to the zones identified based on the switch locations.
- Minimum number of DER within the cluster is limited to 2 to support the islanded operation. The clustering results are post-processed using the algorithm to meet the requirement for the minimum number of clusters.

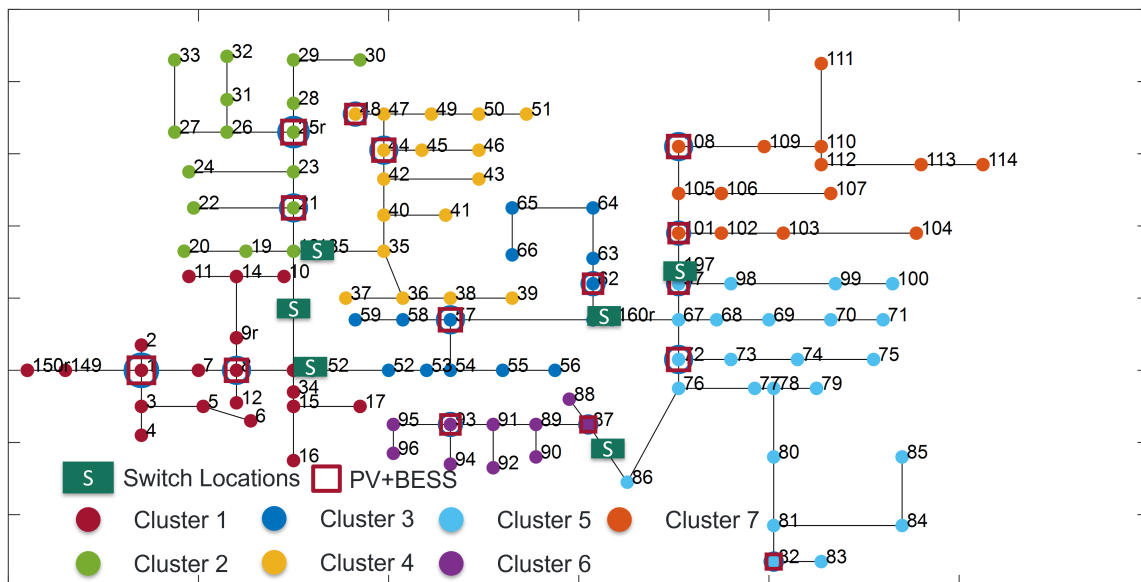


Figure 7.7: Switch locations based clusters

#### 7.4 Resilient cluster control through management of loads

As discussed in section 7.1, the resiliency of the distribution grid is quantified based on the duration and the number of customers affected during an outage. The distribution grids with high penetration of DERs provide an opportunity to support the grid through DERs during outages. However, DERs require the black-start and grid forming functionalities for islanded operations. Modern BESS provides the grid forming functionalities and is often implemented to provide backup power to critical facilities. However, DERs have limitations in power and energy to support the loads. Photovoltaics are intermittent generating resources with availability only during the daytime, and BESS has limited availability based on its capacity and operating SOC at the time of the event. Hence, advance management of loads is required, which considers the limitations based on the operating state of local generation to support the local loads during an outage. This section provides load management based on its criticality factor and available energy from DERs.

### 7.4.1 Load Management Problem Formulation

As discussed in the section, the loads on the distribution system can be classified based on their criticality levels. In the current work, the loads are classified among 5 critical levels. For every cluster ( $k$ ), the aggregated load for each criticality level is given by

$$P_{kw}^k(c, t) = \sum_{n=1, n \in C, k}^{N_L} p_n(t) \quad (7.7)$$

The primary objective of load management is to maximize the interval of the load support for loads belonging to each criticality level. If  $T(c)$  is the interval for which a load of criticality level  $c$  is kept on during an outage of duration  $T_{out}$ , the objective function to balance the duration among each load is given as

$$\min \sum_{c=1}^{N_c} ||T_{out} - T(c)||^2 \quad (7.8)$$

If the available energy from DER is known, an equality constraint for equation 7.8 is formulated as follows.

$$\sum_{c=1}^{N_c} P_{kw}^k(c, t) * T(c) = \sum_{i=1, i \in k}^{N_{BESS}} SOC_i(t) * E_{bess_i} + E_{PV}(5) \quad (7.9)$$

Here, both BESS and PV are considered for the calculation of the available energy.

$E_{PV}(c)$ , where  $c = 5$  is the total energy generated by PVs by end of support duration for critical load level 5. For PV, it is assumed that the PV generation forecast is available. Based on the forecast, the available energy  $E_{PV}(5)$  till time  $T(5)$  is calculated using the following equation.

$$E_{PV}(c) = \sum_{i=1, i \in k}^{N_{PV}} \sum_{t=T_o}^{T_o+T(c)} P_{PV}^{forecast}(i, t) \quad (7.10)$$

It is to be noted here that the  $T(5)$  is an optimization variable. Hence the pro-

posed optimization is initiated with an initially assumed/estimated value of  $T(5)$  with updates performed at the end of each iteration. The optimization ends when the norm of optimization values between the consecutive iterations is less than the given threshold.

The minimum support duration required for each criticality level is implemented through the lower bounds of the optimization variable.

$$T_{lb}(c) \leq T(c) \leq T_{ub}(c) \quad (7.11)$$

The values of  $T_{lb}(c)$  and  $T_{ub}(c)$  can be set by the distribution system operators based on customer requirements derived through the surveys.

The support duration of the critical loads can be prolonged if the DERs are utilized efficiently. The equality constraint looks at an overall energy distribution. However, an additional set of objectives is required to ensure that the PV generation is utilized efficiently and with a higher priority than BESS. The BESS can support the PV dispatch by either charging or discharging the energy. Efficient utilization of the PV generation is represented as a least square problem to reduce the difference between the total energy produced by DER and total energy consumption by the active loads till  $T(c)$ .

$$\min \sum_{c=1}^{Nc} \|T_{out} - T(c)\|^2 + w_{der} * \sum_{c=1}^{Nc} \|(E_{PV}(c) - P_L^k(c) * T(c))\|^2 \quad (7.12)$$

Here  $E_{PV}(c)$  is the forecasted energy from local PVs calculated using equation at the end of each iteration based on the updated values of  $T(c)$ . Here  $P_L^k(c)$  is the total active load just before the load shedding time  $T(c)$ . It is calculated using the following equation.

$$P_L^k(c) = \sum_{i=c}^{Nc} P_{kw}^k(i, t) \quad (7.13)$$

As discussed in the section, the economic loss during an outage contributes to grid

resiliency. However, the scale of economic loss may not correlate with the criticality level of the load. Hence, if each load  $i$  on the distribution feeder has an economic loss  $\epsilon(i)$  associated with it, the total economic loss for each category of critical load can be represented as

$$\epsilon_L^k(c) = \sum_{i=1, i \in c}^N \epsilon(i) * P_{kw}^k(i, t) \quad (7.14)$$

Similarly, the social discomfort can also be aggregated based on the criticality levels of the load.

$$\psi_L^k(c) = \sum_{i=1, i \in c}^N \psi(i) \quad (7.15)$$

The final optimization problem for the load management, including the economic loss and social discomfort components, is represented as

$$\begin{aligned} \min \sum_{c=1}^{N_c} \|T_{out} - T(c)\|^2 + w_{der} * \sum_{c=1}^{N_c} \|(E_{PV}(c) - P_L^k(c) * T(c))\|^2 + \\ w_{el} * \sum_{c=1}^{N_c} \|\epsilon_L^k(c) * (T_{ub}(5) - T(c))\|^2 + \\ w_{sd} * \sum_{c=1}^{N_c} \|\psi_L^k(c) * (T_{ub}(5) - T(c))\|^2 \quad (7.16) \\ s.t. \sum_{c=1}^{N_c} P_{kw}^k(c, t) * T(c) = \sum_{i=1, i \in k}^{NBESS} SOC_i(t) * Ebess_i + E_{PV}(5) \\ T_{lb}(c) \leq T(c) \leq T_{ub}(c) \end{aligned}$$

Here  $T_{ub}(5)$  is the feasible duration of support during an outage. Its value could be derived from the historical outage data for a feeder. The weights  $w_{der}$ ,  $w_{el}$  and  $w_{sd}$  changes the priority of the additional objectives of optimization. The values of the weights can be set based on the field requirements and planning studies.

Table 7.1: Sample loads for the sensitivity study

Load ID ( $i$ )	Load $P_{kW}$	Criticality level ( $C$ )	Economic loss factor ( $\epsilon$ )	Social Discomfort factor ( $\psi$ )
1	18.7991	4	60	3
2	9.3996	3	40	4
3	9.3996	4	40	5
4	18.7991	3	80	5
5	18.7991	2	100	3
6	18.8078	5	80	5
7	18.7991	1	60	5

#### 7.4.2 Prioritization of the objectives

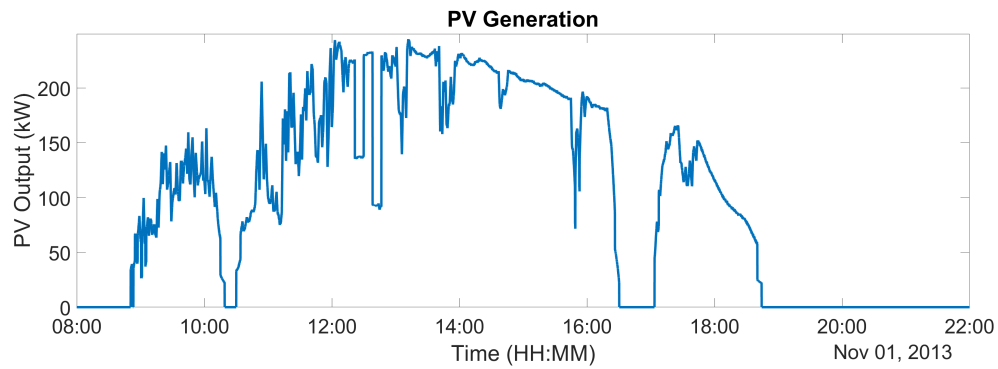


Figure 7.8: PV Generation for the sensitivity study

Table 7.2: Inter-correlation of objectives and weights

	$w_{der}$	$w_{el}$	$w_{sd}$	$f_{tout}$	$f_{der}$	$f_{el}$	$f_{sd}$
$f_{tout}$	0.35	-0.71	0.04	1			
$f_{der}$	-0.76	0.56	0.08	-0.75	1		
$f_{el}$	0.55	-0.72	0.01	0.95	-0.91	1	
$f_{sd}$	0.59	0.10	-0.36	-0.08	-0.48	0.15	1

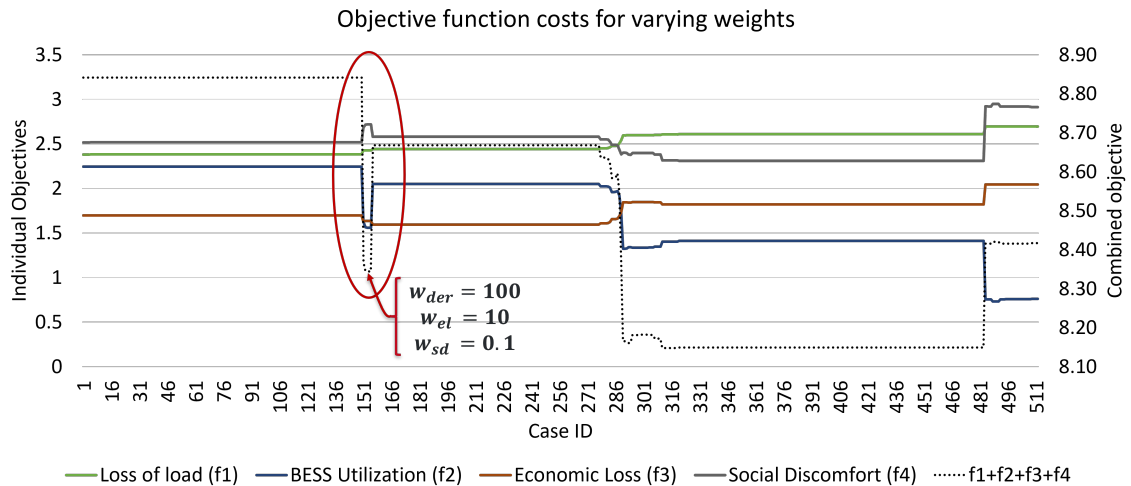


Figure 7.9: Variation in the objective function cost due to varying weights

The multi-objective-based optimization framework serves 4 different objectives. The units and scales of these objective functions are different. However, the optimization variables are the same for all. The primary objective of the optimization is to minimize the outage time of the loads based on the criticality. The secondary objectives are to minimize BESS usage and reduce economic losses and social discomfort. The sensitivity of the local and global objectives is different for each of the weights. Hence, it is essential to tune the weights as per the DSO's commitments to customers and the customer requirement.

Here, the estimation of the weights is performed using a sample cluster with 7 load values and 2 PVs. The Table 7.1 shows the consumption of each load along with its critically level, economic loss factor, and social discomfort factor. The figure 7.8

shows the total PV generation considered as a forecast for the sensitivity study.

The weight of the primary objective is set as one. The remaining weights are determined through the sweep analysis. The weights of  $w_{der}, w_{el}$  and  $w_{sd}$  are logarithmically varied (with base 10) from 0.0001 to 100. The figure 7.9 shows the variations in the objective costs for the 512 combinations of the weights. The self and cross-sensitivity of the weights and the local objectives are summarized in the Table 7.2. Following insights can be derived from the figure 7.9 and the Table 7.2.

- As expected, the weights negatively correlate with the local objectives.
- Local objectives  $f_{der}$  and  $f_{el}$  have similar sensitivity to the local weights, whereas the sensitivity of  $f_{el}$  is lower for the local weight  $w_{el}$
- The economic loss factor for the loads negatively co-relates with the social discomfort factor. Hence, the correlation between  $f_{der}$  and  $f_{el}$  is low.
- The loss of load and economic losses are reduced at the expense of higher BESS support. Hence,  $f_{tout}$  and  $f_{el}$  negatively co-relate with  $f_{der}$ . Also, the higher weight  $w_{der}$  increases the cost of  $f_{tout}$ ,  $f_{el}$ , and  $f_{sd}$ .

Based on the above insights, the weight  $w_{der}$  plays a vital role in deciding an optimized cost for global and other local objectives. As shown in the figure 7.9, the cost of  $f_{el}$  has three levels. Hence, the combination of weights corresponding to the middle level is accepted for the current study.

#### 7.4.3 Effect of BESS SOC level and the event time on the critical load support

Critical loads are expected to be supported entirely by the DERs (PV and BESS) during an event. Here, PVs are intermittent generating resources with availability only during the daytime, whereas BESS has limited energy available. Hence, the time of fault and energy stored in the battery is crucial to the duration throughout which the critical loads can be supported through DERs. The planning studies, as

presented here, may help grid operators in preparing for the outage scenarios. Here, the proposed load management is implemented for the irradiance profile (as shown in figure 7.8) and varying BESS SOC levels. Figure 7.10-7.14 represents 143 scenarios/ combinations of BESS SOC level and time of an outage event for loads with critical level 1 to 5. The value at every intersection of the row and column represents the duration of support for the load of the corresponding critical level. The load support matrix provides the following insights.

- It can be noted that the load support capacity decreases during the high inter-mittencies at 10 am and 4 pm.
- The loads are supported atleast for 36 seconds, wherever possible, to reduce the momentary disruptions due to the temporary faults.
- The load support can be longer for events during the daytime since PVs would primarily support the loads. Excess energy generated will be utilized in replenishing the BESS SOC for support after the PV generation.
- During the night, the load support capacity decreases since the BESS is utilized at its full capacity. Following the lower bound of optimization, the critical level 5 loads are supported for at least 1 hour (if sufficient capacity is available).

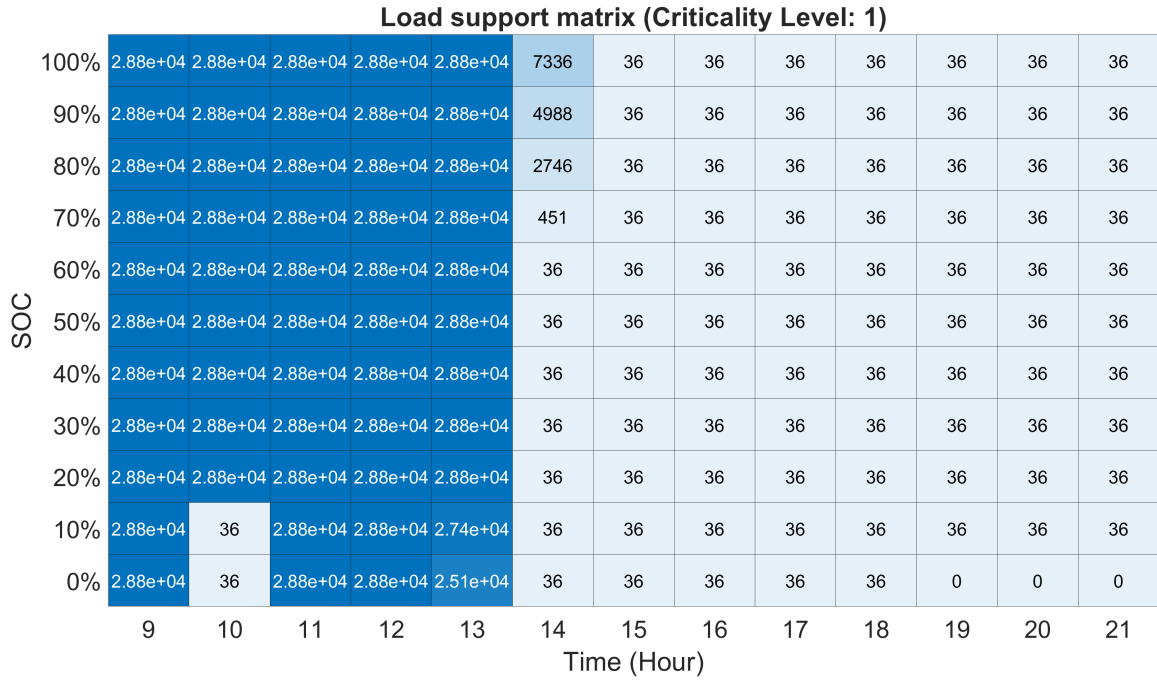


Figure 7.10: Support matrix for critical level 1 loads

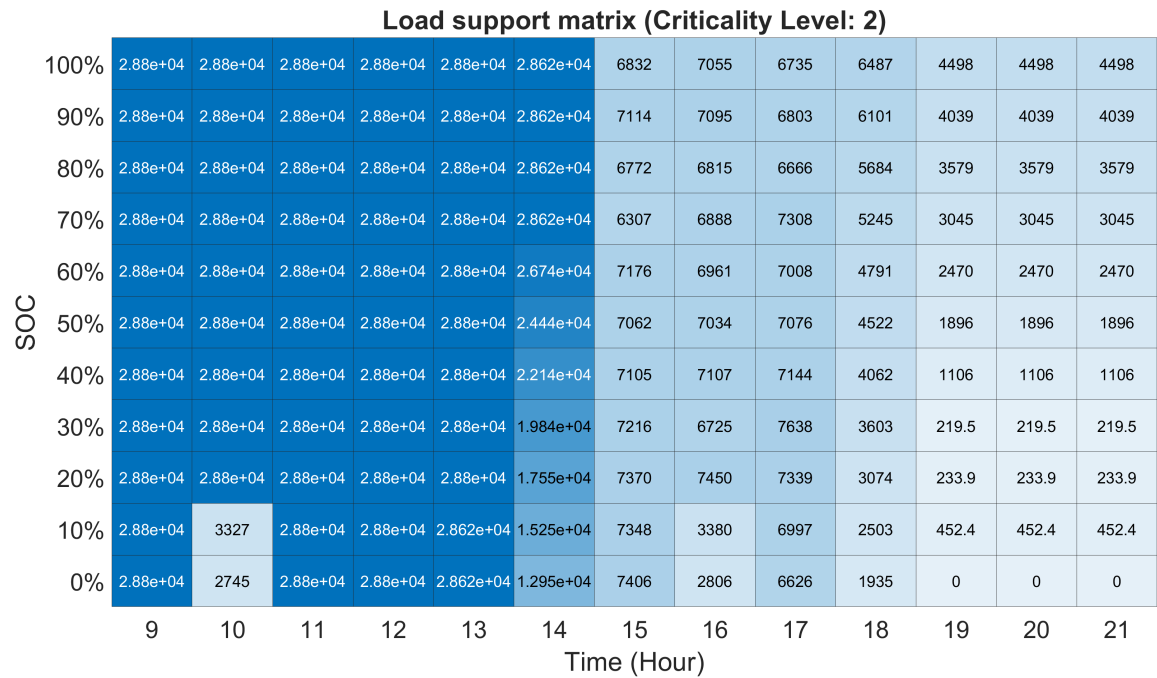


Figure 7.11: Support matrix for critical level 2 loads

**Load support matrix (Criticality Level: 3)**

100%	2.88e+04	2.88e+04	2.88e+04	2.88e+04	2.88e+04	2.868e+04	2.051e+04	1.238e+04	1.015e+04	6547	4558	4558	4558
90%	2.88e+04	2.88e+04	2.88e+04	2.88e+04	2.88e+04	2.868e+04	1.879e+04	1.226e+04	9705	6161	4099	4099	4099
80%	2.88e+04	2.88e+04	2.88e+04	2.88e+04	2.88e+04	2.868e+04	1.982e+04	1.219e+04	9315	5744	3639	3639	3639
70%	2.88e+04	2.88e+04	2.88e+04	2.88e+04	2.88e+04	2.868e+04	1.91e+04	1.174e+04	8770	5305	3105	3105	3105
60%	2.88e+04	2.88e+04	2.88e+04	2.88e+04	2.88e+04	2.868e+04	1.759e+04	1.129e+04	8368	4851	2530	2530	2530
50%	2.88e+04	2.88e+04	2.88e+04	2.88e+04	2.88e+04	2.868e+04	1.726e+04	1.083e+04	7922	4582	1956	1956	1956
40%	2.88e+04	2.88e+04	2.88e+04	2.88e+04	2.88e+04	2.868e+04	1.677e+04	1.039e+04	7476	4122	1166	1166	1166
30%	2.88e+04	2.88e+04	2.88e+04	2.88e+04	2.88e+04	2.868e+04	1.622e+04	1.01e+04	7698	3663	224.5	224.5	224.5
20%	2.88e+04	2.88e+04	2.88e+04	2.88e+04	2.88e+04	2.868e+04	1.56e+04	9441	7399	3134	238.9	238.9	238.9
10%	2.88e+04	3387	2.88e+04	2.88e+04	2.868e+04	2.868e+04	1.557e+04	3440	7057	2563	452.4	452.4	452.4
0%	2.88e+04	2805	2.88e+04	2.88e+04	2.868e+04	2.868e+04	1.527e+04	2866	6686	1995	0	0	0
	9	10	11	12	13	14	15	16	17	18	19	20	21

Time (Hour)

Figure 7.12: Support matrix for critical level 3 loads

**Load support matrix (Criticality Level: 4)**

100%	2.88e+04	2.88e+04	2.88e+04	2.88e+04	2.88e+04	2.874e+04	2.874e+04	1.378e+04	1.021e+04	6607	4618	4618	4618
90%	2.88e+04	2.88e+04	2.88e+04	2.88e+04	2.88e+04	2.874e+04	2.874e+04	1.281e+04	9765	6221	4159	4159	4159
80%	2.88e+04	2.88e+04	2.88e+04	2.88e+04	2.88e+04	2.874e+04	2.64e+04	1.225e+04	9375	5804	3699	3699	3699
70%	2.88e+04	2.88e+04	2.88e+04	2.88e+04	2.88e+04	2.874e+04	2.59e+04	1.18e+04	8830	5365	3165	3165	3165
60%	2.88e+04	2.88e+04	2.88e+04	2.88e+04	2.88e+04	2.874e+04	2.53e+04	1.135e+04	8428	4911	2590	2590	2590
50%	2.88e+04	2.88e+04	2.88e+04	2.88e+04	2.88e+04	2.874e+04	2.417e+04	1.089e+04	7982	4642	2016	2016	2016
40%	2.88e+04	2.88e+04	2.88e+04	2.88e+04	2.88e+04	2.874e+04	2.311e+04	1.045e+04	7536	4182	1800	1800	1800
30%	2.88e+04	2.88e+04	2.88e+04	2.88e+04	2.88e+04	2.874e+04	2.204e+04	1.016e+04	7758	3723	1800	1800	1800
20%	2.88e+04	2.88e+04	2.88e+04	2.88e+04	2.88e+04	2.874e+04	2.103e+04	9501	7459	3194	243.9	243.9	243.9
10%	2.88e+04	3447	2.88e+04	2.88e+04	2.874e+04	2.874e+04	1.954e+04	3500	7117	2623	452.4	452.4	452.4
0%	2.88e+04	2865	2.88e+04	2.88e+04	2.874e+04	2.874e+04	1.827e+04	2926	6746	2055	0	0	0
	9	10	11	12	13	14	15	16	17	18	19	20	21

Time (Hour)

Figure 7.13: Support matrix for critical level 4 loads

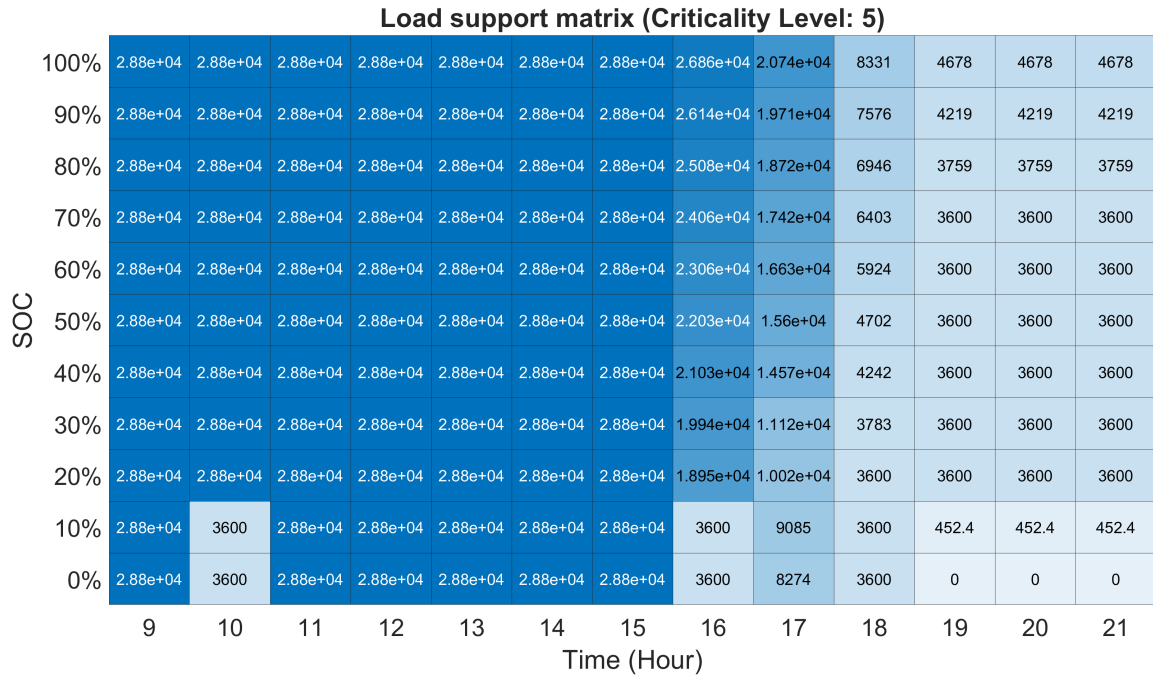


Figure 7.14: Support matrix for critical level 5 loads

## 7.5 Implementation on IEEE 123 bus system

The proposed approach for load management during a long-term outage is implemented on IEEE 123 bus system with 15 PV and BESS. The ratings of the PV and BESS has been discussed in chapter 3. The cluster control during regular operation with model predictive control is discussed in chapter 6. Here, the loads and the DERs within the clusters are controlled to improve the overall resiliency of the affected part of the distribution grid.

The breaker locations are shown in the figure 7.7. Here, the fault is simulated at bus 67(cluster 5). Immediately upon the detection of the fault, the breaker will isolate the affected clusters (5, 6, and 7) from the grid. The proposed implementation assumes the grid-forming capacities of the BESS inverters and the deployment of an efficient protection and reconfiguration scheme for the distribution system. The reconfiguration scheme will isolate cluster 6 and cluster 7, which is then supported

Table 7.3: Load Information

Load	kW	Clevel	$\epsilon(\$/kW/Hr)$	$\psi(Discomfort/Hr)$
Cluster 1				
S87B	18.83	4	60	3
S88A	18.96	1	60	5
S90B	19.58	5	80	5
S92C	18.89	2	100	3
S94A	18.92	3	80	5
S95B	9.42	3	40	4
S96B	9.42	4	40	5
Cluster 2				
S102C	9.42	3	100	1
S103C	18.83	4	80	5
S104C	18.83	3	60	5
S106B	18.83	1	40	2
S107B	18.83	2	40	2
S109A	18.83	5	40	5
S111A	9.42	4	60	4
S112A	9.82	1	80	1
S113A	20.42	2	40	1
S114A	9.42	5	60	1

by the local grid forming DERs.

Each load is characterized by the critical load level, economic loss factor, and social discomfort factor (Table 7.3). The resiliency improvement by implementing the proposed load management approach is compared against the base case scenario with a non-load shedding-based cluster control. The base case scenario assumes that all loads have the same criticality level, and the support is provided till the depletion of the BESS SOC.

### 7.5.1 Results and discussion

Here, the three-phase to ground fault is applied at cluster 5. Immediately upon the detection of the fault, the breaker operates and isolates the clusters 1, 2, and 3. However, the reconfiguration algorithm isolates the healthy clusters 1 and 3 to reduce the impact of an outage (figure 7.15).

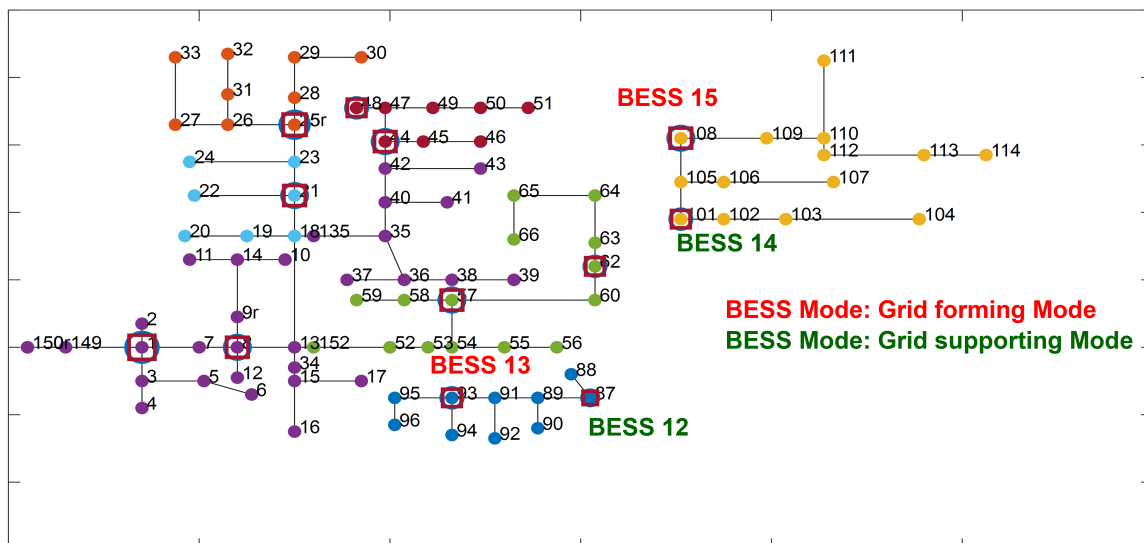


Figure 7.15: Economic loss during an outage

BESS 13 and BESS 15 are the higher-rated BESS in clusters 2 and 3, respectively. Hence, they seamlessly transition into grid forming mode and continues to support the islanded grid. BESS 12 and BESS 14 are controlled through the MPC-based net-load minimization. Hence, as shown in figure 7.17 and 7.19, any variations in the net load are primarily addressed by the BESS 12 and BESS 14, followed by BESS 13 and BESS 15.

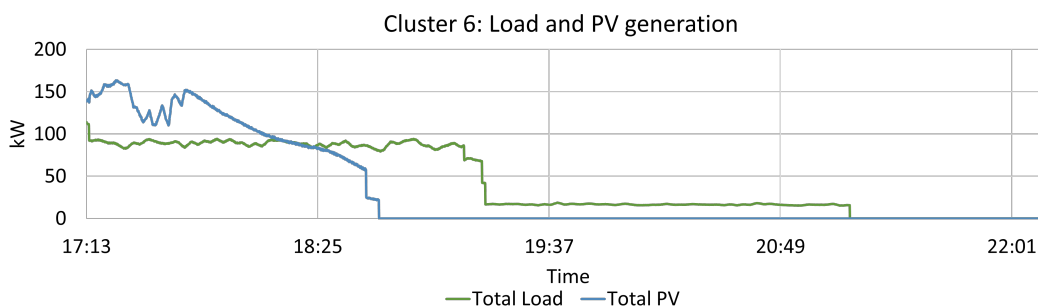


Figure 7.16: Economic loss during an outage

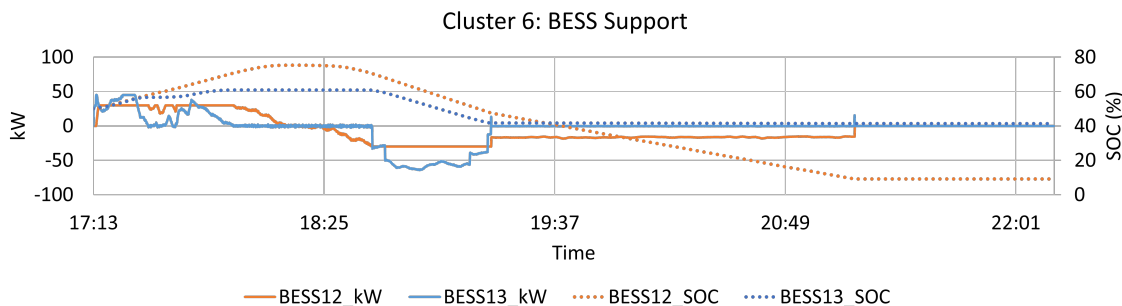


Figure 7.17: Economic loss during an outage

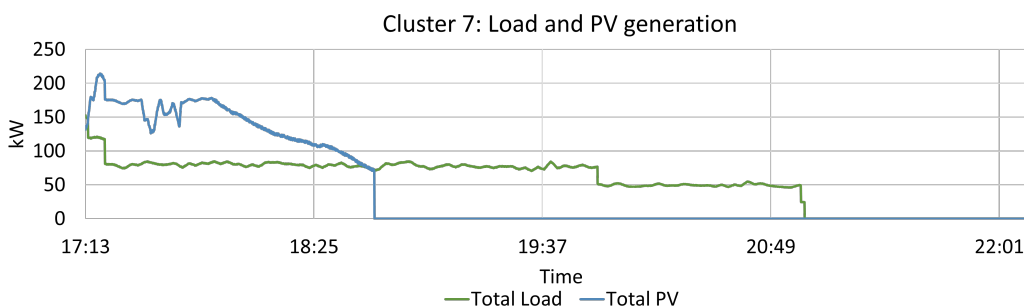


Figure 7.18: Economic loss during an outage

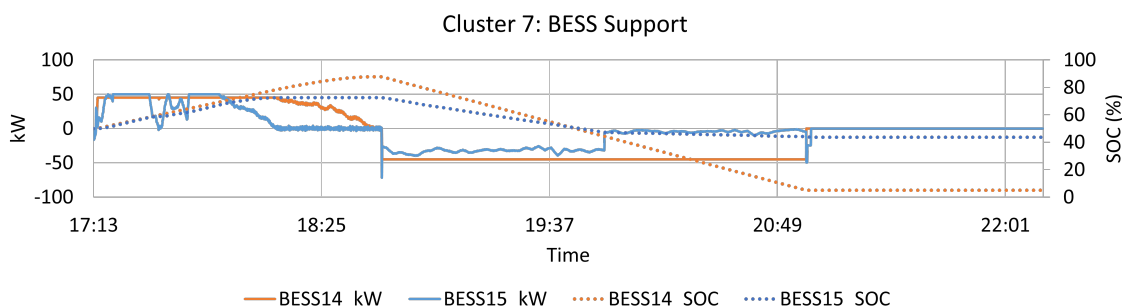


Figure 7.19: Economic loss during an outage

Figure 7.16 and figure 7.16 shows the load and PV generation during the event. The step reduction in the total cluster load because of the implementation of the proposed load management approach can be observed in 7.16 and figure 7.16. Since PVs are

generating till 17:00, the loads are primarily supported through the PV generation, and the BESS absorbs any additional generation. This helps BESS replenish the state of charge for an extended support duration for the critical loads in the absence of PVs. After the PVs go offline, the local storage supports the complete cluster load. The SOC for grid supporting BESS is between the range of 5%-8% at the end of load support for critical level 5 loads, indicating an efficient utilization of the BESS. Table shows the time at which each load is turned off from clusters 1 and 2. It can be noted that the load support duration is identical for all loads within each cluster for the base case (without load management). The total energy served is identical for both cases. Hence, the comparison provides accurate quantification of improvements in resilience.

Table 7.5 compares and quantifies the grid's resilience in load loss, economic loss, and social discomfort for both - the base case and proposed load management. It can be noted here that the individual load level resiliency is identical for all loads without managed load shedding scheme. However, the individual load level resiliency ranges from 0.005% for critical level 6 load to 77% for critical level 5 loads. The average cluster level resiliency improves 5% for cluster 6 and 14% for cluster 7. The improvement is more significant for cluster 7 because of higher loads at critical level 5. Also, the economic loss is reduced by 8% for cluster 6 and 12% for cluster 7. The social discomfort improves by 5% for cluster 6 and 29% for cluster 7. The variation in the improvements between cluster 6 and cluster 7 is due to differences in the total load magnitude, economic loss, and social discomfort factors. However, the improvements in all aspects of resiliency (summarized in Table 7.6) are observed by implementing the proposed load management approach.

## 7.6 Chapter summary

The chapter leverages the control capability of the framework to support the distribution network through DERs during the grid contingencies. The chapter proposes

Table 7.4: Loads during an islanded operation: Base Case and With proposed load management

Load	Event time (s)	Toff (s) (Base Case)	Restoration time (s)	Toff (s) (With Load Management)	$T_{out}(i)$ (s) (Base Case)	$T_{out}(i)$ (s) (With Load Management)	$T_{out}(i)$ (h) (Base Case)	$T_{out}(i)$ (h) (With Load Management)
S87B	62010	68713	80000	69455	11287	10545	3.14	2.93
S88A	62010	68713	80000	62055	11287	17945	3.14	4.98
S90B	62010	68713	80000	76265	11287	3735	3.14	1.04
S92C	62010	68713	80000	69060	11287	10940	3.14	3.04
S94A	62010	68713	80000	69395	11287	10605	3.14	2.95
S95B	62010	68713	80000	69395	11287	10605	3.14	2.95
S96B	62010	68713	80000	69455	11287	10545	3.14	2.93
S102C	62010	68363	80000	71690	11637	8310	3.23	2.31
S103C	62010	68363	80000	75535	11637	4465	3.23	1.24
S104C	62010	68363	80000	71690	11637	8310	3.23	2.31
S106B	62010	68363	80000	62055	11637	17945	3.23	4.98
S107B	62010	68363	80000	62375	11637	17625	3.23	4.90
S109A	62010	68363	80000	75605	11637	4395	3.23	1.22
S111A	62010	68363	80000	75535	11637	4465	3.23	1.24
S112A	62010	68363	80000	62055	11637	17945	3.23	4.98
S113A	62010	68363	80000	62375	11637	17625	3.23	4.90
S114A	62010	68363	80000	75605	11637	4395	3.23	1.22

Table 7.5: Quantification of the resilience for the impacted loads and the corresponding cluster

Load	Without Load Management			With Load Management				
	$E_{grid}^o$	$R_l$	$R_{SD}$	$E_{grid}^o$	$R_l$	$R_{SD}$		
Cluster 6								
S87B	59.04	0.37	3542.69	9.41	55.16	0.40	3309.76	8.79
S88A	59.45	0.37	3567.01	15.68	94.52	0.00	5671.07	24.92
S90B	61.39	0.37	4911.25	15.68	20.31	0.77	1625.17	5.19
S92C	59.22	0.37	5922.26	9.41	57.40	0.38	5740.13	9.12
S94A	59.33	0.37	4746.48	15.68	55.75	0.39	4459.64	14.73
S95B	29.52	0.37	1180.90	12.54	27.74	0.40	1109.53	11.78
S96B	29.52	0.37	1180.90	15.68	27.58	0.40	1103.25	14.65
Total	357.48	0.37	25051.48	94.06	338.46	0.39	23018.55	89.17
Cluster 7								
S102C	30.44	0.35	3043.88	3.23	21.74	0.52	2173.55	2.31
S103C	60.88	0.35	4870.23	16.16	23.36	0.73	1868.58	6.20
S104C	60.88	0.35	3652.67	16.16	43.47	0.52	2608.27	11.54
S106B	60.88	0.35	2435.10	6.47	93.87	0.00	3754.93	9.97
S107B	60.88	0.35	2435.10	6.47	92.20	0.02	3687.97	9.79
S109A	60.88	0.35	2435.11	16.16	22.99	0.74	919.64	6.10
S111A	30.44	0.35	1826.33	12.93	11.68	0.73	700.71	4.96
S112A	31.75	0.35	2540.38	3.23	48.97	0.00	3917.27	4.98
S113A	66.00	0.35	2640.11	3.23	99.96	0.02	3998.47	4.90
S114A	30.44	0.35	1826.35	3.23	11.50	0.74	689.74	1.22
Total	493.46	0.35	27705.26	87.28	469.73	0.40	24319.15	61.98

Table 7.6: Improvement in the resiliency of the cluster through the proposed management of the loads

Metrics	Without Load Management	With Load Management	% Improvement
Cluster 6			
$E_{grid}^o$	357.48	338.46	5.32
$R_l$	0.37	0.39	4.94
$R_{EL}$	25051.48	23018.55	8.12
$R_{SD}$	94.06	89.17	5.19
Cluster 7			
$E_{grid}^o$	493.46	469.73	4.81
$R_l$	0.35	0.40	14.16
$R_{EL}$	27705.26	24319.15	12.22
$R_{SD}$	87.28	61.98	28.99

improvements to the clustering approach to adapt to the varying grid conditions and topologies. A multi-objective optimization-based load management approach is also proposed to improve resiliency and reduce the impacts on the customers during grid outages. The proposed approach is demonstrated for a grid outage scenario on IEEE 123 bus system. The improvements in the grid resilience are quantified through the consequence-based metrics and compared against the conventional islanded operation without managing loads.

## CHAPTER 8: CONCLUSIONS AND FUTURE WORK

In this dissertation, we have proposed an approach to form clusters on the distribution grid based on the active power flow and reactive power to voltage sensitivity. The DERs within the clusters are then controlled to manage the cluster level net-load and the voltages.

### 8.1 Conclusions

Chapter 3 proposes an improved spectral clustering based approach for identifying the active powerflow based clusters. The chapter also proposes an approach to find clusters based on reactive power to voltage sensitivity.

- The approach improve the accuracy of cluster detection.
- The discontinuities in the cluster formation are substantially reduced through the proposed approach.
- The active powerflow based cluster configuration varies based dynamically based on the powerflow.
- The reactive power sensitivity based clusters varies dynamically based on the availability of the reactive power.

Chapter 4 proposed an approach for net-load smoothing and voltage management through cluster control.

- The variations in the net-load reduces by 58% through cluster control approach.
- The losses are lower compared to centralized control approach.
- The voltage variations are lower for active power managed through cluster control approach.
- Dynamic clustering improves the local load support through improved balance in the cluster net-load

- Reactive power control reduces the voltage variation significantly for all nodes on the system.

Chapter 5 proposes an ADMM based approach for area set-point sharing among the clusters based on the state of charge and tie-line flows for all clusters.

- The approach shares the area set-points among the clusters with a global objective of minimizing the tracking error.
- The tracking error is reduced by 71% for the area set-point tracking and by 53% for net-load minimization.

Chapter 6 proposes an MPC based cluster control approach. An ADMM based transfer function approach is proposed for the identification of the system transfer function at a given operating states based on the measurements.

- The transfer function predicts the system state with good accuracy irrespective of an actual order of the system.
- MPC based cluster control accurately tracks the references of each cluster. An implementation on 650 bus system also proves the scalability of the control approach.

Chapter 7 quantifies the grid resilience in terms of load loss, economic loss, and social discomfort. A multi-objective optimization-based framework is proposed to manage the critical loads on the system during an outage. The complete framework of load management and cluster control is demonstrated on the IEEE 123 bus system for an outage scenario.

- The approach ensures the continuity of the power to the local loads on the healthy cluster during the islanded period.
- The cluster configurations adapt dynamically based on the grid topology to maximize the load support.

- The proposed approach aims to maximize the support to loads at a higher criticality level.
- The proposed approach of management of loads through cluster control of DERs improves the grid resilience in terms of loss of loads, economic losses, and social discomfort.

## 8.2 Future Works

Future work in this direction includes

- Implement the proposed approach on 2500 node system.
- Implement the proposed approach on a use-case of continued critical load support during long term system outage.
- Quantify the improvement in grid resiliency through the proposed control in terms of critical load support, total energy served, financial loss and social discomfort.
- Implement the complete framework on the real-time simulator.

## LIST OF PUBLICATIONS

[J1] Patel, Shyamal, Muhammad Ahmed, and Sukumar Kamalasan. "A novel energy storage-based net-load smoothing and shifting architecture for high amount of photovoltaics integrated power distribution system." *IEEE Transactions on Industry Applications* 56.3 (2020): 3090-3099.

[J2] Patel, Shyamal, Krishna Murari, and Sukumar Kamalasan. "Distributed Control of Distributed Energy Resources in Active Power Distribution System for Local Power Balance with Optimal Spectral Clustering." *IEEE Transactions on Industry Applications* (Accepted for publication)

[J3] Patel, Shyamal, Krishna Murari, and Sukumar Kamalasan. "Spectral clustering and ADMM based distributed control of distribution grid" (In progress)

[J4] Patel, Shyamal, Krishna Murari, and Sukumar Kamalasan. "Cluster control and load management-based resiliency improvement" (In progress)

[C1]. Patel, Shyamal, and Sukumar Kamalasan. "A Graph Theory-Based Two-Level Spectral Clustering Approach for Active Power Grouping of DER Integrated Power Distribution System." 2021 IEEE Power Energy Society Innovative Smart Grid Technologies Conference (ISGT). IEEE, 2021. (Finalist for the Best Paper Award)

[C2]. Patel, Shyamal, Krishna Murari, and Sukumar Kamalasan. "A Spectral Clustering Based Distributed Control of Distributed Energy Resources (DERs) Integrated Power Distribution System." 2020 IEEE International Conference on Power Electronics, Drives and Energy Systems (PEDES). IEEE, 2020.

[C3]. Patel, Shyamal, Krishna Murari, and Sukumar Kamalasan. "A Spectral Clustering based distributed voltage management using limited measurements in distribution grids through DERs. (In progress)

## REFERENCES

- [1] A. Kenward and U. Raja, "Blackout: Extreme weather, climate change and power outages," *Climate central*, vol. 10, 2014.
- [2] W. House, "Economic benefits of increasing electric grid resilience to weather outages," *Washington, DC: Executive Office of the President*, 2013.
- [3] C. Glenn, D. Sterbentz, and A. Wright, "Cyber threat and vulnerability analysis of the us electric sector," tech. rep., Idaho National Lab.(INL), Idaho Falls, ID (United States), 2016.
- [4] "Electric grid cybersecurity," tech. rep., Congressional research service, 2018.
- [5] "Ieee recommended practice for monitoring electric power quality," *IEEE Std 1159-2019 (Revision of IEEE Std 1159-2009)*, pp. 1–98, Aug 2019.
- [6] R. E. Brown, S. Gupta, R. D. Christie, S. S. Venkata, and R. Fletcher, "Distribution system reliability assessment: momentary interruptions and storms," *IEEE Transactions on Power Delivery*, vol. 12, pp. 1569–1575, Oct 1997.
- [7] M. Baran, J. Cavaroc, A. Kelley, S. Peele, and Z. Kellum, "Stresses on induction motors due to momentary service interruptions," in *2006 IEEE Industrial and Commercial Power Systems Technical Conference-Conference Record*, pp. 1–8, IEEE, 2006.
- [8] N. Cumbria, M. Dereg, and N. Rao, "Effects of power disturbances on sensitive loads," in *Engineering Solutions for the Next Millennium. 1999 IEEE Canadian Conference on Electrical and Computer Engineering (Cat. No. 99TH8411)*, vol. 2, pp. 1181–1186, IEEE, 1999.
- [9] M. Abir, S. Jan, L. Jubelt, R. M. Merchant, and N. Lurie, "The impact of a large-scale power outage on hemodialysis center operations," *Prehospital and Disaster Medicine*, vol. 28, no. 6, p. 543–546, 2013.
- [10] K. H. LaCommare and J. H. Eto, "Understanding the cost of power interruptions to u.s. electricity consumers,"
- [11] T. Thasananutariya and S. Chatratana, "Investigation of voltage sags due to faults in mea's distribution system," pp. 1–5, June 2005.
- [12] T. Thasananutariya, S. Chatratana, and M. McGranaghan, "Economic evaluation of solution alternatives for voltage sags and momentary interruptions," *Electrical Power Quality and Utilisation, Magazine*, vol. 1, no. 2, 2005.
- [13] J. Seymour and T. Horsley, "The seven types of power problems," *APC, USA*, 2005.

- [14] “Ieee recommended practice for the analysis of fluctuating installations on power systems,” *IEEE Std 1453-2015 (Revision of IEEE Std 1453-2011)*, pp. 1–74, Oct 2015.
- [15] R. Cai, J. Cobben, J. Myrzik, J. Blom, and W. Kling, “Flicker responses of different lamp types,” *Generation, Transmission Distribution, IET*, vol. 3, pp. 816 – 824, 10 2009.
- [16] N. E. M. Association *et al.*, *American National Standard for Electric Power Systems and Equipment-Voltage Ratings (60 Hertz)*. National Electrical Manufacturers Association, 1996.
- [17] A. H. Bonnett, “The impact that voltage and frequency variations have on ac induction motor performance and life in accordance with nema mg-1 standards,” in *Conference Record of 1999 Annual Pulp and Paper Industry Technical Conference (Cat. No.99CH36338)*, pp. 16–26, June 1999.
- [18] A. Peiravi and R. Ildarabadi, “A fast algorithm for intentional islanding of power systems using the multilevel kernel k-means approach,” *Journal of Applied Sciences*, vol. 9, no. 12, pp. 2247–2255, 2009.
- [19] X. Wang, Z. Yan, L. Li, and D. Xie, “A new kernel-based clustering algorithm for the multi-machine equivalent of large power systems,” in *2008 International Conference on Electrical Machines and Systems*, pp. 3936–3939, IEEE, 2008.
- [20] M. S. Uddin, A. Kuh, Y. Weng, and M. IliÄ, “Online bad data detection using kernel density estimation,” in *2015 IEEE Power Energy Society General Meeting*, pp. 1–5, 2015.
- [21] M. Davodi, H. Modares, E. Reihani, M. Davodi, and A. Sarikhani, “Coherency approach by hybrid pso, k-means clustering method in power system,” in *2008 IEEE 2nd International Power and Energy Conference*, pp. 1203–1207, IEEE, 2008.
- [22] M. Ankerst, M. M. Breunig, H.-P. Kriegel, and J. Sander, “Optics: Ordering points to identify the clustering structure,” *ACM Sigmod record*, vol. 28, no. 2, pp. 49–60, 1999.
- [23] K. Zheng, Y. Wang, Q. Chen, and Y. Li, “Electricity theft detecting based on density-clustering method,” in *2017 IEEE Innovative Smart Grid Technologies-Asia (ISGT-Asia)*, pp. 1–6, IEEE, 2017.
- [24] F. Znidi, H. Davarikia, M. Arani, and M. Barati, “Coherency detection and network partitioning based on hierarchical dbscan,” in *2020 IEEE Texas Power and Energy Conference (TPEC)*, pp. 1–5, IEEE, 2020.
- [25] J. Mora-Florez, J. Cormane-Angarita, and G. Ordonez-Plata, “K-means algorithm and mixture distributions for locating faults in power systems,” *Electric Power Systems Research*, vol. 79, no. 5, pp. 714–721, 2009.

- [26] E. Khaledian, S. Pandey, P. Kundu, and A. K. Srivastava, “Real-time synchrophasor data anomaly detection and classification using isolation forest, kmeans, and loop,” *IEEE Transactions on Smart Grid*, vol. 12, no. 3, pp. 2378–2388, 2020.
- [27] Z. Sun, S. Zhao, and J. Zhang, “Short-term wind power forecasting on multiple scales using vmd decomposition, k-means clustering and lstm principal computing,” *IEEE Access*, vol. 7, pp. 166917–166929, 2019.
- [28] W. Wu and M. Peng, “A data mining approach combining  $k$ -means clustering with bagging neural network for short-term wind power forecasting,” *IEEE Internet of Things Journal*, vol. 4, no. 4, pp. 979–986, 2017.
- [29] S. Satsangi, A. Saini, and A. Saraswat, “Clustering based voltage control areas for localized reactive power management in deregulated power system,” *International Journal of Electrical & Computer Engineering*, vol. 6, no. 1, pp. 1348–1354, 2011.
- [30] T. Guo and J. Milanović, “Identification of power system dynamic signature using hierarchical clustering,” in *2014 IEEE PES General Meeting| Conference & Exposition*, pp. 1–5, IEEE, 2014.
- [31] D. Kiran, A. Abhyankar, and B. Panigrahi, “Hierarchical clustering based zone formation in power networks,” in *2016 National Power Systems Conference (NPSC)*, pp. 1–6, IEEE, 2016.
- [32] M. Eissa and A. Kassem, “Hierarchical clustering based optimal pmu placement for power system fault observability,” *Heliyon*, vol. 4, no. 8, p. e00725, 2018.
- [33] M. Jasiński, T. Sikorski, Z. Leonowicz, K. Borkowski, and E. Jasińska, “The application of hierarchical clustering to power quality measurements in an electrical power network with distributed generation,” *Energies*, vol. 13, no. 9, p. 2407, 2020.
- [34] M. J. Zaki, M. Peters, I. Assent, and T. Seidl, “Clicks: An effective algorithm for mining subspace clusters in categorical datasets,” *Data & Knowledge Engineering*, vol. 60, no. 1, pp. 51–70, 2007.
- [35] R. J. Sánchez-García, M. Fennelly, S. Norris, N. Wright, G. Niblo, J. Brodzki, and J. W. Bialek, “Hierarchical spectral clustering of power grids,” *IEEE Transactions on Power Systems*, vol. 29, no. 5, pp. 2229–2237, 2014.
- [36] I. Jayawardene, P. Herath, and G. K. Venayagamoorthy, “A graph theory-based clustering method for power system networks,” in *2020 Clemson University Power Systems Conference (PSC)*, pp. 1–8, IEEE, 2020.
- [37] F. Znidi, H. Davarikia, K. Iqbal, and M. Barati, “Multi-layer spectral clustering approach to intentional islanding in bulk power systems,” *Journal of Modern Power Systems and Clean Energy*, vol. 7, no. 5, pp. 1044–1055, 2019.

- [38] J. Quirós-Tortós and V. Terzija, “A graph theory based new approach for power system restoration,” in *2013 IEEE Grenoble Conference*, pp. 1–6, IEEE, 2013.
- [39] S. Tosserams, M. Kokkolaras, L. Etman, and J. Rooda, “A nonhierarchical formulation of analytical target cascading,” *Journal of Mechanical Design*, vol. 132, no. 5, 2010.
- [40] A. Kargarian, M. Mehrtash, and B. Falahati, “Decentralized implementation of unit commitment with analytical target cascading: A parallel approach,” *IEEE Transactions on Power Systems*, vol. 33, no. 4, pp. 3981–3993, 2017.
- [41] A. Mohammadi and A. Kargarian, “Accelerated and robust analytical target cascading for distributed optimal power flow,” *IEEE Transactions on Industrial Informatics*, vol. 16, no. 12, pp. 7521–7531, 2020.
- [42] G. Cohen, “Auxiliary problem principle and decomposition of optimization problems,” *Journal of optimization Theory and Applications*, vol. 32, no. 3, pp. 277–305, 1980.
- [43] D. Hur, J. Park, and B. H. Kim, “Evaluation of convergence rate in the auxiliary problem principle for distributed optimal power flow,” 2002.
- [44] A. Losi and M. Russo, “On the application of the auxiliary problem principle,” *Journal of optimization theory and applications*, vol. 117, no. 2, pp. 377–396, 2003.
- [45] D. Zhu and G. Hug, “Decomposed stochastic model predictive control for optimal dispatch of storage and generation,” *IEEE Transactions on Smart Grid*, vol. 5, no. 4, pp. 2044–2053, 2014.
- [46] J. J. Yamé, F. Gabsi, T. Darure, T. Jain, F. Hamelin, and N. Sauer, “Optimality condition decomposition approach to distributed model predictive control,” in *2019 American Control Conference (ACC)*, pp. 742–747, IEEE, 2019.
- [47] A. Rabiee and M. Parniani, “Voltage security constrained multi-period optimal reactive power flow using benders and optimality condition decompositions,” *IEEE Transactions on Power Systems*, vol. 28, no. 2, pp. 696–708, 2012.
- [48] A. Rabiee, B. Mohammadi-Ivatloo, and M. Moradi-Dalvand, “Fast dynamic economic power dispatch problems solution via optimality condition decomposition,” *IEEE Transactions on Power Systems*, vol. 29, no. 2, pp. 982–983, 2013.
- [49] Z. Li, Q. Guo, H. Sun, and J. Wang, “Coordinated economic dispatch of coupled transmission and distribution systems using heterogeneous decomposition,” *IEEE Transactions on Power Systems*, vol. 31, no. 6, pp. 4817–4830, 2016.

- [50] H. Everett III, "Generalized lagrange multiplier method for solving problems of optimum allocation of resources," *Operations research*, vol. 11, no. 3, pp. 399–417, 1963.
- [51] R. Halvgaard, J. B. Jørgensen, and L. Vandenberghe, "Dual decomposition for large-scale power balancing," in *18th Nordic Process Control Workshop*, Cite-seer, 2013.
- [52] S. Mhanna, A. C. Chapman, and G. Verbič, "Component-based dual decomposition methods for the opf problem," *Sustainable Energy, Grids and Networks*, vol. 16, pp. 91–110, 2018.
- [53] P. Pflaum, M. Alamir, and M. Y. Lamoudi, "Comparison of a primal and a dual decomposition for distributed mpc in smart districts," in *2014 IEEE International Conference on Smart Grid Communications (SmartGridComm)*, pp. 55–60, 2014.
- [54] T. Romijn, M. Donkers, J. T. Kessels, and S. Weiland, "A dual decomposition approach to complete energy management for a heavy-duty vehicle," in *53rd IEEE Conference on Decision and Control*, pp. 3304–3309, IEEE, 2014.
- [55] A. Falsone, K. Margellos, S. Garatti, and M. Prandini, "Dual decomposition for multi-agent distributed optimization with coupling constraints," *Automatica*, vol. 84, pp. 149–158, 2017.
- [56] J. Mohammadi, G. Hug, and S. Kar, "Role of communication on the convergence rate of fully distributed dc optimal power flow," in *2014 IEEE International Conference on Smart Grid Communications (SmartGridComm)*, pp. 43–48, IEEE, 2014.
- [57] S. Kar and G. Hug, "Distributed robust economic dispatch in power systems: A consensus+ innovations approach," in *2012 IEEE Power and Energy Society General Meeting*, pp. 1–8, IEEE, 2012.
- [58] J. Mohammadi, S. Kar, and G. Hug, "Distributed approach for dc optimal power flow calculations," *arXiv preprint arXiv:1410.4236*, 2014.
- [59] S. Kar, G. Hug, J. Mohammadi, and J. M. Moura, "Distributed state estimation and energy management in smart grids: A consensus + innovations approach," *IEEE Journal of selected topics in signal processing*, vol. 8, no. 6, pp. 1022–1038, 2014.
- [60] T. Erseghe, "Distributed optimal power flow using admm," *IEEE transactions on power systems*, vol. 29, no. 5, pp. 2370–2380, 2014.
- [61] Y. Zhang, E. Dall'Anese, and M. Hong, "Dynamic admm for real-time optimal power flow," in *2017 IEEE Global Conference on Signal and Information Processing (GlobalSIP)*, pp. 1085–1089, IEEE, 2017.

- [62] R. Gupta, F. Sossan, E. Scolari, E. Namor, L. Fabietti, C. Jones, and M. Paolone, "An admittance-based coordination and control strategy for pv and storage to dispatch stochastic prosumers: Theory and experimental validation," in *2018 Power Systems Computation Conference (PSCC)*, pp. 1–7, IEEE, 2018.
- [63] C. Feng, F. Wen, L. Zhang, C. Xu, M. Salam, S. You, *et al.*, "Decentralized energy management of networked microgrid based on alternating-direction multiplier method," *Energies*, vol. 11, no. 10, p. 2555, 2018.
- [64] K. A. Horowitz, Z. Peterson, M. H. Coddington, F. Ding, B. O. Sigrin, D. Saleem, S. E. Baldwin, B. Lydic, S. C. Stanfield, N. Enbar, *et al.*, "An overview of distributed energy resource (der) interconnection: Current practices and emerging solutions," tech. rep., National Renewable Energy Lab.(NREL), Golden, CO (United States), 2019.
- [65] Ó. Gonzales-Zurita, J.-M. Clairand, E. Peñalvo-López, and G. Escrivá-Escrivá, "Review on multi-objective control strategies for distributed generation on inverter-based microgrids," *Energies*, vol. 13, no. 13, p. 3483, 2020.
- [66] I. Tyuryukanov, *Graph Partitioning Algorithms for Control of AC Transmission Networks: Generator Slow Coherency, Intentional Controlled Islanding, and Secondary Voltage Control*. PhD thesis, Delft University of Technology, 2020.
- [67] A. Thakallapelli, S. J. Hossain, and S. Kamalasan, "Coherency based online wide area control of wind integrated power grid," in *2016 IEEE International Conference on Power Electronics, Drives and Energy Systems (PEDES)*, pp. 1–6, IEEE, 2016.
- [68] A. Thakallapelli, S. J. Hossain, and S. Kamalasan, "Coherency and online signal selection based wide area control of wind integrated power grid," *IEEE Transactions on Industry Applications*, vol. 54, no. 4, pp. 3712–3722, 2018.
- [69] N. Ganganath, J. V. Wang, X. Xu, C.-T. Cheng, and K. T. Chi, "Agglomerative clustering-based network partitioning for parallel power system restoration," *IEEE Transactions on Industrial Informatics*, vol. 14, no. 8, pp. 3325–3333, 2017.
- [70] C. Shen, P. Kaufmann, and M. Braun, "Fast network restoration by partitioning of parallel black start zones," *The Journal of Engineering*, vol. 2017, no. 8, pp. 418–426, 2017.
- [71] G. Xu, S. Wu, and Y. Tan, "Island partition of distribution system with distributed generators considering protection of vulnerable nodes," *Applied Sciences*, vol. 7, no. 10, p. 1057, 2017.
- [72] Y. Li and S. Wu, "Controlled islanding for a hybrid ac/dc grid with vsc-hvdc using semi-supervised spectral clustering," *IEEE Access*, vol. 7, pp. 10478–10490, 2019.

- [73] S. Blumsack, P. Hines, M. Patel, C. Barrows, and E. C. Sanchez, “Defining power network zones from measures of electrical distance,” in *2009 IEEE Power & Energy Society General Meeting*, pp. 1–8, IEEE, 2009.
- [74] Yu and Shi, “Multiclass spectral clustering,” in *Proceedings Ninth IEEE International Conference on Computer Vision*, pp. 313–319 vol.1, 2003.
- [75] W.-Y. Chen, Y. Song, H. Bai, C.-J. Lin, and E. Y. Chang, “Parallel spectral clustering in distributed systems,” *IEEE transactions on pattern analysis and machine intelligence*, vol. 33, no. 3, pp. 568–586, 2010.
- [76] U. Von Luxburg, “A tutorial on spectral clustering,” *Statistics and computing*, vol. 17, no. 4, pp. 395–416, 2007.
- [77] U. Von Luxburg, M. Belkin, and O. Bousquet, “Consistency of spectral clustering,” *The Annals of Statistics*, pp. 555–586, 2008.
- [78] I. Tyuryukanov, J. Quirós-Tortós, M. Naglič, M. Popov, M. A. van der Meijden, and V. Terzija, “A post-processing methodology for robust spectral embedded clustering of power networks,” in *IEEE EUROCON 2017-17th International Conference on Smart Technologies*, pp. 805–809, IEEE, 2017.
- [79] J. R. Lee, S. O. Gharan, and L. Trevisan, “Multiway spectral partitioning and higher-order cheeger inequalities,” *Journal of the ACM (JACM)*, vol. 61, no. 6, pp. 1–30, 2014.
- [80] R. J. Sánchez-García, M. Fennelly, S. Norris, N. Wright, G. Niblo, J. Brodzki, and J. W. Bialek, “Hierarchical spectral clustering of power grids,” *IEEE Transactions on Power Systems*, vol. 29, no. 5, pp. 2229–2237, 2014.
- [81] S. Hasanvand, M. Nayeripour, S. A. Arefifar, and H. Fallahzadeh-Abarghouei, “Spectral clustering for designing robust and reliable multi-mg smart distribution systems,” *IET Generation, Transmission & Distribution*, vol. 12, no. 6, pp. 1359–1365, 2017.
- [82] T. Jiang, L. Bai, H. Jia, H. Yuan, and F. Li, “Identification of voltage stability critical injection region in bulk power systems based on the relative gain of voltage coupling,” *IET Generation, Transmission Distribution*, vol. 10, no. 7, pp. 1495–1503, 2016.
- [83] J. Hongjie, Y. Xiaodan, and Y. Yixin, “An improved voltage stability index and its application,” *International Journal of Electrical Power Energy Systems*, vol. 27, no. 8, pp. 567 – 574, 2005.
- [84] E. Cotilla-Sanchez, P. D. H. Hines, C. Barrows, S. Blumsack, and M. Patel, “Multi-attribute partitioning of power networks based on electrical distance,” *IEEE Transactions on Power Systems*, vol. 28, no. 4, pp. 4979–4987, 2013.

- [85] V. C. Gungor, D. Sahin, T. Kocak, S. Ergut, C. Buccella, C. Cecati, and G. P. Hancke, "A survey on smart grid potential applications and communication requirements," *IEEE Transactions on Industrial Informatics*, vol. 9, pp. 28–42, Feb 2013.
- [86] M. Saleh, Y. Esa, M. E. Hariri, and A. Mohamed, "Impact of information and communication technology limitations on microgrid operation," *Energies*, vol. 12, no. 15, 2019.
- [87] K. Sridharan and N. N. Schulz, "Outage management through amr systems using an intelligent data filter," *IEEE Transactions on Power Delivery*, vol. 16, pp. 669–675, Oct 2001.
- [88] S. Ghosh, D. Ghosh, and D. K. Mohanta, "Situational awareness enhancement of smart grids using intelligent maintenance scheduling of phasor measurement sensors," *IEEE Sensors Journal*, vol. 17, pp. 7685–7693, Dec 2017.
- [89] M. K. Penshanwar, M. Gavande, and M. F. A. R. Satarkar, "Phasor measurement unit technology and its applications - a review," in *2015 International Conference on Energy Systems and Applications*, pp. 318–323, Oct 2015.
- [90] "Advanced metering infrastructure and customer systems: Results from the smart grid investment grant program," *Department of Energy*, Sep 2016.
- [91] "Distribution automation: Results from the smart grid investment grant program," *Department of Energy*, Sep 2016.
- [92] "Communications requirements of smart grid technologies," *Department of Energy*, Oct 2010.
- [93] G. Lou, W. Gu, Y. Xu, W. Jin, and X. Du, "Stability robustness for secondary voltage control in autonomous microgrids with consideration of communication delays," *IEEE Transactions on Power Systems*, vol. 33, pp. 4164–4178, July 2018.
- [94] K. Sun, D.-Z. Zheng, and Q. Lu, "Splitting strategies for islanding operation of large-scale power systems using obdd-based methods," *IEEE transactions on Power Systems*, vol. 18, no. 2, pp. 912–923, 2003.
- [95] M. Paramasivam, S. Dasgupta, V. Ajjarapu, and U. Vaidya, "Contingency analysis and identification of dynamic voltage control areas," *IEEE Transactions on Power Systems*, vol. 30, no. 6, pp. 2974–2983, 2015.
- [96] K. Morison, X. Wang, A. Moshref, and A. Edris, "Identification of voltage control areas and reactive power reserve; an advancement in on-line voltage security assessment," in *2008 IEEE Power and Energy Society General Meeting - Conversion and Delivery of Electrical Energy in the 21st Century*, pp. 1–7, 2008.

- [97] S. Abapour, K. Zare, and B. Mohammadi-Ivatloo, "Dynamic planning of distributed generation units in active distribution network," *IET Generation, Transmission Distribution*, vol. 9, no. 12, pp. 1455–1463, 2015.
- [98] S. Patel, M. Ahmed, and S. Kamalasadán, "A novel energy storage-based net-load smoothing and shifting architecture for high amount of photovoltaics integrated power distribution system," *IEEE Transactions on Industry Applications*, vol. 56, no. 3, pp. 3090–3099, 2020.
- [99] R. Yousefian and S. Kamalasadán, "A lyapunov function based optimal hybrid power system controller for improved transient stability," *Electric Power Systems Research*, vol. 137, pp. 6–15, 2016.
- [100] S. Abdelrazek and S. Kamalasadán, "A weather-based optimal storage management algorithm for pv capacity firming," *IEEE Transactions on Industry Applications*, vol. 52, no. 6, pp. 5175–5184, 2016.
- [101] R. Yousefian, A. Sahami, and S. Kamalasadán, "Hybrid energy function based real-time optimal wide-area transient stability controller for power system stability," in *2015 IEEE Industry Applications Society Annual Meeting*, pp. 1–8, IEEE, 2015.
- [102] S. Moghadasi and S. Kamalasadán, "Real-time optimal scheduling of smart power distribution systems using integrated receding horizon control and convex conic programming," in *2014 IEEE Industry Application Society Annual Meeting*, pp. 1–7, IEEE, 2014.
- [103] S. Kamalasadán, *A new generation of adaptive control: An intelligent supervisory loop approach*. PhD thesis, University of Toledo, 2004.
- [104] E. D. Vugrin, A. R. Castillo, and C. A. Silva-Monroy, "Resilience metrics for the electric power system: A performance-based approach," tech. rep., Sandia National Lab.(SNL-NM), Albuquerque, NM (United States), 2017.
- [105] B. Chiu and A. Bose, "Resilience framework methods and metrics for the electricity sector," *Resource Center, IEEE Power & Energy Society*, 2020.

APPENDIX A: Simulator

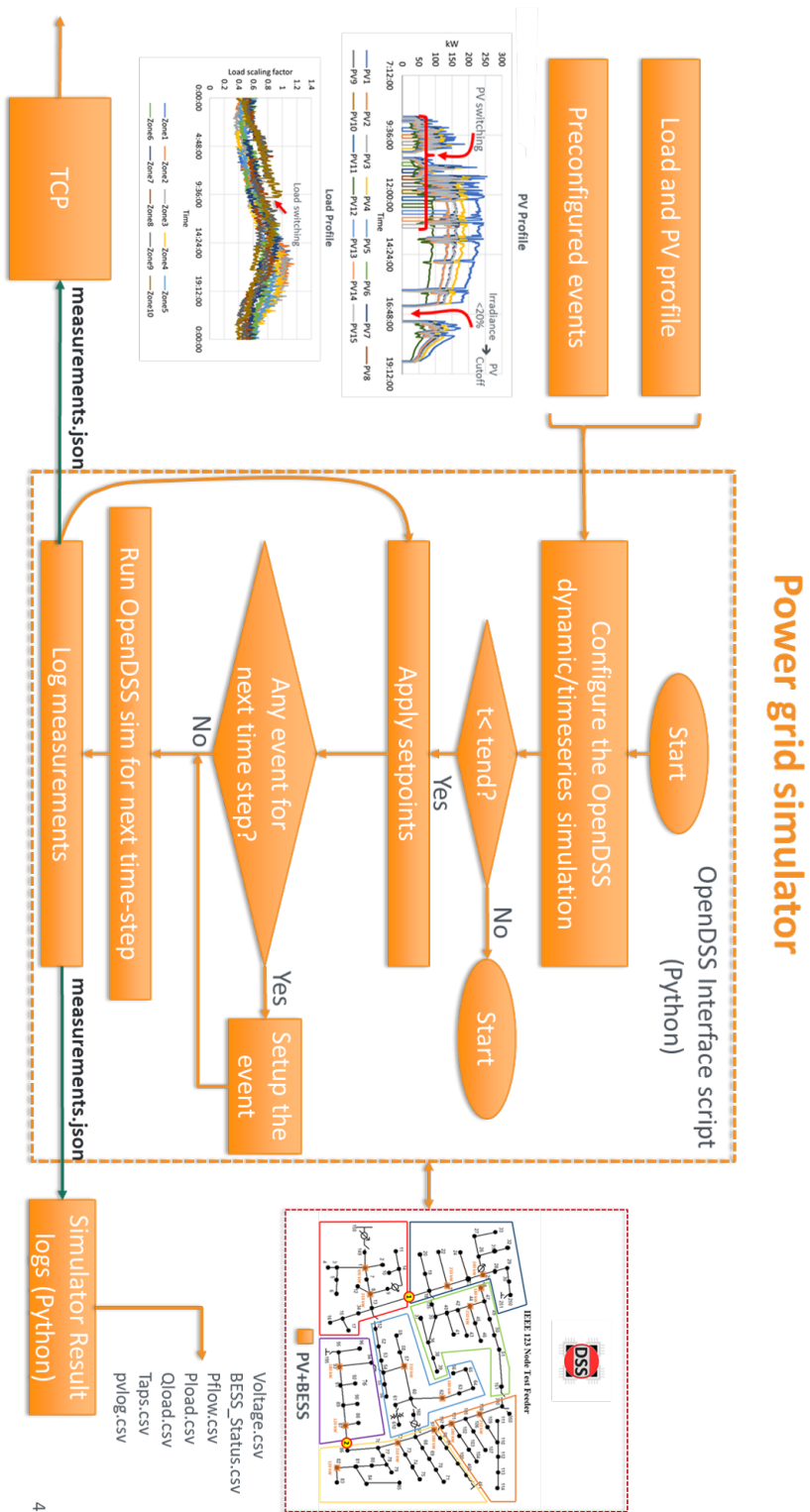


Figure A.1: Python interface for OpenDSS simulator

## APPENDIX B: Measurements

## Measurement points

<ul style="list-style-type: none"> <li>Capacitor</li> </ul>	
<ul style="list-style-type: none"> <li>Capacitor (214233779056)</li> <li>C83 (2142339366056)</li> <li>busdata (214228479056)</li> <li>V (2141692442976)</li> <li>Q (2141692442920)</li> <li>Status (2142339365944)</li> </ul>	<pre>dict: {'C83': {'busdata': [83, 1.678, 4275.0, 175.0] &lt;class 'list'&gt;: [83, 1.678, 4275.0, 175.0] V: {'busdata': [83, 1.678, 4275.0, 175.0] &lt;class 'list'&gt;: [1.003623, 1.060899, 1.067751] Q: {'busdata': [-234.8479, -225.1013, -228.0201] str: [ ]</pre>
<ul style="list-style-type: none"> <li>PV</li> </ul>	
<ul style="list-style-type: none"> <li>PV/system (214233778352)</li> <li>PV1 (2142339363984)</li> <li>busdata (214228479056)</li> <li>P (2141678592384)</li> <li>Q (2141692442920)</li> <li>V (2141692442976)</li> <li>A (2141684679488)</li> <li>Irad (2142339363928)</li> </ul>	<pre>dict: {'PV1': {'busdata': [1, 0.122, 700.0, 1500.0] P: {'busdata': [1, 0.122, 700.0, 1500.0] P: [-74.0976] &lt;class 'list'&gt;: [1, 0.122, 700.0, 1500.0] Q: {'busdata': [1, 0.122, 700.0, 1500.0] &lt;class 'list'&gt;: [-74.0976, -74.0976] V: {'busdata': [1, 0.122, 700.0, 1500.0] &lt;class 'list'&gt;: [-0.0001, -0.0, -0.0001] A: {'busdata': [1.038985, 1.044604, 1.04005, 1.041211] &lt;class 'list'&gt;: [-0.2018, -119.9525, 120.014] float: 0.776</pre>
<ul style="list-style-type: none"> <li>Energy Storage</li> </ul>	
<ul style="list-style-type: none"> <li>Storage (2142339398956)</li> <li>BESS1 (2142339398956)</li> <li>busdata (214228479056)</li> <li>P (2141678592384)</li> <li>Q (2141692442920)</li> <li>V (2141692442976)</li> <li>SOC (2142339340024)</li> <li>State (2142339340136)</li> <li>Mode (2142339340304)</li> </ul>	<pre>dict: {'BESS1': {'busdata': [1, 0.122, 700.0, 1500.0] P: {'busdata': [1, 0.122, 700.0, 1500.0] P: [0.0, -0.0] &lt;class 'list'&gt;: [1, 0.122, 700.0, 1500.0] Q: {'busdata': [1, 0.122, 700.0, 1500.0] &lt;class 'list'&gt;: [-0.0, 0.0, 0.0] V: {'busdata': [1.038985, 1.044604, 1.04005, 1.041211] float: 50.0 str: IDLING int: 0</pre>
<ul style="list-style-type: none"> <li>Transformer/Regulator</li> </ul>	
<ul style="list-style-type: none"> <li>Transformer (214233778992)</li> <li>REG1A (214228479336)</li> <li>busdata (214228479056)</li> <li>Vprim (2142339366392)</li> <li>Vsec (2142339366784)</li> <li>Pprim (2142339366280)</li> <li>Psec (2142339366224)</li> <li>Qprim (2142339365888)</li> <li>Qsec (2142339365776)</li> <li>Tap (2142339365720)</li> </ul>	<pre>dict: {'REG1A': {'busdata': [150, 0.0, 100.0, 1500] Vprim: {'busdata': [150, 0.0, 100.0, 1500.0] &lt;class 'list'&gt;: [150, 0.0, 100.0, 1500.0] Vsec: {'busdata': [150, 0.0, 100.0, 1500.0] &lt;class 'list'&gt;: [1.043742, 1.043746, 1.043745] Pprim: {'busdata': [401.9994, 22.4594, 202.5461] &lt;class 'list'&gt;: [-401.9994, -22.4594, -202.5461] Psec: {'busdata': [323.3943, 171.9187, 211.376] &lt;class 'list'&gt;: [-323.3927, -171.9185, -211.3755] str: 7</pre>
<ul style="list-style-type: none"> <li>Load</li> </ul>	
<ul style="list-style-type: none"> <li>Load (2142339340920)</li> <li>S1A (2142339340864)</li> <li>busdata (214228479056)</li> <li>P (2141678592384)</li> <li>Q (2141692442920)</li> <li>V (2141692442976)</li> </ul>	<pre>dict: {'S1A': {'busdata': [1, 0.122, 700.0] P: {'busdata': [1, 0.122, 700.0, 1500.0] &lt;class 'list'&gt;: [1, 0.122, 700.0, 1500.0] Q: {'busdata': [1, 0.122, 700.0, 1500.0] &lt;class 'list'&gt;: [28.9783, 0.0] V: {'busdata': [1.038985, 1.044604, 1.04005, 1.041211] &lt;class 'list'&gt;: [1.038985, 0.000416]</pre>
<ul style="list-style-type: none"> <li>Switch</li> </ul>	
<ul style="list-style-type: none"> <li>Switch (2142339254400)</li> <li>SW1 (2142339254568)</li> <li>busdata (214228479056)</li> <li>Vprim (2142339366392)</li> <li>Pprim (2142339366280)</li> <li>Qprim (2142339365888)</li> <li>Enabled (2142339255016)</li> </ul>	<pre>dict: {'SW1': {'busdata': [150, 0.0, 100.0, 150] Vprim: {'busdata': [150, 0.0, 100.0, 1500.0] V: {'busdata': [150, 0.0, 100.0, 1500.0] &lt;class 'list'&gt;: [150, 0.0, 100.0, 1500.0] Pprim: {'busdata': [401.9994, 22.4594, 202.5461] &lt;class 'list'&gt;: [401.9994, 22.4594, 202.5461] Qprim: {'busdata': [323.3927, 171.9185, 211.3755] &lt;class 'list'&gt;: [323.3927, 171.9185, 211.3755] bool: True</pre>

→ "busdata" for all elements can be ignored

Figure B.1: Measurement format for all devices